Materials Horizons

REVIEW

Cite this: *Mater. Horiz.*, 2017, **4**, 155

Materials aspects of semiconductor nanocrystals for optoelectronic applications

Stephen V. Kershaw,†[a] Lihong Jing,†[bc] Xiaodan Huang,[bc] Mingyuan Gao*[bc] and Andrey L. Rogach*[a]

Received 1st November 2016,
Accepted 19th December 2016

DOI: 10.1039/c6mh00469e

www.rsc.li/materials-horizons

Semiconductor nanocrystal quantum dots are at last starting to emerge in commercial applications such as flat panel displays. Meanwhile, they are also showing seriously attractive performance levels in other types of optoelectronic devices. This maturing has been driven to a large degree by a deep level of understanding of materials related aspects of semiconductor nanocrystals themselves and in combination with other materials in the form of composite films to build optoelectronic components. We examine the synthetic and post synthetic chemical strategies that have led to semiconductor quantum dot structures with robust and strong device performance, and review the current work-in-progress as well as longer term developments in the areas of photovoltaics and photoelectrochemical cells, photodetectors, solid state lighting, photocatalysts, and sensing applications.

1. Introduction

This review addresses the progress in colloidal semiconductor quantum dot (QD) optoelectronic devices: solar cells,[1–4] photodetectors,[5–8] light emitting diodes (LEDs),[3,9–11] photocatalytic hydrogen generation devices[12–15] and sensors, with a focus on the materials aspects of the semiconductor nanocrystals involved. It examines which QD synthesis and processing strategies were successful in improving device performance and highlights what needs to be done to push some of this work closer to being commercially useful. Chemists have evolved

[a] *Department of Physics and Materials Science & Centre for Functional Photonics, City University of Hong Kong, 83 Tat Chee Avenue, Kowloon, Hong Kong SAR, China. E-mail: andrey.rogach@cityu.edu.hk*
[b] *Institute of Chemistry, Chinese Academy of Sciences, Bei Yi Jie 2, Zhong Guan Cun, Beijing 100190, China*
[c] *School of Chemistry and Chemical Engineering, University of Chinese Academy of Sciences, Beijing 100049, China. E-mail: gaomy@iccas.ac.cn*
† S. V. K. and L. J. contributed equally to this work.

Stephen V. Kershaw

Dr Stephen V. Kershaw is a Senior Research Fellow at City University of Hong Kong. He received his BSc in Physics and Chemistry (1980) and PhD in Physics (1984) from Manchester University, UK. Following postdoctoral research on liquid crystals at Manchester he joined British Telecom Laboratories (1989). His research continued on joining Corning's UK Research Labs in 2000 and in 2002 he co-founded a quantum dot applications startup company, acting as managing director until 2010. His current research includes the synthesis and spectroscopy of low bandgap semiconductor nanocrystal materials for solar, optical sensing and mid-infrared photodetector applications.

Lihong Jing

Dr Lihong Jing is an associate professor in the Institute of Chemistry, Chinese Academy of Sciences. She received her PhD in Physical Chemistry (2011) under the supervision of Prof. Mingyuan Gao in that institute. She worked as a Research Assistant and Research Associate at Prof. Andrey L. Rogach's group at City University of Hong Kong in 2011 and 2013, respectively. Her major research focuses on the synthesis and applications of semiconductor quantum dots and their associated multifunctional nanomaterials.

numerous synthetic methods that result in an impressive range of nanoheterostructured QDs: core–shells,[16–18] nanorods,[19–21] tetrapods,[21,22–27] *etc.*, and these can be functionalized with a rich variety of ligands or linked to other types of nanoparticles or specific surfaces to form composite assemblies. Whilst this toolbox of synthetic methods is impressive in its own right, many of these structures have been derived to solve or address very specific needs in making or improving QD-based optoelectronic devices. This review is an attempt to highlight the correlation between the chemistries involved and the device performance and engineering. For selected applications we've followed some of the twists and turns along the way rather than simply presenting the story as just a snapshot state-of-the-art view. It is sometimes instructive to see what was tried but didn't prove to be as effective as envisaged alongside the strategies that did lead to decisive improvements. In some cases, the good ideas may yet still prove to be useful, perhaps with improved materials, or they may prove to be beneficial for other applications.

QD displays have already proved to be a success story.[28] This is interesting since this is a particularly crowded application area: there are many different technologies – liquid crystal displays, organic LEDs and other traditional technologies all competing for the same or at least highly overlapping markets. This generally makes it difficult for a new technology to enter, so it must bring something special in terms of operating specifications (low power/improved colour performance) or the fabrication process (*e.g.* low cost) to make it more attractive than the incumbent technologies.

QD lighting is highly likely to be one of the next big breakthroughs in mass markets,[11,29–31] whilst infrared (IR) photodetectors, though not such a high volume market and more specialized, may soon be an attractive application for low bandgap QDs. The latter may soon reach performance levels of current IR detector technologies but without the need for expensive and cumbersome cooling in many cases, making such detectors attractive for portable/low power detection systems.[7,32–34]

QD based photocatalysis as a potential clean hydrogen fuel source is a longer term game.[12] Much interesting work is being done, especially on combining QDs with co-catalysts borrowed from nature – either directly or by synthetic mimicry.[35–38] However, there is still much to do in improving the long term operating stability of the QDs and finding durable and regeneratable hole scavengers.[13] Coupling robust O_2 generation with H_2 in a QD based water splitting system also seems a long way ahead.[39]

Photovoltaic (PV) QD solar cell breakthroughs are likewise a harder prospect. The power conversion efficiency (PCE) of commercial silicon PV solar cells has moved ever closer to the Shockley-Queisser limit[40] whilst the PCE of solar cells based on

Xiaodan Huang

Xiaodan Huang is a postgraduate student in the Institute of Chemistry, Chinese Academy of Sciences. She started her PhD degree in Physical Chemistry under the supervision of Prof. Mingyuan Gao in that institute in 2014. She is interested in the synthesis and applications of multifunctional inorganic nanomaterials.

Mingyuan Gao

Prof. Mingyuan Gao is a Full Professor in the Institute of Chemistry, Chinese Academy of Sciences (CAS). He received his BS degree (1989) and PhD degree (1995) in Polymer Chemistry and Physics at Jilin University, China. He worked as research assistant and research associate in Germany from 1996 to 2002 and was an Alexander von Humboldt fellow between 1996 and 1998. He took his current position under the "Hundred-talents Program" of CAS in 2001. He received the "National Science Fund for Distinguished Young Scholars" from NSFC in 2002. His research focuses on the synthesis as well as biological and biomedical applications of functional nanomaterials.

Andrey L. Rogach

Prof. Andrey L. Rogach is a Chair Professor of Photonics Materials and the founding director of the Centre for Functional Photonics at City University of Hong Kong. He received his Diploma in Chemistry (1991) and PhD in Physical Chemistry (1995) from the Belarusian State University in Minsk, and worked as a staff scientist at the Institute of Physical Chemistry at the University of Hamburg, Germany, from 1995 to 2002. During 2002–2009, he held a tenured position of lead staff scientist at the Department of Physics of the Ludwig-Maximilians-Universität in Munich, where he completed his habilitation in Experimental Physics. His research focuses on the synthesis, assembly and optical spectroscopy of colloidal semiconductor and metal nanocrystals and their hybrid structures, and their use for photovoltaic, photocatalytic, and optoelectronic applications.

This journal is © The Royal Society of Chemistry 2017

a perovskite film[41] has rapidly overtaken that of QD PVs for the time being at least. However, there are materials developments in the pipeline that may offer QD solar technologies something of an eventual boost as we will describe in the outlook section.

In the following sections we describe some optoelectronic applications of QDs including work on solar cells, photodetectors, LEDs, and photocatalysis as well. Each of these areas could warrant a specialist review in their own right, and we have tried to maintain a materials scientist's perspective rather than straying too deeply into the device physics, though it helps to at least try to meet half-way, *i.e.* for chemists to understand the issues facing QD device engineers and physicists in order to better tailor materials for applications, and for the engineers to better understand the chemistry to make best use of the materials' properties. Many groups produce QDs by organic solvent methods but deploy the materials in devices coated with water soluble ligands because for optoelectronic applications short chain ligands are a prerequisite. For some QD materials the highest solution photoluminescence quantum yields (PL QYs) are obtained *via* organic solvent based syntheses, whilst for other materials aqueous routes hold sway.[42] But in translating the QD solutions into QD films, *etc.*, for devices, the solution PL QY can be substantially compromised. For this reason, for the purposes of this review we take the view that it does not matter which synthetic route was taken, each has its own merits but also potentially some downsides, which chemists are nonetheless working to minimize. Due to the space constrains, we do not consider group IV QDs such as carbon/graphene dots, and silicon and germanium QDs; the interested reader is referred to a number of recently published related reviews on the optoelectronic applications of these materials.[43–48]

2. QD based solar cells

The following sections review some of the work on solar cells using QD-based materials. This has become a burgeoning field with many different types of QDs, synthetic routes and post synthetic treatments that are carried out primarily in order to consolidate QD films during multilayer deposition and to give good short range coupling between a QD and its surroundings to enhance carrier transport and extraction. There are a wide range of different solar cell device architectures, each designed to harness the QDs' electronic properties to separate and remove the photogenerated charges. In addition, there are other device types which make use of the optical properties of QDs alone to form solar cells in conjunction with other types of conventional photovoltaic cells. These sections are intended to give a flavor of which QD materials are used and how they are used but it is by no means a device specialist review. More detailed discussion and informed overviews of the device aspects can be found in the works by Nozik *et al.*,[49] Emin *et al.*,[50] Carey *et al.*,[1] Sargent,[2] Kim *et al.*[51] and Lan *et al.*[52] and more general reviews of the field by Kim and Ma[53] and Zhang *et al.*[54] In more specific review articles, Hetsch *et al.*[55] compared progress earlier in the development of the field in QD sensitized solar cells (QDSSCs), heterostructure and Schottky QD devices, whilst Ruhle *et al.*[56] and Hines and Kamat[57] cover QDSSCs and QD material properties affecting their operation. Liu *et al.*[58] focus specifically on electron acceptor materials for QD solar cells including different oxides, types, forms and precursors and how they may be optimized to improve the overall cell performance. Similarly Ip *et al.*,[59] also from the Sargent group, have published very useful work on encapsulation methods to protect Pb chalcogenide-based solar cells from oxidation problems, which have more general applicability. Ramasamy *et al.*[60] present a chemists' view of developments in QD PV materials in general, whilst the short reviews by Mondal *et al.*[61] and Fu and Tsang[62] focus more narrowly on CdS rods, tetrapods, wires and QDs, and PbS, PbSe and PbTe QD based devices respectively. Purcell-Milton and Gun'ko[63] review luminescent solar concentrators in general, including those based on other fluorophores as well as QDs and nanorods. We have not included solar cells combining plasmonic particles and QDs specifically, though these combinations are touched upon in the later section on photodetectors. For these types of devices the excellent recent review by Jiang *et al.*[64] is recommended.

A number of different types of device design have evolved in the last decade of QD solar cell research as shown in Fig. 1. Early work focused on QDSSCs in which the QDs substituted for the previous organic dyes that had been successfully used in the so-called Grätzel-type solar cells. However, QDSSCs have struggled to realize PCEs anything like those achievable with dyes. Barriers include the control of competing recombination pathways and the redox compatibility (stability) between the QDs and the electrolyte. The use of a liquid electrolyte is also a potential barrier to commercialization in terms of product lifetimes, but these problems continue to be addressed by various research groups.

Another early type of solar cells involved blends of semiconducting polymers and QDs, including nanorods and branched heterostructures such as tetrapods. In some cases, these mixtures were intimately and homogeneously mixed, whereas in other cases it emerged that there was some degree of phase separation. The latter gave rise to bulk heterojunction cell designs where if the two phases had different carrier types, p- and n-, charge separation could occur at the distributed interface between them. In the case of the fully mixed polymer/QD devices charges could be photogenerated in either the semiconducting polymer or the QDs, but then exciton dissociation would lead to hole transport *via* the polymer to the anode and electron transport *via* the QD network to the cathode. This of course is very abbreviated and leaves out much of the additional cell structure such as carrier blocking layers, *etc.*

From this early work, cell designs with discrete p type and n type semiconducting layers emerged, giving rise to planar heterojunction designs where charges go their separate ways after photogeneration and exciton dissociation happens in a depletion region close to the interface between the two layers. Most often the p-type layer is the QD material, PbS NCs being the most common example. Not only semiconducting polymers have been used as n-type materials, but also n-type wide bandgap oxides as well. In some cases, these materials can also be more

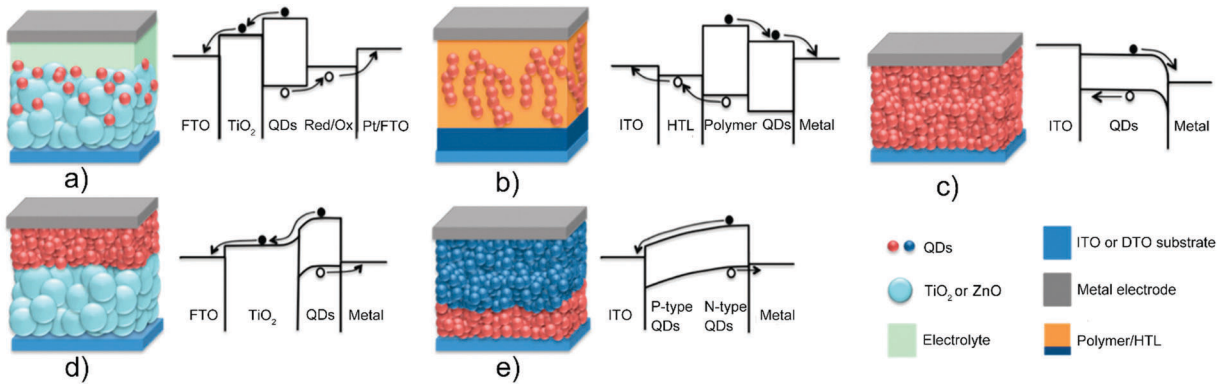

Fig. 1 Schematic illustration of device configurations and energy band diagram of QD-based solar cells: (a) QD-sensitized solar cell, (b) hybrid QD–polymer solar cell, (c) Schottky junction solar cell, (d) p–n heterojunction solar cell, and (e) p–n homojunction solar cell. Reproduced with permission from ref. 53. Copyright 2015 American Chemical Society.

highly doped by the addition of appropriate cation dopants. It is also possible to make some QDs n-type, either by doping or by choosing certain types of ligands. This has led to the construction of heterojunctions made entirely of different or differently treated QD layers, which are sometimes referred to as quantum (hetero)junctions.

Much of the more recent leading research (in terms of the all-important PCE bottom line) has focused on heterostructure design and optimization. Schottky cell designs were quite popular for a while, being able to match if not exceed QDSSC performance without the need for any liquid electrolyte. Here a junction was formed between a metal electrode layer and the QD semiconducting layer and photocharges were generated and collected from a depletion region in the latter adjacent to the QD/metal contact. However, the focus seems to be more upon heterojunction designs nowadays; often Schottky cell performance is something that is measured along the way when fabricating QD-based heterojunctions, essentially the former device being a part of the fabricated heterojunction with a metal contact deposited directly on the (usually p-type) QD layer.

Apart from a purely photovoltaic role in solar cells, QDs offer other potentially useful functions: in an extension of the QDSSC concept they may be used to form electrochemical cells in which photocatalysed chemical reactions can take place; some QD materials, most notably CdTe, may be deposited as thin layers and then sintered to form polycrystalline thin films of bulk semiconductors which can have sufficiently good enough quality to function as a photovoltaic with a good PCE themselves; QDs may be combined with plasmonic metal nanoparticles to form more strongly or broader spectral range absorbing PV materials, making use of radiative energy transfer between the two particle types, and the metal nanoparticles may offer improvements in exciton dissociation efficiencies; radiative energy transfer between monolayer thick stacks of different sized QDs can act as so called Förster Resonant Energy Transfer (FRET) funnels,[65] channelling energy to a photovoltaic heterojunction for example; both radiative and non-radiative transfer (energy and charge transfer respectively) in QD layers deposited directly on the surface of conventional PV cells can improve the energy harvesting capacity of the latter; finally the regular down-shifted fluorescence from QDs embedded in optical polymer films can be used to enhance the spectral efficiency of regular bulk PVs (without being in direct contact), or they may be used as luminescent solar concentrators in conjunction with regular bulk PVs to gather and convert the solar flux at lower cost per Watt generated than conventional PVs alone.

In principle QDs synthesized in either aqueous or organic solvents can be used in QD solar cells. In practice, some are more effectively grown by hot injection or alternative organic solvent methods whilst the aqueous approach suits other materials better. By effective we mean that size, size dispersion, composition and heterostructures can be controlled to precisely manipulate band gaps and band alignments, and that high PL QYs of the materials in solution as synthesized can be obtained. Traditional hot injection methods still generally suffer from the problem of limited batch sizes however which, although not a problem for research, might not be so useful for commercial scale manufacture. Some of the so-called heat-up synthetic methods which are conducted in organic solvents for ternary and quaternary QDs, which don't rely on the rapid and precise temperature profiles used in hot injection growth, may be more attractive in this respect.[54,66] Whichever synthetic method is used, for solar cell applications requiring the QD to be part of a photovoltaic structure, good carrier mobility, rapid exciton dissociation and charge extraction are all necessary, and these are facilitated by using short chain length ligands, or in some cases no ligands at all, when the device is fabricated. Organic syntheses use long chain ligands (*e.g.* oleic acid, *etc.*) relying on steric hindrance to prevent QDs from aggregating together. Mostly these ligands are exchanged for much shorter ligands or cross-linkers such as benzene dithiol, ethanedithiol, MPA, butylamine, *etc.*, at the device stage. Aqueous QDs in contrast use ionic stabilization and the same ligands, such as short chain mercapto-acids, may already be present during their synthesis. There is thus no need for ligand exchange on incorporating them into a device. The fact that they are dispersed in water, this being far less volatile than many organic solvents, can

 This journal is © The Royal Society of Chemistry 2017

present fabrication problems for some types of solar cells, yet be advantageous for others. There are now many methods by which water soluble ligands can be exchanged for organic solvent compatible ligands and *vice versa* allowing QDs to be shifted between hydrophilic and hydrophobic environments. This may be done in solution prior to device fabrication or alternatively post QD film deposition in the solid phase, by washing out the previous ligand and soaking/rinsing with the shorter desired ligands prior to adding further layers of the structure. Ligand exchange may however present potential penalties that must be weighed against the benefits and include incomplete ligand exchange, incomplete passivation of surface sites with the new ligand, ligand (dipole) induced shifts in the band alignments, film cracking, and QD surface damage in the process (surface etching, oxidation, impurity doping), though some of these effects may be usefully exploited in their own right.

In terms of the QD materials used in solar cells, although many have been studied, and new materials such as perovskite QDs are starting to emerge, a few dominate the QD solar cell literature: CdSe and CdSe-based heterostructures; PbS; and to a lesser extent but more recently CdTe. In part this is because these materials can be made with bandgaps that allow good coverage of the majority of the solar spectrum and can be synthesized reproducibly and with good PL QYs. They are also exceptionally well characterized in terms of their electronic properties both at the nanoparticle level and in conjunction with a wide range of ligands. Sticking to these mainstay materials has allowed several groups to focus on the device structure aspects – how to optimize the overall photogeneration, exciton fission, and charge collection to maximize the conversion efficiency by trying different designs, structures and the other materials involved in solar cells (other hybrid semiconductors, electrodes, charge blocking and transport materials, electrolytes, *etc.*). As other new QD materials emerge, much of this body of device knowledge is readily transferable.

In the following sub-sections we review some of the progress, topics of interest and problems for QDs in solar cells, grouped by device types. Whilst this Review is more aimed at QD materials, we do include some of the structural research particularly where this has some bearing on the QDs or on how they are processed or perform. However, we do not trespass too far into the device physics, as we are more concerned with the QD materials themselves.

The all-important comparator is of course solar cell performance. Where figures are given (though in some cases studies are cited on some aspects of the power conversion process that are not reduced to a simple set of performance statistics) we will list them in the format [PCE (%), V_{oc} (V), J_{sc} (mA cm^{-2}), FF (0–1)] under AM 1.5G 1 Sun test conditions unless stated otherwise.

2.1. QD sensitized solar cells

Before describing the different facets of QDSSC research over the past decade it is important to stress that such devices are quite complex, involving several components: QDs; wide bandgap host semiconductor; ligand and QD to host linker molecules; passivating layers and electrolyte. There are multiple interfaces and parallel pathways for carriers to negotiate between the different semiconductors, which makes for a difficult optimization task. Many of the researches (especially the earlier works) which we will describe below focused on one or two of the constituent parts of QDSSCs but not upon the global optimization of the whole device, so the incremental improvements in solar cell performance metrics were often not so outstanding despite the valuable insight gained. Only more recently have some groups started to report PCE values exceeding 10% as the accumulated know-how for all the component parts is beginning to be dovetailed together into single solar cell designs.[67] We have attempted to give a full flavour of the battles fought to improve QDSSC performance on several different fronts but in doing so perhaps it may seem as though much of the early work cited was not leading to very targeted breakthroughs in performance. However, around 2013 there were a number of reports of QDSSC PCE performance exceeding 5%, and there has been further rapid progress during 2016 leading to a doubling of the efficiency to over 10%. We hope that the readers will appreciate the accounts of the, sometimes good, ideas that proved to have perhaps less radical impact on performance than envisaged, and the distillation of what does make for good and practical QDSSC designs.

Dye sensitized solar cells are now reaching PCEs of 17% or better, whilst QDSSCs still lag behind, mostly at $<10\%$ and also have stability problems that are still to be addressed in many instances. In most cases the substrate to be sensitized is a porous TiO_2 n-type layer with a wide bandgap, though other wide bandgap porous substrates such as ZnO are sometimes used. The oxide may consist of a layer of partly sintered nanospheres, nanowires or nanotubes on a transparent electrode layer (*e.g.* FTO) and QDs are introduced into and attached to the surfaces of the porous oxide structure. The contact to the counter electrode (often CuS_2 coated brass) is typically formed *via* a liquid electrolyte redox couple such as polysulfide (S^{2-}/S_n^{2-}), iodide (I^{3-}/I^-) or cobalt (Co^{II}/Co^{III}).

Early studies extensively used mercaptopropionic acid (MPA) and other thioacids as bifunctional linker molecules to tether QDs such as CdSe to the oxide, with the thiol coordinating to the QD and the carboxylic acid to the TiO_2. Robel *et al.*[68] studied the electron to photon conversion factor in such QDSSCs (12%) and found that the main locations where carriers were being lost to recombination were at the TiO_2/QD interface and also at internal TiO_2 grain boundaries. In this work the linker was applied to the surfaces of the TiO_2 pores and QDs introduced by soaking afterwards. There is no indication that the original organic ligands (trioctylphosphine oxide, TOPO) were removed during the incorporation of the QDs into the oxide. Electron transfer rates (CdSe/TiO_2) of 0.07 to 1.95×10^{11} s^{-1} were determined from transient absorption measurements on TiO_2/QDs linked complexes in solution. Later work on CdSe QDs grown in water with thioglycolic acid (TGA) as the ligand and linker molecule in subsequent deposition in TiO_2 films by Mora-Sero *et al.*[69] used surface photovoltage measurements to establish that the

latter (in normalized form) follows the film's optical density spectrum and as such the electron injection rates were similar for all sizes of QDs over the range within the size distribution of the ensemble as synthesized.

Leschkies *et al.*[70] incorporated organically grown CdSe QDs onto ZnO nanowire substrates grown on FTO electrodes using MPA as a linker. In their approach the original TOPO and hexadecylamine (HDA) ligands were removed prior to deposition by a solution based ligand exchange that involved an overnight reflux in a mixture of MPA, methanol and tetramethylammonium hydroxide. Subsequent solar performance testing under AM 1.5G conditions gave a still low result [0.4%, 0.6 V, 2.1 mA cm^{-2}, 0.3].

A comparison of particulate TiO_2 and TiO_2 nanotubes with CdSe QDs found the latter to favour better charge injection into the oxide.[71] Again the substrates were treated with MPA as a linker molecule but no indication of TOPO ligand removal was cited. In this study evidence of more favourable injection efficiency was seen for smaller QDs, but the best PCE values remained below 1%.

Shen *et al.*[72] addressed the issue arising from the poor stability of the QDs with the standard polysulfide electrolytes by using an over-coating layer of ZnS after QD deposition, applied using the successive ionic layer adsorption and reaction (SILAR) method. In this case the CdSe QDs were grown from aqueous precursors but *in situ* using the chemical bath deposition (CBD) method such that the CdSe QDs were in direct contact with the oxide and did not require a linker molecule. The subsequent ZnS layer coated both CdSe and exposed TiO_2 surfaces. Photovoltaic conversion efficiency increased with the CdSe QD diameter but reached a maximum limited by CdSe/CdSe boundaries. The ZnS coating was found to improve V_{oc} and PCE values: without the layer performance was [1.12%, 0.48 V, 5.34 mA cm^{-2}, 0.43] but with the coating [2.02%, 0.53 V, 12.2 mA cm^{-2}, 0.31]. Lee *et al.*[73] approached the problem by using an alternative to the usual polysulfide couple, replacing it with a Co^{II}/Co^{III} electrolyte. They also explicitly removed the organic ligands present during the growth of their CdSe QDs by treating them with pyridine prior to deposition into a MPA treated porous TiO_2 layer. With this approach, they reached [1.17%, 0.61 V, 3.15 mA cm^{-2}, 0.61], and higher PCE values at lower light intensities. Bang and Kamat[74] turned their attention to lower bandgap CdTe QDs. Not only should CdTe have broader coverage of the solar spectrum into the NIR than CdSe, but the larger conduction band offset between CdTe and TiO_2 should give faster electron injection rates (2.4×10^8 s^{-1} and 2.1×10^9 s^{-1} for CdSe and CdTe respectively). Despite this however, CdTe presented a greater problem than CdSe with regard to the electrolyte, with anodic corrosion of Te with S severely limiting both hole scavenging effectiveness and stability. Other redox couples were also tried (I^{3-}/I^-, Co^{II}/Co^{III}, ferrocene/ferrocene$^+$) but without any significant improvement.

In further work with the CdSe QD and Co^{II}/Co^{III} electrolyte and an improved SILAR method to furnish the selenide for *in situ* formation of the QDs within the porous TiO_2 layer, Lee *et al.*[75] improved their performance level, crediting the slower recombination rates and the resulting longer effective carrier diffusion lengths to their better deposition method. In an effort to improve charge collection efficiencies, they made a preliminary study of CdSe/CdTe core/shell QDs where the Te layer was a single SILAR cycle thick. Owing to the already known poor stability of tellurides with many electrolytes they also compared the performance with the alternative solid hole conductor Spiro-OMeTAD, reaching a level of [0.84%, 0.7 V, 2.15 mA cm^{-2}, 0.55] with stability of a few months under room light and ambient atmosphere. With the Co^{II}/Co^{III} electrolyte [4%, 0.67 V, 4.94 mA cm^{-2}, 0.54] was achieved with the Te terminated surface.

Mora-Seró *et al.*[76] reviewed the state of the art around that time (2009) concerning the factors governing recombination in QDSSCs. The benefits of the ZnS layer passivation to improve QD stability with respect to the liquid electrolytes were discussed, along with the potential alternative redox couples; though there was no clear outstandingly better alternative, the ZnS passivation was seen as indispensable. However, surface states arising from the TiO_2 were also known to be a potential recombination site that impacted the fill factors achievable. Methods to incorporate the QDs into porous wide bandgap electrodes were compared: *in situ* growth (SILAR and CBD); linker coated QD deposition; and linker treated oxides were reviewed with regard to efforts to increase QD loading. Poor photocurrents and limited fill factors were seen as major challenges at that time, as dye based devices were able to achieve far higher FF values of >0.7.[76]

Gimenez *et al.*[77] examined the need for a molecular linker such as MPA by trying direct adsorption of pre-synthesized (autoclave/solvothermal method) CdSe QDs originally grown using oleic acid ligands in organic solvents. Prior to deposition in the TiO_2 pores the toluene solvent was replaced by (more volatile) dichloromethane to improve the effectiveness of the deposition process and force precipitation of the QDs within the pores. Here again a ZnS over-coating layer was employed, and, in comparison with CdSe attached to TiO_2 with a cysteine bifunctional linker, direct absorption without any linker was found to give better performance [1.83%, 0.53 V, 7.13 mA cm^{-2}, 0.48]. The approach of Im *et al.*[78] to direct attachment was to grow CdSe/ZnS core/shell QDs *ex situ* and then adsorb them into the porous TiO_2 layer. They termed the ZnS thin shell as a functional layer that ensured that the QDs bonded and had good contact with the TiO_2 substrate. The band alignment of the ZnS according to bulk band levels is type I but as a thin layer, carriers were assumed to be sufficiently able to tunnel from the QD to the titania (electrons) and from the QDs to the electrolyte (holes) to yield a reasonable photocurrent. Additional CdSe loading was obtained by adding a further spray pyrolysis stage to form more QDs *in situ* on top of the initial layer of ZnS coated CdSe QDs. The final performance figure was [2.2%, 0.57 V, 11.2 mA cm^{-2}, 0.34] again; despite promising V_{oc} and photocurrent values the fill factor still remained low.

An alternative method to drive QDs into porous TiO_2 substrates without the need for linker molecules was the electrophoretic deposition (EPD) method investigated by Salant *et al.*[79] A range of different sized CdSe QDs and also nanorods, grown in organic solution, were deposited from toluene onto TiO_2

 This journal is © The Royal Society of Chemistry 2017

coated FTO electrodes with cell voltages up to 200 V. The charge on the QDs was simply that due to the net stoichiometric imbalance of the QD and any ligand contributions. There was no attempt to enhance the charge as in aqueous QD materials where ligand deprotonation (by varying the pH) can be used to form highly charged ligand/QD complexes. Highly loaded TiO_2 films were formed nonetheless, and solar cell test values up to [1.7%, 0.554 V, 9 mA cm^{-2}, 0.35] were achieved after coating the loaded films with a further ZnS passivating layer.

Around 2011, the focus in QDSSCs started to switch from mainly regular CdSe QDs and nanorods to other QD sensitizers. Hu *et al.*[80] prepared $CuInS_2$ (CIS) QDs by an aqueous room temperature synthesis with mercapto acetic acid as the ligand. After immersing the TiO_2 coated FTO photoanode in the resulting QD solution, and rinsing, the QD loaded substrates were heat treated at 280 °C and then a CdS passivation layer was added using a CBD step. An 80 second heat treatment gave an optimum solar cell performance of [1.47%, 0.489 V, 8.12 mA cm^{-2}, 0.37].

Ning *et al.*[81] compared both type II band alignment with organic solution grown ZnSe/CdS core/shell QDs, and the inverse CdS/ZnSe heterostructures. The bandgap of ZnSe/CdS type II QDs is red shifted relative to the bulk bandgaps because of the spatially indirect nature of the band edge transition, and this should improve solar spectral coverage. In both cases, after adsorption into the TiO_2 photoanodes, a passivating layer of ZnS was also added. MPA linker based deposition was used with the TiO_2 being treated with the latter prior to adsorption. Rather than the regular polysulfide electrolyte, Ning *et al.* used an organic sulfide electrolyte based on a tetramethylthiourea/tetramethylthiourea-trifluoromethanesulfonic anhydride couple, also used with dye sensitized solar cells. For the type II structure with the organic sulfide electrolyte the best performance was obtained: [0.86%, 0.66 V, 2.25 mA cm^{-2}, 0.58]. Whilst the FF and V_{oc} values were quite promising, poor photocurrent limited the PCE.

McDaniel *et al.*[82] turned their attention to $CuInSe_xS_{2-x}$ QDs, the alloying with Se allowing the quaternary QDs to be compositionally tuned further into the IR than $CuInS_2$ QDs. As with CdSe QDs however, ZnS passivation was still necessary to protect the Se surface sites from the electrolyte, and to limit unwanted back recombination between electrons in the QDs and holes in the electrolyte. A surface treatment to the QDs using Cd-oleate was also added in order to form a CdS shell around the QDs. This improved the carrier lifetimes and both V_{oc} and J_{sc} values, though it came with the penalty of slower electron extraction rates. With relatively good QD loading a solar cell performance of [3.45%, 0.55 V, 9.4 mA cm^{-2}, 0.604] was obtained. Further work by the same group using the same QDs but replacing the aqueous polysulfide electrolyte with a methanol based polysulfide formulation led to further improvements. They also surveyed the use of a range of different bifunctional linker molecules: MPA, *t*-butyl amine, *n*-butyl amine, *s*-butyl amine (and pyridine as a comparison). The best test device performance data improved to [5.5%, 0.56 V, 16.8 mA cm^{-2}, 0.59].

Wang *et al.*[83] turned their attention to CdTe/CdSe core/shell QDs, first synthesizing the CdTe cores by organic methods, then applying CdSe by solution SILAR reaction to deposit a precise number of CdSe layers. Prior to deposition in their TiO_2 photoanodes, the oleic acid/oleylamine ligands were removed and replaced with MPA ligands, allowing the QDs to be incorporated into the oxide by simply soaking and rinsing. The choice of this type II QD again extended the spectral coverage, accelerated the electron injection rate into the oxide and retarded the radiative recombination rate. The use of the standard ZnS passivation and polysulfide electrolyte limited the V_{oc} but a still respectably improved performance of [6.75%, 0.606 V, 19.59 mA cm^{-2}, 0.569] was reported. Rather than core shells, Pan *et al.* used $CdSe_xTe_{1-x}$ alloy QDs and achieved a very similar level of performance.[84] Using a one-pot organic solvent heating method, $CdSe_{0.45}Te_{0.55}$ alloys were synthesized. Again, prior to deposition in the TiO_2 substrate, ligand exchange for MPA rendering the QDs water soluble was carried out. After deposition, a ZnS SILAR passivation and polysulfide electrolyte were used and the cell performance achieved was [6.36%, 0.571 V, 19.35 mA cm^{-2}, 0.575].

Whilst some studies of QDSSCs including those just mentioned carried out complete replacement of organically soluble ligands such as TOPO (or oleic acid, oleylamine, *etc.*) with water soluble thiols, others simply let the organic ligands remain, but relied on MPA already bound at the carboxylate functional group to the TiO_2 substrate to make contact with the QD surface through the organic ligand shell during deposition of the QDs. This led Hines and Kamat[85] to make a comparative study of the effectiveness of thiol and amine linker molecules (MPA and β-alanine) under such circumstances, with regard to hole and electron transfer rates and hole trapping. Both linkers reduced the rate of electron transfer to TiO_2 but the authors suggested that β-alanine may offer the advantage of remediating surface hole traps on CdSe at low ligand concentrations and some increase in photogenerated electrons in the QD cores due to ligand charging effects. Alternative water soluble ligands have also been investigated by other groups. Cysteinate capping was used on both magic sized CdSe clusters and larger CdSe QDs[86] giving cell performance figures of [0.43%, 0.4 V, 1.4 mA cm^{-2}, 0.45] and [0.83%, 0.48 V, 2.3 mA cm^{-2}, 0.46] respectively.

Pan *et al.*[87] made improvements to $CuInS_2$ QDSSCs by adding a ZnS layer during *ex situ* growth to form core/shell heterostructures. By now it had become more usual to render the organic solvent soluble QDs water soluble *via* solution ligand exchange into an MPA ligand environment. Post deposition in the TiO_2 photoanode, further ZnS was added *via* a SILAR reaction to passivate against the electrolyte. The core/shell structure in this case was type I, improving confinement of both carriers to the QD core and cell performance to [7.04%, 0.586 V, 20.65 mA cm^{-2}, 0.581].

The relative merits of type I and type II band alignments and the differing types of carrier confinement were studied by Luo *et al.*[88] with $CdSe_xTe_{1-x}$ alloyed cores. During synthesis, a thin layer of CdS was added giving rise to type I confinement because the shell was thin. However, this could be increased

post deposition in the TiO_2 porous substrate by further SILAR CdS deposition cycles, leading to a transition to type II confinement. Again, MPA was the chosen linker and also the stabilizing ligand used in the water based QD synthesis. With type I band alignment, cell performance was [2.72%, 0.502 V, 10.23 mA cm^{-2}, 0.53] but this improved to [5.04%, 0.578 V, 14.79 mA cm^{-2}, 0.59] on spatially segregating the electrons and holes within the type II QDs, and extended the spectral coverage into the IR.

Whilst most of the work on QDSSCs had used II–VI QDs and CIS based ternaries and quaternaries, most work on lead chalcogenide-based QDs had centred on their use in heterojunction and Schottky type solar cells. However, there are a few and increasing instances of groups investigating their performance in QDSSCs. PbS and PbSSe QDs grown with organic solvent soluble ligands (*e.g.* oleic acid) were electrophoretically deposited in TiO_2 photoanodes from toluene solution, and subsequently over-coated with a CdS SILAR passivating layer to protect the QDs against the polysulfide electrolyte. Relatively modest performance [2.1%, 0.46 V, 8 mA cm^{-2}, 0.58] was seen and evidence of some oxidation to form PbO was observed. Slightly better performance was obtained from PbS QDs deposited by electrophoresis (EPD) into TiO_2 nanotube array photoanodes by Tao *et al.*[89] They attributed their higher photocurrent to increased QD loading by using EPD method, with performance figures of [3.41%, 0.64 V, 8.84 mA cm^{-2}, 0.63].

The issue of the need to highly load a microporous TiO_2 substrate with QDs when a thicker more open macroporous substrate might be more effectively loaded with QDs was examined by Jumabekov *et al.*[90] The problem becomes more acute for organically grown QDs where the stabilizing ligands (if not exchanged) are hydrophobic whereas their intended deposition site is hydrophilic. Their paper in fact opens with a very useful yet succinct review of the various QD deposition methods relevant to hydrophobic PbS QDs. However, Jumabekov *et al.* improved the situation by ligand exchange, moving from their oleylamine synthesis ligand to water soluble glutathione (GSH) prior to deposition. They deposited the GSH stabilized PbS QDs into macroporous TiO_2 layers with large pores formed by PMMA sphere templates of 100 nm diameter mixed with the TiO_2 sol–gel precursor but removed by calcination during high temperature drying and partial consolidation of the oxide films. The much larger pore sizes allowed far more efficient PbS QD deposition by simple repeated soaking and rinsing cycles. After deposition, a SILAR ZnS layer was applied as usual. Performance was [1.11%, 0.343 V, 7.4 mA cm^{-2}, 0.44] with the low V_{oc} and fill factor attributed to slow hole transfer and limitations of using the polysulfide electrolyte.

The electrolyte issue was addressed by Kim *et al.*,[91] who used a solid P3HT hole transporting polymer in this role. Their TiO_2 nanorod array substrate was formed by first depositing a layer of sacrificial ZnO nanorods which are then converted to TiO_2 nanorods by treatment with ammonium hexafluorotitanate boric acid. The resulting TiO_2 nanorod layer was then treated with MPA and organically stabilized PbS QDs introduced by multiple rounds of spin coating. After each PbS deposition a treatment with ethanedithiol was employed to displace the incumbent ligand and cross-link the PbS to obtain a multi-QD thick dense coating on the nanorods. The hole transport layer was introduced by spin coating from dichlorobenzene solution and a layer of PEDOT:PSS spin coated on top of that, before a gold top contact was added by thermal evaporation. The short radial path of charge transport between the QDs and the rods for the electrons and the QDs and the surrounding P3HT improved the fill factor, V_{oc} and photocurrent: [3.9%, 0.53 V, 12.1 mA cm^{-2}, 0.603].

A similar but all-aqueous process was used by Chen *et al.*[92] to avoid the use of a liquid electrolyte. In their case they used water soluble methoxy poly(phenylene vinylene) (MPPV) as a wide bandgap hole acceptor in conjunction with aqueously synthesized CdTe with mercaptoethylamine as the ligand. The device was formed in a planar geometry for the TiO_2 electron acceptor rather than as a mesoporous oxide, whilst the CdTe/MPPV layer was spin coated as a blend from aqueous solution and then baked at 300 °C for 60 min in a glove box (Fig. 2).[92] With this approach, the donor and acceptor were in close contact despite the fact that the MPPV loading was quite low (3% by weight, 16% by volume). With the polymer present, all of the device test parameters were improved [4.84%, 0.612 V, 14.8 mA cm^{-2}, 0.534] relative to

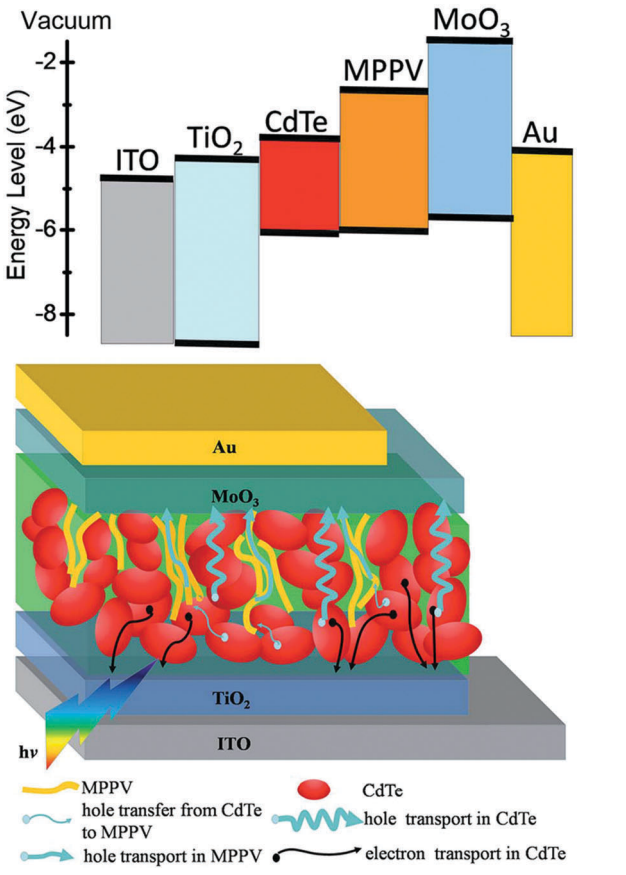

Fig. 2 Energy level, device structure diagrams and proposed carrier transfer and transport in the CdTe based QDSSCs studied by Chen *et al.* Reproduced with permission from ref. 92. Copyright 2015 The Royal Society of Chemistry.

This journal is © The Royal Society of Chemistry 2017

reference devices containing no polymer, with the polymer functioning as both a hole acceptor and a hole transporter.

In the work on PbS heterojunction solar cells running in parallel with QDSSC development, it was found that halide treatment of such QDs as an atomic surface ligand shell could passivate surface defects more effectively than MPA (or other comparatively large molecular ligands) alone. A hybrid method with both MPA (at less than full surface coverage) and halide passivation allows the benefits of both types of passivant to be realized in QDSSCs. This approach was adopted by Huang *et al.*,[93] who used mixed I^-/MPA stabilized CdSe QDs (dispersed in chloroform). After pipetting the solution onto mesoporous TiO_2 substrates and rinsing away the surface excess, a protective SILAR coating was added. The use of the hybrid ligands brought an improvement with cell test values of [3.31%, 0.52 V, 10.87 mA cm^{-2}, 0.585].

Although CIS-based ternaries and quaternaries have made big improvements in the PCE values, work on the II–VI materials also continues to push the QDSSC performance ever higher. Jiao *et al.*[94] improved upon CdTe/CdSe core/shell QD sensitized cells with ZnTe/CdSe type II heterostructures where the conduction band offset between the core and the shell is almost 1 eV greater. The benefit of this greater offset is an increase in charge accumulation across the QD/TiO_2 interface (under illumination) and *via* stronger dipole effects an upward shift of the TiO_2 conduction band, increasing the photovoltage. The electron injection rate is increased, as is the photocurrent. The spectral range is almost the same as that of the earlier CdTe/CdSe QD materials.[83] The standard procedure of changing the organic soluble growth ligands for water soluble MPA prior to deposition and ZnS SILAR overcoating after deposition was followed. The performance with this type II core shell improved to [7.17%, 0.642 V, 19.65 mA cm^{-2}, 0.57].

The final example we cite in this class of solar cells is an update of work published during the writing of this review. Du *et al.*[67] have obtained PCEs of 11.6% [11.6%, 0.739 V, 25.25 mA cm^{-2}, 0.622], with 4 nm diameter Zn–Cu–In–Se alloy QDs deposited inside a nanoporous TiO_2 photoanode with the usual MPA linker applied to the QDs before deposition. The use of quaternary alloys allowed smaller diameter particles (compared to previous work employing 5–6 nm diameter QDs) whilst still covering the solar spectrum up to around 1100 nm, thus improving the ease of deposition within the porous titania structure and thereby the QD deposition density. The broadened absorption spectrum contributed to an improved J_{sc} value, assisted by a higher conduction band edge which improved the electron extraction rate. The alloy structure is also credited with suppression of carrier recombination at the photoanode/electrolyte interfaces leading to an improved V_{oc}.

2.2. QD/polymer composite solar cells

The first work on QD/semiconducting polymer blends sprang from earlier studies of photovoltaic conversion in organic polymers where the electron acceptor was a second, high electron affinity (*e.g.* cyano-substituted) polymer or a fullerene. QDs offered an alternative electron acceptor to bring about dissociation of the exciton generated in the polymer and to assist in the transport of the latter through the hybrid material. Ginger and Greenham[95] were one of the first to investigate such blends combining organically grown CdSe QDs with MEH-PPV (poly[2-methoxy-5-(2′-ethyl-hexyloxy)-*p*-phenylenevinylene]), MEH-CN-PPV and DHeO-CN-PPV derivatives. Although blended, TEM images showed CdSe QD aggregated areas where the structure might more properly be regarded as a heterojunction between two phases. Transient absorption studies compared the degree of charge transfer between the QDs and the polymers, with the DHeO-CN-PPV showing a lack of charge transfer to the QDs possibly partly due to strongly competing delocalization of the photogenerated exciton across several adjacent chains, and partly because the alkyloxy side chains on either side of the conjugated polymer would sterically impede close approach of the QDs to the site of the photogenerated excitons. Charge transfer was not found to be strongly dependent on the QD size however.

Huynh *et al.*[96] extended the investigation of QD polymer blends to include CdSe nanorods (60 nm × 7 nm) using P3HT as the conducting polymer and were among the first to report AM 1.5G performance figures for such devices in a solar cell test structure. 90% by weight CdSe nanorod/P3HT blends were spin cast from solution onto an ITO glass substrate coated with PEDOT:PSS. An aluminium top contact was directly deposited on the nanorod/P3HT blend layer. The cell test values at this early stage were [1.7%, 0.7 V, 5.7 mA cm^{-2}, 0.4].

Although conducting polymers such as MEH-PPV and its derivatives are readily engineered to absorb light and thereby generate excitons that can be dissociated and extracted as a photocurrent, the role of the blended NCs in the early devices was seen as mainly electronic, *i.e.* in assisting the exciton dissociation and transport of electrons. However, coverage of the near IR portion of the solar spectrum was not readily achievable with the polymer absorption spectrum. McDonald *et al.*[6] recognized that PbS QDs could also contribute to the photocurrent and extend the photosensitivity further into the IR than the polymer alone. Photocurrent studies on blends with different sized PbS QDs demonstrated spectral responses to as far as 1600 nm.

Gur *et al.*[97] investigated the morphology – in particular what could be done to maximize the QD/polymer heterojunction contact and limit the exciton diffusion length in the polymer before reaching the heterojunction (here again photogeneration was assumed to be mainly in the P3HT polymer chosen). Hyperbranched, so called urchin, CdSe QDs were blended with the conducting polymer to form a solution suitable for spin-coating. In solar cell tests the V_{oc} *vs.* CdSe loading dependence was almost flat at around 0.6 V as was the fill factor, varying only slightly between 0.5 and 0.55. The PCE then essentially followed the J_{sc} *vs.* loading characteristic, rising to a maximum value around 1%, corresponding to a photocurrent of 3.5 mA cm^{-2}.

The theme of extended IR response was taken further by Jiang *et al.*[98] this time combining IR bandgap PbSe QDs with P3HT and MEH-PPV conducting polymers. For the smaller PbSe QDs the heterojunction in the P3HT blend test devices was

type II. Polymer blends with PbSe QDs with bandgaps up to 1.85 μm were explored, with the anticipation that these might be useful not just for extended solar spectrum absorption but also may have allowed use to be made of carrier multiplication in low bandgap QDs. However, the test device performance in these early devices was very poor at [0.04%, 0.3–0.4 V, 0.02 mA cm^{-2}, <0.37].

Thus far, little mention has been made of the influence of the QD's ligands on the interaction with the conducting polymer at the interface. However, in their study of CdS multiarmed (tetrapodal) nanorods blended with MEH-PPV, Wang *et al.*[99] purposefully removed the original HDA ligand before device fabrication by refluxing their particles in pyridine. FTIR spectra confirmed the removal of the HDA. Pyridine was also the solvent used to spin coat the nanorod/polymer blend. The pyridine ligand strip was attributed with an enhancement in the photocurrent and PCE value. Further improvements were obtained by heat treating the films at 150 °C after spin coating, resulting in test values of [1.17%, 0.85 V, 2.96 mA cm^{-2}, 0.466]. Bang *et al.*[100] also used a pyridine treatment on their ZnTe/ZnSe type II core/shell QD/P3HT blends. These were spin coated onto PEDOT:PSS coated ITO electrodes and top electrodes of aluminium added to form test devices. However, very low test values were observed: [0.0063%, 0.38 V, 0.055 mA cm^{-2}, 0.30]. Band engineering of the nanocrystals before pyridine treatment can be used to tune charge separation between polymer and QDs as well as modify the electron transport properties.[101–105] For example, the blends of alloyed tetrapod $CdSe_xTe_{1-x}$/MEH-PPV,[103] and the branched heterostructure CdTe–CdSe/P3HT[105] showed improved performance with PCEs around 1%.

Rather than using polymer/QD blends, Wei *et al.*[106] instead selected a planar heterojunction solar cell design, combining a layer of PPV with a layer of $Cd_xHg_{1-x}Te$ QDs, the latter alloy QDs being grown in water with MPA as the ligand. After synthesis, the MPA coated QDs were treated with dodecyltrimethylammonium bromide (DTAB) in order to transfer them into chloroform for spin coating onto the PPV layer. The ammonium salt coupled with the carboxylic acid group of the MPA and in the process both terminated the ligand shell with a long alkyl chain conferring organic solvent compatibility and also modified the surface dipole moment of the ligand shell (Fig. 3). This was suggested as the reason for the marked uplift in the V_{oc} of the planar heterojunction (to 1.4 V). However, the price for this increase in the photovoltage appears to be relatively low photocurrent due to the effective thickening of the insulating ligand dielectric layer and a consequently low PCE. The performance figures were [0.06%, 1.4 V, 0.2 mA cm^{-2}, 0.2].

The geometry of the electron acceptor layer has often received attention in solar cells in an effort to improve the contact between QD layers. Wide bandgap oxide nanorod substrates are a frequent choice in both bulk heterostructures and QDSSCs. Briscoe *et al.*[107] investigated QD coating techniques to bring ZnO nanorods into close and controlled proximity to CdTe QDs. Layer by layer solution deposition methods using TGA-capped, ionically charged CdTe QDs in water at high pH, alternating with oppositely charged poly(diallyl-dimethylammonium chloride)

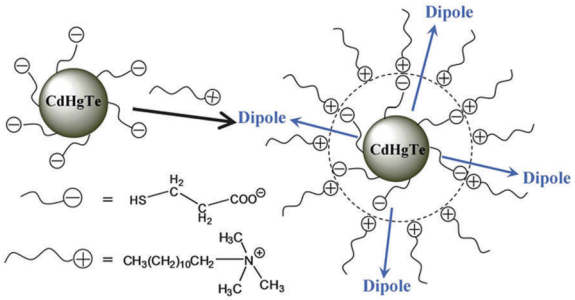

Fig. 3 The surface dipole change at the hybrid heterojunction interface. The CdHgTe QDs are covered with MPA as stabilizer. After the surface modification of the QDs with the DTAB, the dipole moment at the QD surface shifts from inside to outside. Reproduced with permission from ref. 106. Copyright 2012 The Royal Society of Chemistry.

(PDDA) polyelectrolyte solutions, were used to build up coatings of up to 50 bilayer cycles on the nanorods. This resulted in bands of CdTe QDs with 0.2–0.3 nm layers of PDDA in between. Over the coated ZnO substrate, layers of p-type CuSCN or PEDOT:PSS were spin coated as solid hole collecting layers (rather than using a liquid electrolyte) before applying gold anodes. The best efficiencies were obtained for test devices that were annealed at 350 °C for 1 h and where the CuSCN was used as the hole collecting layer [0.0066%, 0.12 V, 0.19 mA cm^{-2}, 0.29].

2.3. Bulk and depleted planar heterojunction solar cells

Donor–acceptor heterojunctions (rather than p–n type heterojunction devices) featured quite early in the development of QD-based solar cells. Gur *et al.*[108] formed such a type II junction between two layers of CdTe and CdSe nanorods, each spin coated from pyridine solution having been synthesized by organic solvent based methods. The substrate was an ITO coated glass slide with a 0.2 nm thick alumina coating. Photogenerated excitons could be created in either layer and dissociated at the junction due to the band offsets. However, the authors proposed that the extraction of charges towards the respective terminals was *via* carrier diffusion rather than by any built-in field in the absence of any dopant depletion region. The top aluminium electrode was applied directly to the CdSe nanorod layer, without any additional charge blocking layers, but this simple test device gave a performance of [2.9%, 0.41 V, 0.58 mA cm^{-2}, 0.4].

Whilst many of the early conducting polymer/QD hybrid solar cells were bulk heterojunction devices (on some scale), other types of organic/inorganic hybrid heterojunction combinations have also been investigated. Kitada *et al.*[109] combined PbSe QDs with a tetrabenzoporphyrin (TBP). In their device, the photosensitive and charge separating layer was a blend of PbSe QDs with this organic photoconductor, but on top of this blend a further buffer layer of PbSe QDs was also added to prevent direct contact between the Al cathode and the TBP. As with other types of QD solar cells, it was realized that the oleic acid ligands used in the PbSe QD synthesis impeded electrical contact between the respective parts of the heterojunction and restricted carrier transport, so the long chain ligand was exchanged for butylamine and the PbSe buffer layer treated

 This journal is © The Royal Society of Chemistry 2017

with ethanedithiol (EDT) to both cross link it and enhance conductivity. However, in spite of this the performance was rather low [3.1–3.5 × 10^{-3}%, 0.63–0.65 V, 22.5–25.8 μA cm^{-2}, 0.21–0.22].

Fullerenes (C_{60}, and in particular its PCBM derivative) are yet another set of electron acceptor/transport layers often employed in such solar cells. Li *et al.*[110] combined the latter with CdSe/CdTe tetrapods in a blended donor–acceptor heterojunction layer in their devices. The electron transport may have been aided by partial aggregation of the C_{60} in the blended layer, providing an electron collection pathway. Again, contact between the junction layer and the top Al electrode was ensured by adding a thin C_{60} layer between the two. At the opposite ITO electrode a PEDOT:PSS electron blocking layer/hole transport layer was used. The phosphonic acids used in the tetrapod synthesis were again stripped by a 24 h reflux in pyridine and the latter used as a coordinating (but volatile) solvent during spin coating of the blend along with chloroform. The thin pure C_{60} film was deposited by thermal evaporation at low pressure. With this combination test values were [0.62%, 0.43 V, 3.15 mA cm^{-2}, 0.46].

The work on verifying charge separation in QD layer heterostructures using the surface photovoltage spectroscopy technique by Gross *et al.*[111] was useful in the development and engineering of such structures. Test stacks of various alternating patterns of water soluble CdTe and CdSe QDs with negatively charged TGA ligands interspersed with positively charged (also water soluble) polyelectrolyte layers were deposited using a layer by layer solution dipping technique. Separation of excitonic charges generated by photon absorption could occur at the CdTe/CdSe interface(s) in the stacks (holes in CdTe, electrons in CdSe). The excitation source wavelength was scanned such that the surface photovoltage excitation spectrum could be determined. Referencing the photovoltage spectra to the absorption curves for the two QDs allowed the (energetic) location of the carrier generation and the sign of the carriers to be determined. Both lock-in/chopped source and pulsed excitation modes were used allowing the slow and fast (>1 ns) responses to be monitored, the latter giving insight into carrier diffusion mechanisms (see Fig. 4).

Major improvements in QD heterojunction solar cells came with Pattantyus-Abraham *et al.*'s[112] report of a depleted heterojunction mode of operation with PbS-based devices. PbS QDs were spin coated onto TiO_2 electrodes coated on top of SnO_2:F glass and treated after deposition with MPA to cross link them and improve conductivity. Evidence of cross-linking, *i.e.* binding at both thiol and carboxylate functional groups, was observed *via* FTIR measurements. Differences in the Fermi level of the n-type TiO_2 and p-type PbS forming the heterojunction led to a built-in field with a value depending on the p-type doping of the QDs which was in turn found to depend on the diameter of the nanoparticles. The built-in field led to the formation of a depletion region within the PbS layer and the field assisted in exciton dissociation and drove the separation of the electron and hole charges. The depletion region allowed thicker QD absorbing layers to be used whilst the depletion region still allowed the charge generated in this region to be collected efficiently. It was established that field driven carrier diffusion rather than serial FRET transfer to the junction was the mechanism allowing a greater thickness of material to be used. From FRET transfer rates and exciton lifetimes it was estimated that only a few short-range transfers were likely to occur whereas something of the order of 50 carrier site hops would be needed to transit from the dissociation point to the electrodes (a distance of up to 200–250 nm), which would be beyond the range for multiple stages of FRET. The improvement in performance was quite marked for the optimal QD diameter (and bandgap) of the three chosen for their study:

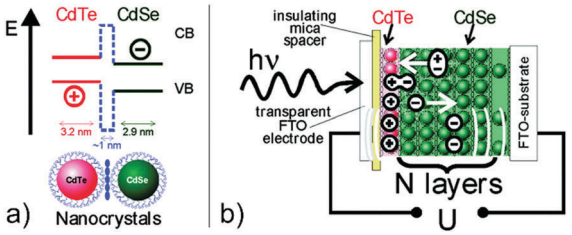

Fig. 4 (a) Type II band alignment of CdTe and CdSe QDs. Conduction band (CB) and valence band (VB) levels are shown. (b) Scheme of the surface photovoltage (SPV) setup applied for the measurements on multi-layered samples of CdTe and CdSe QDs. Excitons are created upon light excitation, which diffuse through the structure and may reach and become separated at the type II CdTe/CdSe interface. The random diffusion of separated charges creates an electric field measured as the SPV signal U by two transparent outer FTO electrodes in a capacitor arrangement. Reproduced with permission from ref. 111. Copyright 2010 American Chemical Society.

$$\text{QD } E_g = 1.3 \text{ eV: } [5.1\%, 0.51 \text{ V}, 16.2 \text{ mA cm}^{-2}, 0.58]$$

compared with

$$\text{QD } E_g = 1.1 \text{ eV: } [2.1\%, 0.45 \text{ V}, 13.2 \text{ mA cm}^{-2}, 0.35]$$

and

$$\text{QD } E_g = 0.9 \text{ eV: } [0.93\%, 0.21 \text{ V}, 11.3 \text{ mA cm}^{-2}, 0.21]$$

The problems inherent in excitonic heterojunction QD devices associated with finding a good electron transport layer (well aligned energy levels) that also functioned as a good hole blocking layer were addressed by Zhao *et al.*[113] For the latter they selected the fullerene derivative, [6,6]-phenyl-C_{61}-butyric acid methyl ester (PCBM), in conjunction with PbS QDs. The influence of various treatments (air annealing the PbS QD films at 110 °C for 30 min during fabrication, room temperature ozone treatments, *etc.*) on performance was compared. For air annealed devices, values of [1.27%, 0.47 V, 4.2 mA cm^{-2}, 0.62] showing improvements in fill factor and V_{oc} were seen, whilst ozone treatment led to higher photocurrents [1.68%, 0.24 V, 14 mA cm^{-2}, 0.5]. Controlled surface oxidation of the PbS QDs was seen as the main mechanism for the improvements.

Bulk heterojunctions consisting of CdTe tetrapods blended with aniline-capped poly[(4,4′-bis(2-ethylhexyl)-dithieno[3,2-*b*:2′,3′-*d*]silole)-2,6-diyl-*alt*-(2,1,3-benzothiadiazole)-4,7-diyl] ($PSBTBTNH_2$) were evaluated by Chen *et al.*[114] Their device structure also

incorporated a 30 nm thick 'gain' layer of C_{60} between the blend layer and the n-type ZnO nanoparticle layer. After deposition of the tetrapod layer the film was treated with benzenedithiol (BDT) vapor and the amine functionalization was chosen to promote surface interaction between the polymer and the tetrapods. Both of these features were designed to improve charge separation across the donor–acceptor interface. The gain in the C_{60} film was suggested to come from improved exciton dissociation efficiency and reduced recombination. The Pd anode was matched with a MoO_3 transport layer to give barrier-less hole extraction. For 80 : 20 tetrapod : PSBTBTNH$_2$ blends by weight, the optimum performance was [3.2%, 1.06 V, 8.3 mA cm^{-2}, 0.56].

Limitations in the V_{oc} achievable by depleted heterojunction cells were countered by Wang *et al.*[115] with a tandem PbS QD depleted heterojunction design. Two PbS cells with offset QD bandgaps (1 eV and 1.6 eV) were fabricated one on top of the other with a recombination layer sandwiched between them. The latter consisted of a MoO_3 hole extraction layer on top of the PbS (1.6 eV) QD film, followed by layers of ITO, AZO (aluminium doped zinc oxide) and then the TiO_2 layer of the top PbS (1 eV) QD half of the cell (Fig. 5). Electrons collected by the TiO_2 layer from the low bandgap PbS QDs could recombine with holes gathered from the MoO_3 film that had originated in the 1.6 eV PbS depletion region. With this stacked tandem arrangement the V_{oc} of the cells was the sum of the two constituent sub-structures and the overall performance was [4.21%, 1.06 V, 8.3 mA cm^{-2}, 0.48]. Again, MPA treatment of the PbS layers was carried out during device fabrication.

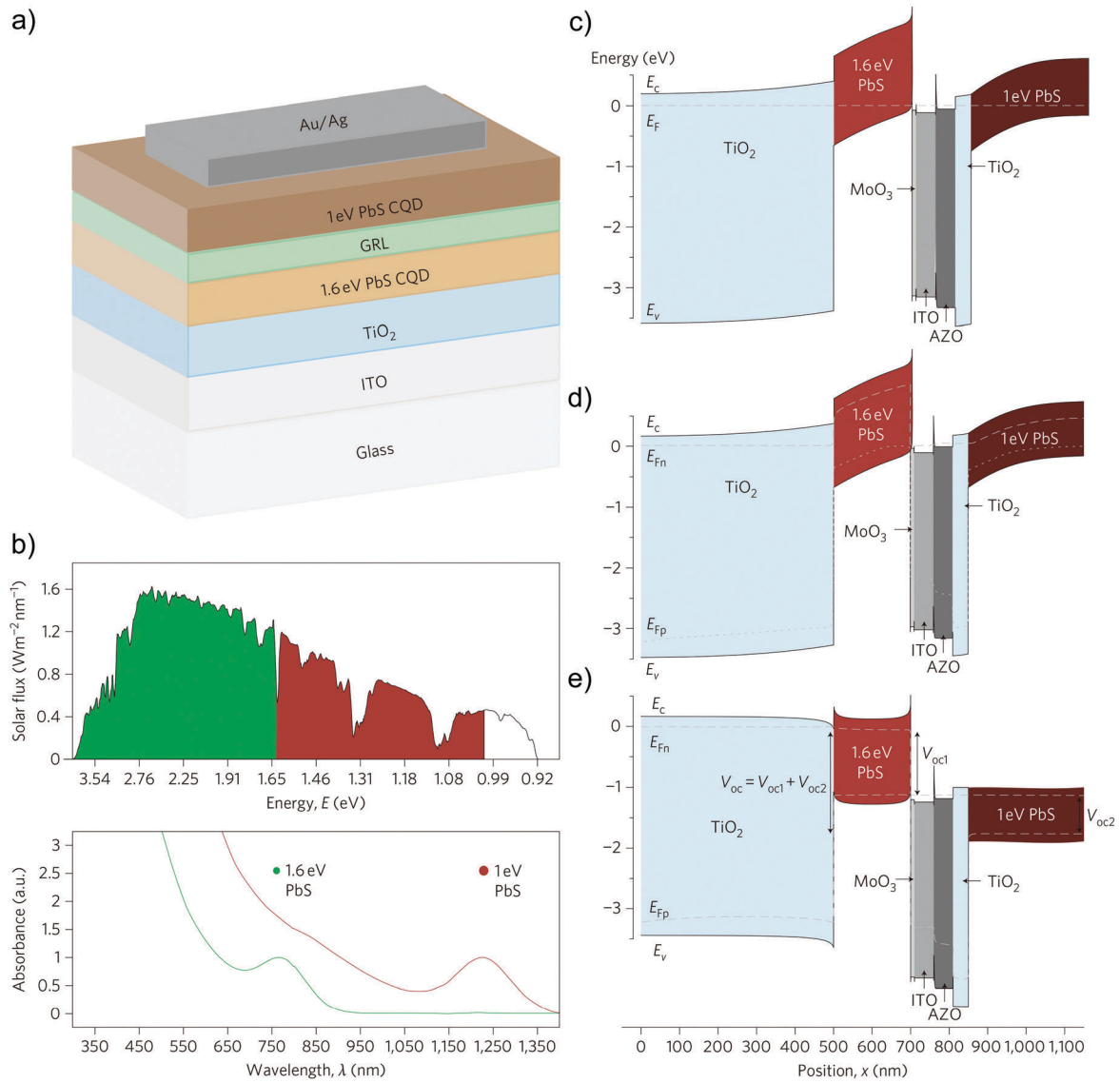

Fig. 5 PbS QD-based tandem solar cells: concept and realization. (a and b) Device architecture (a) and spectral utilization (b) for PbS QD tandem solar cells having quantum-confined bandgaps of 1.6 eV (green) and 1.0 eV (red). (c–e) Spatial band diagrams for PbS QD tandem cells at equilibrium (c) and under short-circuit (d) and open-circuit (e) conditions, where E_F is the Fermi energy (dashed-dotted line in c), E_{Fn} is the electron quasi-Fermi energy (dashed line in d and e), and E_{Fp} is the hole quasi-Fermi energy (dotted line in d and e). Reproduced with permission from ref. 115. Copyright 2011 Nature Publishing Group.

This journal is © The Royal Society of Chemistry 2017

McDaniel *et al.*[18] used nanorod CdSe/CdTe heterostructures to investigate improvements in absorption, charge separation and carrier transport that could be gained by using segmented and curved nanorods. For single component CdSe and CdTe nanorods, test devices gave V_{oc} values of 0.1 V and 0.4 V, whilst linear heterostructures and curved heterostructures performed better with values of 0.6 V and 0.5 V respectively. One of the issues facing such PV devices is the difficulty in ensuring that the CdTe/CdSe type II junction within the nanorod is ideally aligned relative to the adjacent charge collection and electrode structures to ensure good separation and migration of both charges along opposite directions down each rod segment (electrons along the CdSe and holes *via* the CdTe). Rods with the counter-alignment form electron traps at the CdSe/hole collector layer and hole traps at the CdTe/electron collection interface, drastically reducing performance. A further problem is the very thin absorber layer, limiting the total photocurrent. Linear heterojunction nanorods reached photocurrents of 0.161 mA cm^{-2} (FF 0.226) whereas curved heteronanorods generated photocurrents of 0.300 mA cm^{-2} (FF 0.173).

Several groups have considered the effect of the surface ligand groups normally used on the QD films on the V_{oc}. They make a contribution *via* their shift in the valence band offset and thereby also the conduction band offset of the QD layer relative to any n-type junction layer in a heterojunction device. Greaney *et al.*[116] compared the performance of CdSe QDs with the native ligands from the QD synthesis (a mixture of TOPO and oleic acid), and pyridine treated QDs (TOPO displaced) and *t*-butanethiol (TOPO and oleic acid displaced) in bulk heterostructure devices with P3HT as the electron donor. Here the ligand exchanges were made in solution prior to the device fabrication process. The highest V_{oc} and overall conversion efficiency were obtained with the thiol exchanged ligand [1.9%, 0.8 V, 5.62 mA cm^{-2}, 0.43], with poorer photocurrent in the pyridine case being attributed to a greater trap density in that instance.

Another manner in which ligands can be used to engineer improved performance in QD heterojunction cells was explored by Yaacobi-Gross *et al.*[117] in planar CdTe QD/CdSe QD layered structures. In simple test devices (no additional charge collection/blocking layers) a donor/acceptor junction was formed between a CdTe QD layer and a CdSe QD layer. The former were coated with MPA, and the latter were coated with a methylthiophenol (MTP) ligand. Both ligands were applied to the water and organic route QDs used *via* a sequence of solution based ligand exchange steps, prior to forming the device layers. Each QD layer was built up by a number of multiple spinning or dipping cycles interspersed with EDT or ethylenediamine (EDA) treatment and rinsing to consolidate each layer and cross-link to the following one. The use of mixed ligands (with each bearing different dipole moments) introduced a quantum confined Stark shift in the QDs in the junction region which was credited with an improvement in exciton dissociation and charge separation efficiency. In the simple devices used to compare performance, the best results were obtained with devices using EDA as the linker molecule in the upper, CdSe QD/MTP layer [0.25%, 0.81 V, 0.143 mA cm^{-2}, 0.21].

With the effective carrier collection lengths (the sum of the carrier diffusion length and the depletion region thickness) approaching 100–150 nm, Kramer *et al.*[118] investigated the use of regular arrays of TiO_2 nanopillars as the n-type material in conjunction with p-type PbS QDs. Such arrays can be patterned with spacings between adjacent pillars set at twice the collection length maximizing the surrounding volume of PbS from which photogenerated carriers can be collected in a bulk heterojunction cell. 320 nm high nanopillar substrates were filled with PbS QDs spin coated from solution in several passes and treated with MPA between each layer. The filled layer was over-coated with MoO_3 and a combined Ag/Au electrode to complete the test cells. This optimized collection geometry gave improved performance on photocurrent, conversion efficiency and V_{oc} compared with regular TiO_2 collector layers: PCE 5.6% (3.8%), V_{oc} 0.57 V (0.52 V), J_{sc} 19 mA cm^{-2} (16.1 mA cm^{-2}) – regular substrates' values in parentheses.

Further attention to the maximization of the performance of the depletion region in so-called quantum depleted heterojunction cells was given by Liu *et al.*[119] in their work on devices where both the p- and n-type layers were formed from PbS QD films. Doping in the former was augmented by additional silver doping of the QDs and was necessary in order to extend the depletion region into the far more lightly doped n-type PbS layer formed by halide treatment of the QDs (with tetrabutylammonium iodide). Ag doping was performed by introducing AgCl during the organic solvent hot injection synthesis. The depletion and generation regions then spanned both sides of the QD junction. The use of an improved n-type AZO layer (also functioning as a hole blocking layer) combined with this QD engineering to push performance up to [6.1%, 0.52 V, 23.3 mA cm^{-2}, 0.5], driven largely by the improved photocurrent.

Willis *et al.*[120] have demonstrated the transition in the junction mechanism from excitonic mode where carriers generated only within the diffusion length on the absorber side of the junction survive long enough to avoid recombination and be separated and collected, to depletion mode where the built-in field of the p–n junction can extend the volume over which carriers are gathered and assist collection. They formed a junction between PbS QDs and ZnO where the latter was intrinsic, lacking a carrier surplus. Under these circumstances a small depletion zone existed only in the ZnO layer close to the junction, so the test cells functioned as an excitonic donor–acceptor junction. However, exposure to UV light under oxygen free conditions caused absorbed gas species within the ZnO layer to desorb, freeing previously trapped electrons to become mobile carriers once more. This photodoping mechanism increases the electron doping density rendering the ZnO n-type and allows the depletion zone to shift into the PbS region at sufficiently high electron densities. The junction then becomes a p–n type depletion mode device in the same manner that purposefully doped ZnO junctions are designed.

PCE values were increased to 8.5% when Maraghechi *et al.*[121] improved the width of the depletion region in PbS QD/TiO_2 junction devices by increasing the doping density in the p-type semiconductor. This was achieved by using a thin TiO_2 layer

but changing the FTO substrate on which it was deposited to a shallow work function (with respect to that of the TiO_2) FTO version. This arrangement, termed a donor-supply electrode, allowed electrons to be injected into the TiO_2 layer from the FTO *via* a charge transfer doping mechanism, boosting the doping density and further increasing the depletion length to around 260 nm. This benefited both the short circuit current density and the fill factor to give a performance of [8.5%, 0.62 V, 22.7 mA cm^{-2}, 0.61]. The improvements were essentially derived from optimization of the device geometry and carrier collection efficiency, the PbS QD synthesis having settled already to a standard recipe: PbS QDs with an optimal size and bandgap were synthesized by hot organic solvent methods, and after layer by layer spin coating during device fabrication were treated with MPA solution.

The Sargent group has started to investigate the robustness of their photovoltaic cell fabrication process to being adapted to potential large scale manufacturing methods. Kramer *et al.*[122] described a spray coating method for coating curved or flexible substrates that is transferrable to roll to roll manufacture of large area photovoltaic films. Spray coated PbS QDs (which had previously been treated with $CdCl_2$ to halide coat the QDs) were deposited on a curved ITO/PET film-based structure and they maintained very reasonable test device performance figures [7.2%, 0.59 V, 22.9 mA cm^{-2}, 0.54]. Very recently, a new ligand exchange method based on the combination of lead halide (PbX_2) and ammonium acetate (AA) was introduced by the same group to improve the passivation and carrier transport of QDs, which gave rise to a closely packed PbX_3/AA-exchanged PbS film and an enhanced device performance with PCE up to 11.28%.[4] Furthermore, the unencapsulated devices retained around 90% of their initial PCE after 1000 h of storage in air.

Other groups continued to investigate alternatives to PbS QDs for heterojunction devices. Using aqueous QD chemistry, Chen *et al.*[123] formed bulk heterojunction devices *in situ* by using spin coated films of CdTe QDs with mercaptoethylamine ligands. To form a donor–acceptor bulk heterojunction the surface of the QDs was converted to CdS, *i.e.* forming CdTe/CdS core/shell nanocrystals by heat treatment at 300 °C in a glove box typically for 2 min. However, the CdS coverage was suggested to be incomplete thus allowing escape and transport of the photogenerated holes formed within the CdTe cores. Although generation, separation, transport and extraction were all claimed to be highly efficient, the performance figures were relatively modest at [3.98%, 0.5 V, 14.81 mA cm^{-2}, 0.538].

The limitations of the QD depleted heterojunction device structure continue to be challenged. The standard transparent n-type oxide/p-type QD/metal cell construction suffers from the problem that some of the PbS QD layer lies in close proximity to the reflective metallic hole collecting electrode and will be inefficiently excited near the node of the optical electromagnetic field. This limits how the absorption of the PbS layer can be used efficiently whilst minimizing the transport distance through inefficiently used material. This led Kim *et al.*[124] to investigate an inverted structure where a hole collecting PEDOT:PSS p-type layer was first deposited on the FTO before adding the PbS QD layer. The n-type oxide was ZnO furnished by the decomposition of volatile diethyl zinc in air which could then be annealed at only 110 °C. This was subsequently coated with an Al electrode and the completed devices gave test results of [4.21%, 0.58 V, 12.9 mA cm^{-2}, 0.55] for 160 nm thick PbS QD layers.

The benefit of halide treatment of PbS QDs would appear to be one of the QD material chemistry factors (aside from the optimization of other more physical device design parameters) that is supporting better than 8% PCE performance and improved device stability. The latter is often not given so much attention in earlier work, but as PCE values start to move towards the 10% plus level it is becoming more important to address such practicalities. Wang *et al.*[125] treated PbS QDs with cetyltrimethylammonium bromide (CTAB) solution, and saw a drop to only 90% of initial PCE values over 3000 hours of light soaking under AM 1.5G illumination in an ambient atmosphere (initial performance [5.75%, 0.394 V, 29.3 mA cm^{-2}, 0.50]).

Halide treatment was also used in conjunction with the addition of a CdS shell to PbS QDs by Neo *et al.* in planar depleted heterojunction solar cells.[126] Comparing test devices containing PbS and PbS/CdS QDs with just EDT ligand exchange, and the latter with Cl and Br treatments alone and also together with EDT, they found the combination of the CdS shell with both Br and EDT treatment to yield the highest performance of [5.61%, 0.63 V, 21.9 mA cm^{-2}, 0.38]. The use of EDT is credited with maintaining good charge transport (closer interdot spacing), and Br with improving carrier mobilities relative to Cl treated QDs. The halide atoms were believed to bind at exposed Pb sites, exposed after incomplete coverage by the thin CdS shell layer. However, the latter is still largely effective in reducing PbS QD surface traps and decoupling the carriers from surface trap states, but with the penalty of an increased barrier to charge extraction/transport. The three treatments together, CdS shell, EDT and Br treatment, could however be combined with the latter two offsetting some of the negative aspects of the former.

The extension of the bulk p–n heterostructure to nanoscale blends was investigated by Rath *et al.*,[127] who combined nanocrystalline n-type ZnO particles with p-type PbS QDs in a single film, rather than forming a planar bilayer junction between the two materials. Comparison of the V_{oc} and J_{sc}, and dark current density for both bilayer and blended film devices allowed an ideality factor to be calculated which for the latter cells was close to unity. This indicated that such devices were less prone to Fermi level pinning due to trap recombination and therefore could establish depletion more effectively. Comparative performance tests showed that the nanoscale heterojunction devices had better low light PCEs and under AM 1.5G achieved [5.2%, 0.64 V, 16.3 mA cm^{-2}, 0.5].

The mechanisms by which electron trapping can affect electron transfer in QD films treated with bifunctional ligands, including the case where type II QD combinations such as mixed CdTe and CdSe QDs are present, were studied by Boehme *et al.*[128] They combined the transient absorption measurement

 This journal is © The Royal Society of Chemistry 2017

technique with electrochemical gating, for both solutions and QD films (Fig. 6). In this manner, the Fermi level in a solution of QDs could be swept through the range of potentials where electron traps were located in the gaps of the QDs and traps progressively filled from the valence band upwards. As the traps were filled the band edge bleach became progressively deeper and recovered more slowly after the pump pulse as fewer photogenerated electrons were trapped after excitation. In films consisting of alternating layers of CdTe and CdSe QDs (crosslinked with EDT), without any electrochemical gating CdTe surface trapping dominated the fate of electrons generated in the latter. Raising the Fermi level however allowed the transfer of electrons from CdTe to CdSe and the simultaneous decay of the CdTe bleach whilst the CdSe bleach grew in magnitude. At high enough potentials the electron transfer rate could be raised to almost 100% between the two QDs.

An alternative approach to the maximization of the depletion length in QD heterojunction devices has been taken by Ko *et al.*[129] borrowing the p–i–n structure used in amorphous silicon photovoltaics. In their PbSe QD devices the QDs are no longer the p-type layer but are intrinsic (i) and sandwiched between p-type CuI and n-type ZnO films. The doping in these films is then controlled independently of any processing on the QDs to manipulate carrier densities. The PbSe QDs were deposited by spin coating combined with BDT treatments. The much thicker QD absorber layers that this approach permits due to the higher built-in fields that can be obtained by highly doping the CuI and ZnO should lead to higher V_{oc} and the wider depletion region this can support should increase the photocurrent. In practice these devices yielded a performance of [3.58%, 0.49 V, 21.6 mA cm^{-2}, 0.34].

A potential improvement to the band structure within the QD absorber layers in heterojunction (and other types of) solar cells that derives from the QD surface chemistry has been demonstrated by Santra *et al.*[130] Using multilayer PbS QDs as their absorbers in depleted heterojunction cells, they used materials with different thiol ligands in each half of the PbS stack. Three thiophenol ligand derivatives were studied: methyl, fluoro and nitro, having dipole moments −1.82, 0.04 and 4.4 Debye towards the phenol group respectively (see Fig. 7). The dipole moments shift the PbS energy levels to differing degrees, allowing a type II structure to be formed (for two layers with different ligands) or even a graded structure with a greater number of appropriately offset ligand types. This allows more effective carrier separation and directional transfer towards the correct electrode and consequently less recombination within the QD layer, with a 23% improvement over structures without graded ligand dipole moments in terms of power conversion efficiency observed in simple test devices.

An all QD p–n type quantum heterojunction device with Cd_3P_2 QDs as the n-layer and p-type PbS QDs has recently been studied by Hefeng *et al.*[131] Again a driver for this work is to combine the benefits of type II carrier separation at the interface, with the creation of a depletion zone in both QD layers to further improve carrier collection and the thickness of

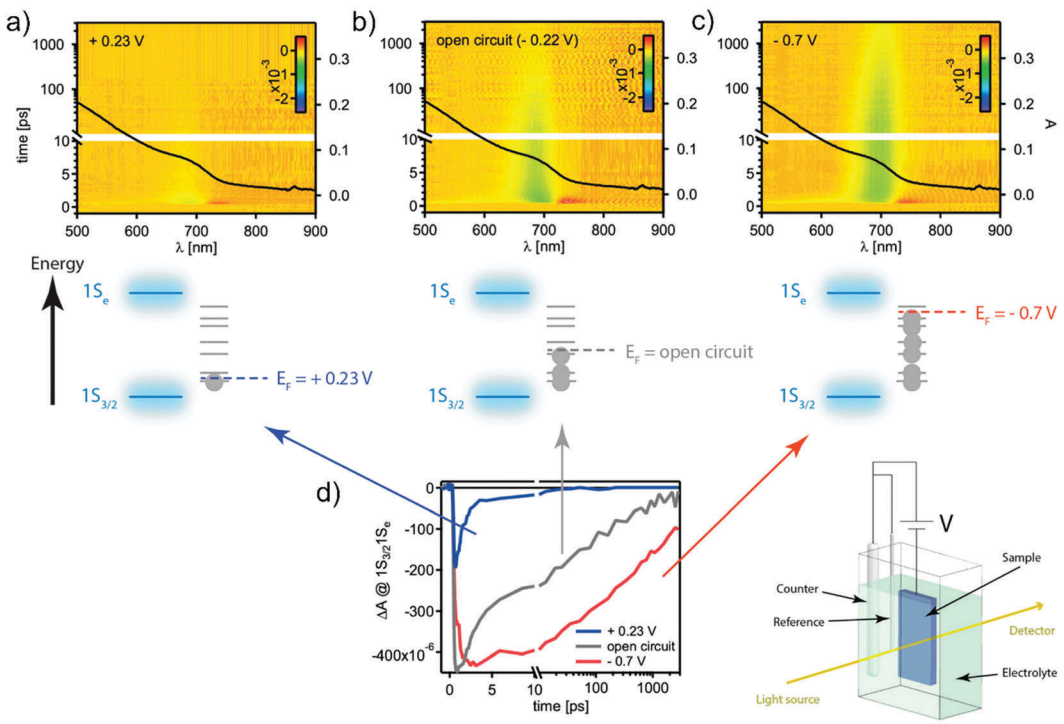

Fig. 6 Switching off electron trapping. 2D TA image of a film of 6.3 nm CdTe QDs with 8DA ligands on an ITO substrate after 460 nm excitation (a) at +0.23 V *versus* Ag pseudoreference electrode, (b) at open circuit, corresponding to −0.22 V, and (c) at −0.7 V, respectively. (d) Kinetics of the $1S_{3/2}1S_e$ transition at 700 nm for all applied potentials. The schematic diagram in the second row sketches the filling of trap states going from (a) to (c), using an electrochemical cell (lower right) to control the Fermi level. Reproduced with permission from ref. 128. Copyright 2014 American Chemical Society.

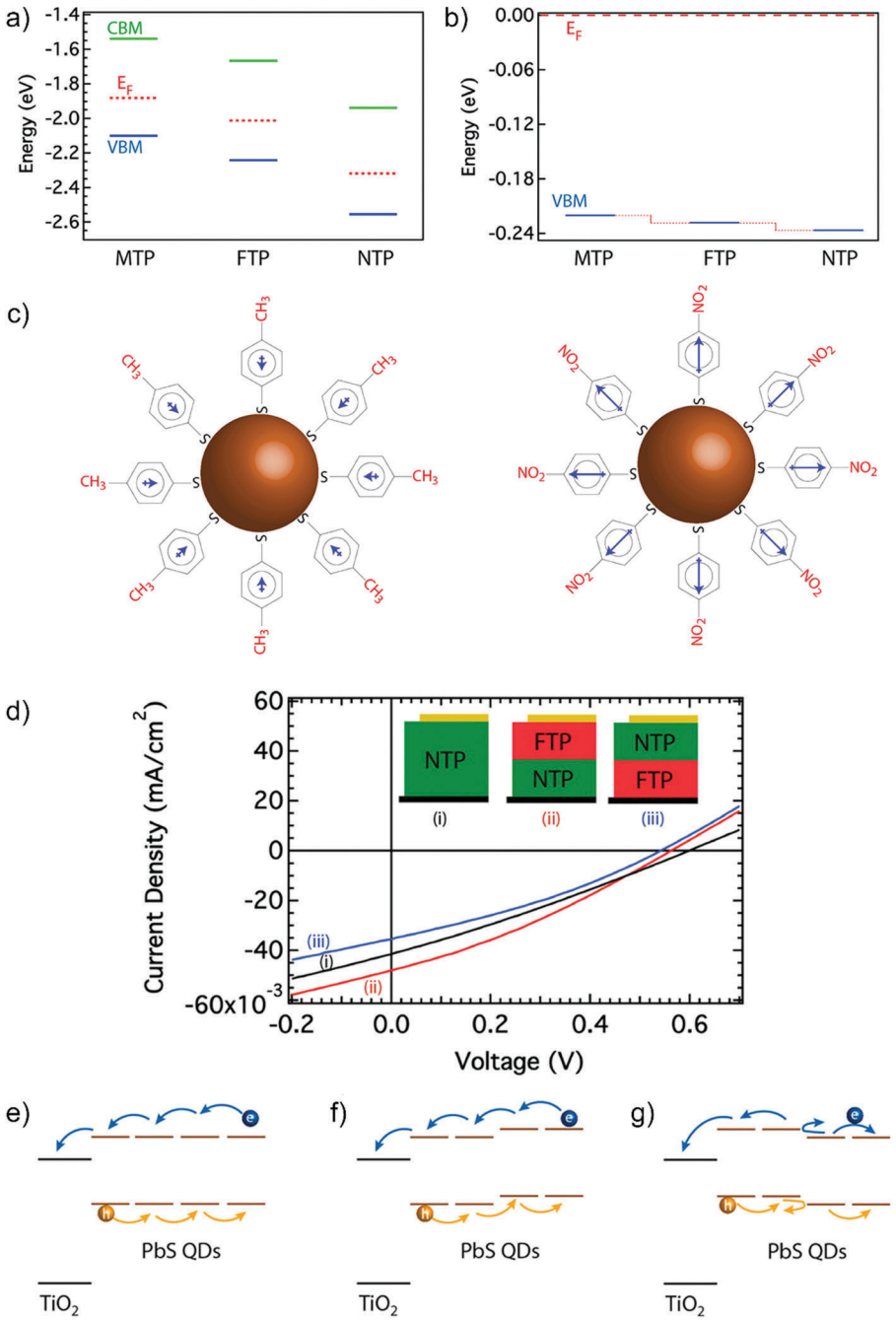

Fig. 7 (a) VBM, CBM, and E_F positions of PbS QDs passivated with different thiophenol ligand molecules as calculated on the $Pb_{80}S_{68}$ cluster passivated with 16 ligands. (b) Variation in VBM positions with respect to E_F of the QDs passivated with different thiophenols shows the change in doping density with the dipole moment of the ligand. (c) Schematic diagram showing the dipole moment of the ligand on PbS QDs passivated with methylthiophenol (MTP) and nitrothiophenol (NTP). (d) *J*–*V* characteristics of solar cells having three different configurations: (i) control, (ii) unidirectional, and (iii) bidirectional. The configurations are shown in the inset. Schematic energy diagram of (e) control, (f) unidirectional, and (g) bidirectional configurations. Reproduced with permission from ref. 130. Copyright 2015 American Chemical Society.

the effective QD layer(s). To improve the depletion, the PbS QDs were also Ag doped during synthesis to increase the hole density. The Cd_2P_3 QDs were treated with tetrabutylaminoiodide after deposition by spin coating to ensure and increase the n-type doping in that layer. Optimum performance from this study was obtained with 1.27 eV bandgap PbS QDs with Ag doping as the p-layer [1.2%, 0.38 V, 7.6 mA cm^{-2}, 0.41].

A problem often encountered when QD and QD/polymer blend films are treated to bring about ligand exchange with EDT in solution is the resultant nanoscale cracking when the film shrinks upon removing the prior longer chain ligands. Where multilayers of QDs are deposited this is often countered by EDT treatment after each spin cycle so that cracks from the previous round may backfill and any cracks from the

 This journal is © The Royal Society of Chemistry 2017

subsequent EDT treatment may occur in different locations so avoiding deep fissures extending through the whole stack. Single layer QD polymer blends may however be more prone to this cracking problem. Nam *et al.*[132] used an additional spin coating stage to deposit a layer of PCBM over treated QD/polymer blend bulk heterostructure films which penetrated the cracks as well as forming a surface layer across the whole device. This material functions as an n-type layer and acts as a hole blocking layer and electron collector and significantly improved the test cell performance to [4.53%, 0.56 V, 14.04 mA cm^{-2}, 0.58].

2.4. QD Schottky devices

Whereas depleted heterojunction devices form the carrier depletion region by bringing a p-type and n-type layer into contact, Schottky devices differ in that a metal/p-type junction is formed, causing depletion in the p-type QD layer.[1,133] In the QD PV field this type of device initially made a great improvement in performance and allowed dry solar cells to be fabricated. However, the even greater design flexibility and better performance from depleted heterojunctions more recently seems to have eclipsed Schottky cells. The latter suffer from a fundamental limit as far as the V_{oc} is concerned in that this is limited to $< E_g/2q$ (where q is the electron charge) and in fact Fermi level pinning at the metal/QD interface may lead to lower values still. Schottky cells are still often used as comparative test devices and for fundamental studies,[134] being relatively simple to fabricate alongside heterojunction cells for comparison, and with similar processing for some of the device layers.

Early examples of Schottky cells used either PbS[135] or PbSe[136] as the p-type QD layer and Al or Ca/Al back electrodes with ITO as the transparent counter electrode. Again, ligand exchange on QDs grown using oleate ligand stabilization during synthesis was used to both improve conductivity and cross link the QD films during multiple dip coating deposition stages. The performance of these early devices was rather modest, representative values being around [1%, 0.17 V, 20 mA cm^{-2}, 0.32], and to some extent the studies were focused upon confirming the Schottky operating mode as much as optimization. However further improvements were rapidly obtained; Luther *et al.*[133] increased the conversion efficiency to over 2% and surveyed the influence of the QD size (bandgap) and choice of back contact metal (Ca, Mg, Ag, Al, Au) on the V_{oc} values. Evidence for Fermi level pinning was seen for metals such as Ca, which did not raise the V_{oc} as far as its work function might have suggested.

Koleilat *et al.*[137] improved the PCE value to 3.6% under IR illumination with PbSe QDs treated with BDT as the cross-linker suggesting that the alternative butyl diamines and butyl dithiols that were often used in both Schottky and other QD solar cells at the time were perhaps too volatile and therefore did not yield stable device performance. They reported device stability of several weeks with the lower vapour pressure aryl cross linker. The higher device efficiencies were found to correlate with relatively long diffusion paths (220 nm and 285 nm for electrons and holes respectively) in their PbSe QD films.

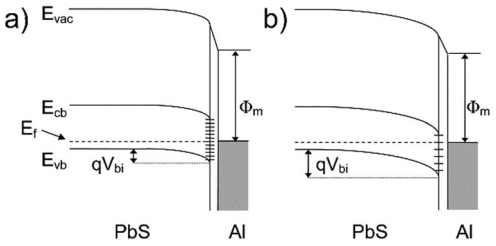

Fig. 8 Schematic diagram showing the reduced band bending in a device with many interfacial traps (a) relative to one with fewer traps (b). Symbols denote the vacuum level (E_{vac}), conduction band (E_{cb}), Fermi level (E_f), valence band (E_{vb}), metal work function (Φ_m), and total band bending (qV_{bi}). Reproduced with permission from ref. 138. Copyright 2008 American Chemical Society.

Barkhouse *et al.*[138] examined the mechanism of the enhancement of performance on treatment with short dithiols (EDT, *etc.*) relative to lesser improvement by diamines, *etc.* In PbS QD/Al based Schottky devices the 10-fold improvement in PCE was found to be partly attributed to a 1.4× factor arising from improved carrier mobility, but a ×4 fold factor of the improvement was derived from the increase in the device V_{oc} (from 0.28 to 0.43) which was symptomatic of the removal of deep mid-gap trap states *via* a passivating effect in the presence of the thiols. Reducing the density of trap states also lessened the impact of Fermi level pinning and allowed increased band bending and improved (deepened) the depletion region (raising the width from 140 nm to 200 nm) (see Fig. 8). Choi *et al.*[139] also addressed the same trap driven Fermi level pinning limitation in the band bending and consequent low V_{oc} in a different manner by purposefully oxidizing the surface of the PbS QDs used in their devices. This approach was also mentioned earlier in connection with depleted heterojunction cells. By reducing the density (and depth) of interface states at the metal/QD junction the stability was improved to only 45% reduction of the initial PCE after 500 h operation under an ambient atmosphere.

Solar PCEs at this early stage were typically as high as 1.8% for PbS QD Schottky cells, with many groups focusing on improving or extending the response in the IR region of the solar spectrum. With a simple Al/PbS QD/ITO device construction, Johnston *et al.*[140] also investigated improvements in performance due to exchange of the oleate synthesis ligand for butylamine in solution (by repeated precipitation and redissolution cycles to displace the oleate in favour of the latter) prior to deposition. This also improved device quality *via* better film homogeneity and reduced cracking. AM 1.5G solar illumination gave performance figures of [1.8%, 0.33 V, 12.3 mA cm^{-2}, FF not specified], with IR PCEs of 4.2% at 975 nm and 2.1% at 1550 nm.

Debnath *et al.*[141] also examined a method to improve device stability, taking the view that perhaps relatively weak diamine or dithiol binding at the QD surface was allowing air and moisture to facilitate surface oxidation and produce potential trap and recombination sites. They used an alternative bidentate conjugated ligand, *N*-2,4,6-trimethylphenyl-*N*-methyldithiocarbamate, carrying out the ligand exchange (with the oleic acid synthesis ligand) in solution prior to QD deposition, refluxing with the

replacement ligand for 4 h. After substituting this ligand, devices could be processed under an ambient atmosphere (rather than under glove box conditions) yet still give good performance figures [3.6%, 0.51 V, 14 mA cm^{-2}, 0.51]. Further attention to the ligand type and density at the QD surface by careful monitoring before and during device fabrication has led to improvements in PbS based Schottky cell performance reaching PCE values of 5.2%.[142]

2.5. QD luminescent converters

One of the major barriers to the adoption of photovoltaic solar energy generation is the reduction of the cost per watt of electricity generated. Most of the cost is embedded in the initial PV manufacturing cost and the whole of the front-loaded expenditure is recouped during the early part of the 25–30 years operating lifetime for mainstream generating applications. Increasing the PV's PCE (without making the manufacture proportionately more expensive) is one way to improve the commercial attractiveness, but another is simply to drive down the PV cost more rapidly than the current operating efficiency. This means that the areal efficiency may drop but the cost per watt may improve, the overall economic margin being dictated by factors such as the site land cost, *etc.*

The fluorescence rather than photovoltaic properties of QDs may be used in either strategy – efficiency improvement or cost reduction – to improve the cost effectiveness of regular bulk semiconductor solar cells. In down converters, a QD containing film is applied to the front surface of photovoltaics having the most useful effect when converting short wavelength solar radiation to emission wavelengths just above the bulk PV's bandgap. Some bulk PVs such as CdTe thin film solar cells have protective window materials such as CdS layers which block and discard shorter wavelengths whereas a preceding QD layer can shift some of the energy in this range into the transmission range of the window layer before the light then passes through the latter.

QD-based luminescent solar concentrators (LSCs) also downshift the solar spectrum by absorption and re-emission. In such devices a slab of optical material such as a transparent polymer doped with QDs absorbs much of the solar spectrum and a proportion of the emission is trapped within the slab and guided to the edges. Along the edges there are strips of conventional bulk PV cells mounted to capture the escaping emission. The area of PV cells used in this configuration must be lower than the area of the slab, and the emitted light concentrated to a higher intensity to a sufficient degree in order to improve the cost effectiveness.

In both cases, apart from optimizing the PL emission to improve the operating margin, a major challenge is to produce QDs that will maintain their PL QY for many years under full sun conditions and with exposure to a range of site weather conditions, but for now the main focus for most groups is upon optimization at the bench.

The QD LSC concept (Fig. 9) is borrowed from earlier dye based-LSCs[143–147] which were limited by the available photostable dye absorption and emission spectra. The extension

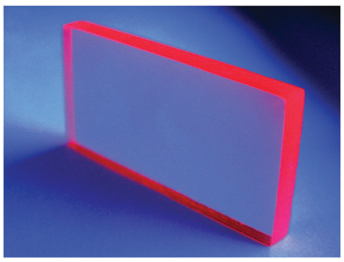

Fig. 9 An LSC design of P(LMA-*co*-EGDM) doped with CdSe/CdS/$Cd_{0.5}Zn_{0.5}S$/ZnS QDs, showing clear red emission of slab-guided fluorescence. Reproduced with permission from ref. 147. Copyright 2011 Elsevier.

using QDs was first investigated by Barnham's group,[148–150] and later by many others,[151–154] who recognized that QDs with broad solar emission that could also extend into the near IR may be very attractive for efficient LSC operation, whilst also bringing the benefit that concentrated near band edge illumination of the edge mounted solar cells could be obtained without much thermal dissipation in the PV itself, allowing it to maintain efficient operation whilst the energy converted to heat during down conversion in the LSC panel was lost to the surroundings more effectively.

The main parameters of interest in LSCs are the geometrical factor, $G = A_{slab}/A_{edge}$, the optical power conversion efficiency $\eta_{opt} = P_{out}/P_{in}$ and the effective concentration factor ECF = $G \times \eta_{opt}$, where A_{slab} and A_{edge} are the area of the top surface of the slab and the edge surface area; and P_{in} and P_{out} are the power measured in through the top surface and out through the edges respectively. Sahin *et al.*[155] modelled the hypothetical performance of QDs with a PL QY of 95% dispersed in a high refractive index (n = 1.7) polymer slab and for a geometrical factor G = 26 predicted a conversion efficiency η_{opt} = 23.7% and a concentration factor ECF = 4 for a particular QD loading. However, better performance could in principle be obtained if aligned nanorods (long axes parallel to slab normal) could be used such that more of the emission would fall within the range of trajectories that would be confined within the LSC by internal reflection. Under those conditions it was predicted that the ECF could rise to 7.6 with a G = 25 slab, and η_{opt} could be improved to 27.9%.

In practice the main material challenges are maintaining the high PL QY of the QDs after embedding them in an optical matrix and ensuring even dispersion without the significant formation of aggregates that scatter light out of the slab guide, and reducing absorption and emission spectral overlap. In the former case, an approach often used to produce low cost LSC panels involves dispersion of the QDs (or nanorods) in a monomer or partly polymerized 'pre-polymer' followed by further free-radical/thermally driven polymerization to a solid high molecular weight sheet. The QD surface must be able to withstand the chemical reactions in the material surrounding it without the formation of additional surface traps, or a core/shell structure that keeps the carrier wavefunctions well shielded from the surface should be used. Sholin *et al.*[156] factored out this problem in their study of the spectral overlap problem by

 This journal is © The Royal Society of Chemistry 2017

using a test slab consisting of fluorophore solutions sandwiched between two glass sheets rather than solid composite slabs. Here the purpose was not to produce a solid practical LSC sheet, but to compare the performance of laser dyes, semiconducting polymers and QDs in relation to the overlap problem. Interestingly they concluded that semiconducting polymers (in solution) outperformed both commercially available QDs and small molecule laser dyes, with QDs having relatively low PL QY and overlap at that time. The optical efficiencies for CdSe/ZnS core/shell QDs were just 10% of those obtained for the best polymer material, Red F.

This poor practical performance was later addressed by Meinardi *et al.*[157] using more elaborate QD heterostructures. Large Stokes shifts could be obtained using giant shell quasi type II CdSe/CdS core/shell QDs, and the thicker shells also better screened the carriers, mostly the holes from any undesirable trap site created during the QD/polymer slab formation. Quasi type II confinement is an important feature since it means that the absorption is mainly governed by the thick CdS shell which appears almost bulk-like, whilst emission takes place mainly in the much smaller CdSe core with a large Stokes shift. For thicker shells this shift could exceed 150 nm even in the visible spectral range. The giant core/shell materials gave much better performance figures: under AM 1.5G illumination, a $G = 43$ slab, showed $\eta_{opt} = 10.2\%$ efficiency and an ECF of 4.4 with a silicon photocell as the PV. The absorption spectrum of the CdS was far from optimal, with the band edge still below 500 nm, and the PL emission peak at around 640 nm, far from realizing full spectral absorption or the full spectral range of the PV (Fig. 10).

The use of QD down-shifting films on crystalline silicon (c-Si) and thin film CdTe with CdS window PV plates has been addressed by Kalytchuck *et al.*[158] Several QD and laser dye fluorophores were compared for each type of solar cell. For CdTe/CdS PVs, aqueously grown CdTe QDs encapsulated in water based polyvinyl alcohol (PVA) polymer films; organically grown CdSe/CdS core/shell QDs and CdSe/CdS tetrapods in poly(methyl methacrylate) (PMMA) polymer films; rhodamine 6G dye in PMMA films were used. For the longer wavelength range c-Si PVs, organically grown PbS QDs in PMMA were compared with PMMA film doped with a range of IR laser dyes (Q-switch 5, IR-26 and rhodamine 800). Figures of merit (PL QYs, absorption–emission spectral overlap, spectral matching of the downshifting layer and the PV absorption spectrum, *etc.*) were calculated in each case for optimum fluorophore loadings (Table 1). In the best cases, the QD downshifting films could increase the CdTe/CdS PV J_{sc} by 16% and the c-Si cell's J_{sc} by 50%.

Recently, large-area LSCs were demonstrated in both experimental and theoretical aspects by employing ternary I–III–VI_2

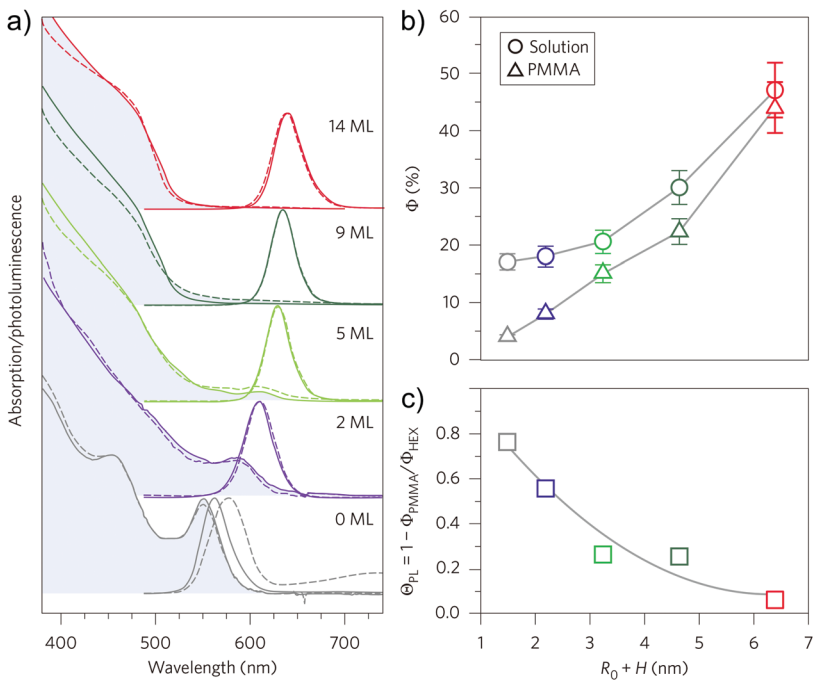

Fig. 10 (a) Absorption (grey shading) and PL spectra (no shading) of hexane solutions (solid lines) and PMMA composites (dashed lines) of CdSe/CdS QDs with increasing H (0, 0.6, 1.5, 2.7 and 4.2 nm from bottom to top). Corresponding shell thicknesses in terms of the number of CdS monolayers (MLs) are reported next to each curve. (b) PL QYs of QD hexane solutions (Φ_{SOL}, circles) and PMMA nanocomposites (Φ_{PMMA}, triangles) measured under weak steady-state excitation at 473 nm. Error bars are standard deviations from the set of five measurements. (c) PL quenching factor, $\Theta_{PL} = 1 - \Phi_{PMMA}/\Phi_{HEX}$, plotted as a function of ($R_0 + H$), showing that for the thickest-shell QDs ($H = 4.2$ nm) the reduction in PL efficiency following QD incorporation into PMMA is negligibly small, but reaches 80% for core-only CdSe QDs. A further increase in shell thickness typically results in a deterioration of the PL efficiency, which can probably be attributed to the formation of interfacial defects. Reproduced with permission from ref. 157. Copyright 2014 Nature Publishing Group.

Table 1 Figure-of-merit values for several combinations of QD based luminescent down-shifting layers (LDSLs) with CdTe/CdS and c-Si solar cells.[a] Reproduced with permission from ref. 158. Copyright 2014 American Chemical Society

Solar cell	LDSL[b]	PL QY[c] (%)	EO[d] (%)	ESM[e] (%)	ASM[f] (%)	PA[g] (%)
CdTe/CdS	CdTe QDs	40–80	25.1	95.1	62.4	15.5
	CdSe/CdS QDs	<98	8.6	99.0	70.0	11.1
	CdSe/CdS tetrapods	35–60	1.4	99.8	50.6	4.6
	Rhodamine 6G	95	30.9	89.6	24.5	13.4
c-Si	PbS QDs	20–90	9.9	79.7	49.7	26.3
	Rhodamine 800	25	16.9	55.9	23.5	14.5
	IR-26	0.05	58.9	31.9	8.5	38.1
	Q switch 5	0.05	21.5	19.0	7.0	44.2

[a] Orange boxes indicate critical areas of poor performance, and green boxes indicate near ideal performance. Solution phase absorption and emission spectra were used in these calculations. [b] Luminescent down-shifting layer. [c] PL quantum yield. [d] Emission overlap. [e] Emission spectral matching. [f] Absorption spectral matching. [g] Parasitic absorption.

based QDs such as $CuInS_2$, $CuInSe_2$, and alloyed $CuInSe_xS_{2-x}$.[159,160] These heavy-metal-free copper-based QDs integrate the merits of broad absorption, large Stokes shifts, size/composition-dependent PL tunability covering the visible to the NIR window, and low toxicity, which render them appealing for LSC applications.

2.6. QD energy transfer based solar cells

In donor–acceptor heterojunction QD devices, only QDs adjacent to the junction are efficiently dissociated and make the major contribution to the photocurrent. Photons absorbed in QDs further away from the heterojunction may create carriers that recombine radiatively or non-radiatively before they can be separated and extracted. The need to extract charges, without the benefit of a depletion region and a built-in field to drive the charge extraction, also leads to the absorbing layer thickness needing to be limited. One method to increase the layer thickness and still efficiently move excitons to the heterojunction is the Förster Resonant Energy Transfer (FRET) funnel approach as introduced by Feldmann and co-authors.[65,161] Here QDs are deposited in a layer by layer fashion with each sequential layer being graded in size, with the lowest bandgap layer closest to the heterojunction. The layer by layer dipping technique is very suitable for water based QDs such as CdTe (with negatively charged TGA ligands), alternating with thin positively charged layers of water soluble PDDA. With adjacent QD layers in close proximity, FRET transfers the higher energy excitation of the topmost layer efficiently to the next lower bandgap layer and so forth in a cascade towards the heterojunction, effectively improving the thickness of the absorbing layer that contributes to the photocurrent at the junction. FRET transfer times are of the order of 250 ps for such materials. This so called FRET funnel principle was employed by Ruland *et al.*[162] in a photoelectrochemical cell rather than a planar heterojunction PV cell, but the photocurrent enhancement relative to a cell with a non-graded CdTe QD reference film was seen to be 180%, with the PCE improving by 155%.

A method using QD films to enhance conventional PV photovoltaics that has elements of down-conversion and FRET based transfer has been investigated by several groups. QDs are deposited as thin layers either on the surface or as in the case of Chanyawadee *et al.*[163] within grooves etched into the surface layers of conventional photovoltaic cells. In the latter case, aqueously synthesized CdTe QDs were deposited into patterned GaAs p–i–n photodiodes. Enhancements in monochromatic (570 nm) photocurrent and power conversion efficiency were observed, the former increasing by 244% and the latter by 433% at room temperature. However, the etching of grooves into these structures drastically reduced the underlying bare photodiode performance, whilst broader spectral measurements would undoubtedly show a net reduction if the QD short wavelength absorption were factored in also. However, the monochromatic measurements demonstrated that non-radiative (QD dipole to GaAs dipole) coupling where the excitonic excitation in the QDs drives the production of an electron–hole pair in the nearby semiconductor surface region occurs in the mid-visible spectral range. Radiative energy transfer (absorption of the QD emission by the bulk semiconductor) also occurs but with far lower efficiency in the visible range. The same two coupling modes have also been studied by Nimmo *et al.*[164] using CdSe/ZnS and also $CdSe_xTe_{1-x}$/ZnS core/shell QDs on Si surfaces. In their case the bulk semiconductor was a uniform planar substrate rather than a photovoltaic device and the energy transfer process was monitored using time resolved fluorescence to observe changes in the QD emission decay rate as the QD/substrate coupling distance was varied. Interposing a thin SiO_2 layer allowed the influence of radiative transfer to be separated from the combination of the radiative and nonradiative (NRET) transfer. Again, they concluded that non-radiative energy transfer with high efficiency (>75%) dominates in the mid-visible range (545 nm) but becomes comparable with radiative transfer in the near IR (800 nm) since lower bandgap QD emitters are larger and the imaginary part of the silicon permittivity decreases with increasing wavelength, both factors reducing the NRET rate.

2.7. QDs as precursors for bulk-like photovoltaic devices

The final contribution of QDs to the field of solar cells does not actually utilize the NCs as photovoltaic entities themselves but instead they are used as precursors for the formation of bulk polycrystalline thin films formed by sintering them. Olson *et al.*[165] formed p-type CdTe Schottky thin film junctions with Al electrodes using CdTe nanorod film precursors with the p-doping originating from the use of TOPO ligands. Under the sintering conditions (400 °C after exposure to $CdCl_2$) the TOPO decomposes leading to phosphorus doping of the sintered film. PCEs of over 5% were measured in the resulting devices.

This journal is © The Royal Society of Chemistry 2017

Jasieniak *et al.*[166] used CdTe QDs rather than nanorods, but avoided cracking problems due to stresses induced by the formation of large size grains that had previously limited the use of QD precursors. In their approach, although TOPO was used as a synthesis ligand, this was subsequently stripped and exchanged in solution for pyridine prior to the QD film deposition. Heterojunction devices (CdTe/ZnO) were fabricated with the CdTe layer deposited by spin casting and sintering in several cycles to build up the required film thickness. This also contributed to minimizing the oversize grain growth and suppressed cracking. PV device characterization gave performance as [6.9%, 0.59 V, 20.7 mA cm^{-2}, 0.56]. The same group extended this approach to fabricate vertically graded alloy compositions by depositing multiple layers of mixed dispersions of CdTe and CdSe QDs (Fig. 11).[167] Within each layer sintering formed alloys with compositions controlled by the ratio of the two components (with some loss of the more volatile Te during the process). Minimal interlayer indiffusion was observed. The benefit of this approach is that the absorption edge can be tuned to vary with depth, allowing lower layers to be better tuned to absorb the more deeply penetrating longer wavelength components of the solar spectrum without contributing too strongly to the absorption spectrum of the upper layers where the shorter wavelength light is effectively absorbed. This spatial bandgap engineering increased the performance with a slightly higher V_{oc} relative to the earlier pure CdTe sintered devices [7.1%, 0.61 V, 20.3 mA cm^{-2}, 0.57].

Several groups have used this so-called nanocrystal ink precursor route to sintered thin film PVs with the doped quaternary Cu_2ZnSnS_4 (CZTS) being a popular choice.[168–170] Kim *et al.*[171] have used this method to produce graded composition Ge doped CZTS films, the grading also contributing to better depletion and a slightly higher built-in field in their depleted heterojunction devices. The Sn/(Sn + Ge) ratio was varied to give a tuned bandgap through their device structures and this was achieved by introducing the Sn in the form of a molecular metal chalcogenide (MMC) ligand on CuZnGeS quaternary nanoparticle precursors. The latter were synthesized by hot injection using oleylamine as the ligand. This was subsequently removed by exchange and replaced with the MMC ligand, Sn_2S_6. During the nanoparticle film deposition mixtures of MMC and oleylamine stabilized CZGeS QDs were deposited in order to vary the Sn content in each layer in a graded manner. Sintering took place at 530 °C for 30 min under an Ar/H_2S atmosphere. The best device performance with this approach was [6.3%, 0.54 V, 23.36 mA cm^{-2}, 0.50].

A final outstanding example of sintered QD precursor thin films is the work of Panthani *et al.*[172] with CdTe QD starting materials. In addition to optimizing the CdTe thin film formation they also improved the ZnO n-type material, comparing the usual nanocrystalline ZnO precursor with In doped sol–gel derived ZnO films. The latter gave improved performance attributed to the smoother conformal interface with the CdTe layer. Improvements were also seen as a result of current (forward biasing) and light soaking of the devices prior to test. This was connected to the presence and location of Cu impurities, suspected to be included with the CdO precursor used in the CdTe synthesis. During fabrication Cu concentration was found to be higher at the CdTe/ZnO interface. The current/light soaking improved the V_{oc} with the small, mobile Cu ions

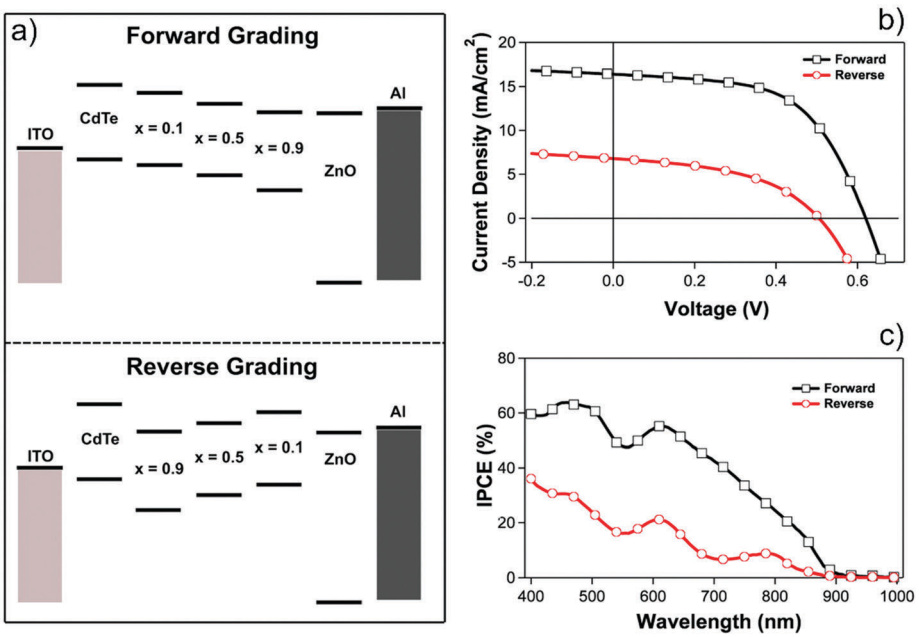

Fig. 11 (a) Flat-band energy diagrams for forward and reverse graded CdTe/CdSe QD solar cells. (b) Current–voltage curves of graded cells under 1 Sun illumination. In both devices the thickness of each individual $CdSe_xTe_{1-x}$ layer was ~100 nm for a total absorber layer thickness of ~400 nm. The thickness of the ZnO layer was 60 nm. (c) IPCE spectra for the same graded devices. The forward graded structure exhibits superior performance across the entire spectral range. Reproduced with permission from ref. 167. Copyright 2012 American Chemical Society.

assumed to be driven towards the CdTe/ITO interface. The beneficial V_{oc} enhancement was observed to decline over days to weeks but could be re-instated by repeating the soaking process. The behavior points to the potential for more stable or even better performance with an alternative ohmic contact in place of ITO. The optimal performance immediately after the current/light soaking process was [12.3%, 0.684 V, 25.8 mA cm^{-2}, 0.71].

3. QD based photodetectors

Whilst much of the materials science – both the QD chemistry and the device physics of QD-based photodetectors – is covered in the works mentioned in the previous section on solar cells, there are a few excellent reviews which take a signal measurement rather than a power generation perspective. The reviews by Konstantatos and Sargent[173,174] and also the later article by Sargent *et al.*[5] are particularly good examples whilst the broader work by Talapin *et al.*[175] also contains a nice summary of the development of both QD solar cells and detectors.

QD photodetectors fall under two main categories of device structures: photodiodes and photoconductors. In the former, the primary photocurrent arises from the collection of charges photogenerated in the QDs and forms the detected signal along with background dark/noise currents. In the photoconductors, some of the primary charges are trapped, modifying the conductivity of the QD material for the duration of the time they remain trapped. A secondary current due to an externally applied voltage then flows, governed by the modified conductivity. This secondary current is the main contributor to the detected signal in this case. Photoconductive gain can occur if the charges remain trapped for longer than the time it takes the secondary charge carriers to circulate through the device and around the external measuring circuit, with the gain being simply the ratio of the circulation time to the carrier trapping time. In photoconductors, the control of trap density, lifetimes and trap depths dictates the trade-off between detector speed, linearity, and signal gain. For some applications, slow but sensitive detectors (up to 10^{13} Jones detectivities have been measured) may be acceptable, whereas for imaging applications, at least video frame rate response times and reasonably linear response are more important. UV response in oxide based NC films has been shown as low as 370 nm wavelength, whilst with other materials such as HgTe QDs the long wavelength response has been extended to over 12 μm. The speed sensitivity trade-offs for photodiodes are not the same as for photoconductors. In photodiodes, the primary photocurrent is collected with the help of a heterojunction and either a built-in or an additional externally applied bias voltage. Photoconductive gain is absent but response times can be much faster than for photoconductors. QD photodiode bandwidths up to a few MHz can be obtained, and the IR response thus far in such devices has reached over 2 μm.

3.1. Photoconductors

The earliest studies of visible range photoconductivity in CdSe QD films by Leatherdale *et al.*[176] were made on relatively insulating TOPO stabilized QD materials and even at low temperatures (10 K) the photocurrents were relatively low with photocurrent gain being of the order of 10^{-4}. The charge separation mechanism was modelled on the basis of resonant tunneling with a QD size and surface dependence, the latter determined from samples with different surface ligands and the addition of CdS or ZnS shells. The role of the ligand was investigated further in studies by the same group[177] on CdSe QDs with treatments including butylamine, aniline, diaminohexane, phenylenediamine, tri-*n*-butylphosphine and sodium hydroxide. Treatments enhanced the photocurrent for a given bias voltage and in some cases the current voltage curve was observed to saturate at high voltages, with this being interpreted as the onset of a regime where both carriers were mobile but the Au electrodes were blocking (injection unable to occur), due to the high work function of the metal and poor alignment relative to the conduction and valence levels of the QDs. Likewise, Yu *et al.*[178] also observed a considerable improvement in photoconductivity on treating CdSe QDs with sodium hydroxide, with around 10 ms response times at low temperatures (4.3 K).

Porter *et al.*[179] replaced the ligand shell around their CdSe QDs with a ZnS shell. This was for two reasons – to reduce the influence of the organic layer through which photogenerated charges had to tunnel in order to escape from the core; and to reduce the non-radiative recombination rate which competed with the charge separation/extraction process. This resulted in 100% internal quantum efficiencies even at room temperature, with the photocurrent limited by the carrier mobilities rather than the charge generation efficiency at higher bias levels. The reduction in the influence of surface states due to the presence of the thin ZnS shell led to lower photoconductive gain (less trapping) but improved the response cut-off frequency to 14 kHz (3 dB).

Some of the earlier work on IR range photoconductors involved aqueously synthesized HgTe QDs. Kim *et al.*[180] observed a photocurrent around 1.7 times greater than the dark current under visible illumination at 514.5 nm with a HgTe QD film passivated with the 1-TG (1-thioglycerol) ligand. In later work[181] however the same group removed the 1-TG ligand, by washing with acetone and methanol after deposition, and this resulted in a more close packed film. Whilst dark currents remained in the pA range, the photocurrent was increased by several orders of magnitude leading to on–off ratios $>1000:1$. The spectral response of the detectors was a little under 1 second, and a photoresponse extending out to 1800 nm was recorded. In addition, room temperature operation was demonstrated. This work was extended further by the Heiss group with Böberl *et al.*[182] fabricating inkjet printed HgTe QD photoconductive detectors with long wavelength responses out to 3000 nm, with detectivity peaking at D^* = 3.9 Jones at 1400 nm. On–off ratios ranged between 20 : 1 and about 60 : 1 depending on the illumination levels.

In addition to planar devices, Böberl *et al.*[183] also fabricated both PbS and HgTe photodetectors where the QDs were infiltrated into vertical nanopores in alumina membranes

 This journal is © The Royal Society of Chemistry 2017

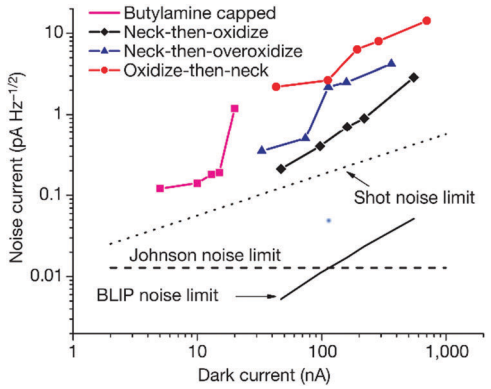

Fig. 12 Measured noise current as a function of measured dark current for PbS QD photoconductor devices. Neck-then-oxidize devices exhibited the lowest noise current that approaches within 3 dB of the shot noise limit. Oxidize-then-neck NC devices had the highest noise current consistent with multiplicative noise. Devices formed from neck-then-over-oxidize NCs showed lower noise levels than the oxidize-then-neck NC devices although they contained larger amounts of oxide. This indicates the criticality of the oxidation step in the fabrication process. The Johnson noise limit, the shot-noise limit, and fundamental background-limited thermodynamic (BLIP) noise current of the best-performing devices (neck-then-oxidize) are also plotted for comparison. Reproduced with permission from ref. 184. Copyright 2006 Nature Publishing Group.

(adapted from 100 μm and 200 μm pore size filtration media). The HgTe QDs were synthesized in water, but for pore infiltration they were transferred into organic solution and the ligand exchanged for dodecanethiol, whilst for PbS QDs the long oleylamine synthesis ligand was exchanged for a shorter butylamine stabilizer. Very low dark currents were observed for the latter, whilst for HgTe QDs the long wavelength response extended to 3000 nm. On–off ratios were 5.4 : 1 and 7 : 1 for HgTe and PbS QDs, respectively.

Konstantatos *et al.*[184] investigated the effect that surface treatments, *i.e.* ligand substitution with butylamine and also ligand removal and oxidation, had on PbS QD devices, finding that the noise/dark current could approach the Shot noise limit with ligand removal and QD oxidation (Fig. 12). Operation up to 1600 nm wavelength was obtained and detectivities exceeded 10^{13} Jones over most of the range from 800 nm to 1400 nm. With responsivities of up to 2700 A W^{-1}, considerable photoconductive gain was obtained (of the order of 10^4) which limited the frequency response to just 18 Hz. The significant trapping that was responsible for this was associated with $PbSO_4$ formation on the surface of the QDs during the treatment if carried out in air. In measuring the dynamic response of their devices Konstantatos *et al.* found that multiple time constant decays were involved in the transport and trapping behaviour of the carriers. This was investigated further in subsequent studies[185] with trap filling observed at higher light levels, resulting in faster response times under bright illumination, and a reduction in responsivity due to the drop in gain as the number of available traps falls. The location of the different traps was determined to be at about 0.1, 0.2 and 0.3 eV below the conduction band[186] by photocurrent quenching measurements and these traps were identified with the 60, 300 and 2000 ms decay time components observed in the room temperature photocurrent decays.

Further work on the relationship between ligands and the electronic properties of QD films by the Sargent group focused on understanding the changes that occurred when exchanging long chain ligands on QDs such as PbS for short chain cross-linkers such as EDT. Klem *et al.*[187] found that such treatments can improve majority carrier mobilities by reducing interdot spacing, but at the same time the majority carrier concentration may drop, as the EDT reduces the extent of surface oxidation in the lead based materials. The surface oxidation functions as a p-type doping mechanism, but is suppressed to a degree with EDT at the surface. Purposefully heating in air post EDT exchange caused the beneficial surface doping to occur in spite of the presence of the latter and allowed both the (ten-fold) mobility increase and the higher carrier concentration (×125%) benefits to be retained.

Whilst earlier work on PbS QD based photodetectors had shown multiple decay component transient responses when butylamine was used as the linker molecule, EDT treated devices were found to show a single time constant decay photoresponse. The long-tailed decays were associated with the presence of carboxylates (from the original synthesis) and sulfates which the EDT was found to displace during the exchange process. This removal improved the temporal response (single 20 ms decay) at the expense of some reduction in photoconductive gain (gain = 26).[188] Selective replacement of the sulfate and carboxylate surface trap sites with lead sulfite similarly allowed the same type and extent of trade-offs.[189] Lower photoconductive gains of around 10 allowed response times of around 25 ms, and device detectivities of 10^{12} Jones were achieved in the visible range (IR wavelength response up to 850 nm). A similar approach was taken with Bi_2S_3 QD photoconductive detectors by Konstantatos *et al.*[190] In this case replacement of the oleate synthesis ligand with EDT did not passivate the trap sites responsible for the long and multiple decay components. High (*e.g.* 1000×) photoconductive gains were obtained but response times were unhelpfully long. However, treatment of the films with methanol (which chelated with the Bi_2O_3) surface was found to reduce the gain to more modest levels (×10) but to allow faster video frame rate compatible response times (*e.g.* 23 ms).

A number of groups have explored the use of QD/organic hybrid materials as photoconductors, teaming materials such as PbS, CdTe, CdSe and InP with conjugated semiconducting polymers and fullerenes. In early studies, on MEH-PPV/PbS QD hybrid films,[191] the hole transport properties of the polymer were combined with the IR response of the QDs to produce detectors with a wavelength response up to 1300 nm, but relatively poorly optimized sensitization of the polymer in terms of charge transfer. Post synthetic ligand exchange for octylamine improved upon the much longer original oleate ligands, but was still relatively long. In addition, the precise band alignment between QDs and the conjugated polymers was not fully understood or optimized to drive charge transfer between the two hybrid components at that stage resulting in quite low internal quantum efficiencies (only up to 10^{-3}%).

An interesting hybrid combination was investigated by Biebersdorf *et al.*[192] C_{60} needle-like crystals several tens of microns in length were cast over gold interdigitated electrodes (10 μm spacing) and current passing along the needles under bias could be collected *via* the contact with the metal fingers. Whilst the C_{60} exhibited a weak photoconductive response, surface decoration of the needles with CdTe, CdSe or InP QDs increased the magnitude of the response by three orders of magnitude, due to transfer of photogenerated electrons from the QDs to the C_{60}, with the QDs themselves acting as hole traps as far as the electron carriers in the C_{60} particles were concerned. The internal quantum efficiency for these hybrids was estimated at around 50% but with a relatively slow (few to tens of seconds) response time.

Chen *et al.*[193] combined more intimately mixed P3HT/PCBM blends with CdTe QDs, with the latter capped with *N*-phenyl-*N*′-methyldithiocarbamate (PMDTC) ligands. All of the blend components were soluble in organic solvents suitable for device processing, allowing composite films to be easily formed by spin coating. The polymer/PMDTC/CdTe interfaces formed a type II junction at which photogenerated charge could be separated. Again, the charge trapped in the QDs (electrons) due to the barrier provided by the ligand led to high photoconductive gain (external quantum efficiencies up to 8000%) as the holes transited around the detection circuit and through the polymer transport pathway through the film many times before recombining with an escaped electron. In addition, QDs containing trapped electrons located near the device cathode lowered the barrier for hole injection under reverse bias.

The somewhat limited response times of the PbS QD photoconductive film devices were modified using a bilayer planar hybrid structure by Osedach *et al.*[194] After depositing PbS QDs over gold interdigitated electrodes and treating with EDT and thermal oxidation in the same manner as by the Sargent group,[188,189] a further layer of PCBM was spin coated on top of the QD layer forming a type II junction with the underlying PbS. This junction then allowed for rapid electron transfer to the PCBM but also for a fast recombination channel (compared with recombination between trapped electrons and holes) across the polymer/QD junction. The net effect of this additional channel was to sacrifice some of the photoconductive gain (less trapping in the QD layer as electrons are driven by the band structure to transfer them into the PCBM) for faster recombination times. Even the spatially indirect recombination of electrons and holes across the type II interface allowed for response times of over 300 kHz at high illumination levels, but with detectivity levels limited by the speed/gain trade-off to $D^{\star} = 4.4 \times 10^{7}$ Jones. At low illumination levels, <100 Hz response times were compensated for by $D^{\star}$ levels increasing to 2.5×10^{9} Jones. Szendrei *et al.*[195] formed devices from a similar combination of materials, PbS QDs and PCBM, but assembled as a single blended layer spin coated over gold interdigitated electrodes. In that instance the detectivity was somewhat higher, $D^{\star} = 2.5 \times 10^{10}$ Jones at 1200 nm, but again the frequency response was much slower with two distinct components, the longer weaker amplitude decay time being a few seconds. However, the linearity of the detectors' dynamic response was found to be good over several orders of magnitude in the illumination level, whereas earlier, multiple surface trap QD-based photodetectors had a much poorer linearity.

In addition to forming hybrid photodetector materials by combining QDs and polymers, the former have also been combined with inorganic materials such as wide bandgap oxide materials deposited by atomic layer deposition (ALD). ZnO has been deposited on and into the voids within QD films, and ZnS is another candidate material for the same type of approach. The oxide was deposited by exposing CdSe QD and CdSe/CdS core/shell QD films alternately to diethyl zinc vapour and water at 100 °C, and was found to coat the internal surfaces of voids within the films in a conformal manner.[196] Prior to the deposition, the films were treated with an ammonia solution to remove most of the organic ligands present after synthesis. Deposition of the n-type oxide into the shell was seen as a potentially useful alternative to ligand cross-linker treatments such as EDT or diamine exposure, filling the interdot space with both a material into which photogenerated electrons could be transferred by tunnelling through the thin oxide barrier and within which electron transport would be much more significantly enhanced than in organic materials. For the core/shell structure this was seen as a particularly attractive scenario for photoconductivity, with holes remaining in the CdSe cores whilst liberated electrons could rapidly circulate through the device taking advantage of the high mobility (10^{-1}–10^{-2} cm^2 V^{-1} s^{-1}, 2–3 orders of magnitude higher than in uncoated QD films). Although the responsivities reported were quite low (10^{-5} A W^{-1}) the response times were exceptionally fast for QD photoconductive detectors, showing a sub-nanosecond rise time and a few nanoseconds fall time in response to a sub-10 ps excitation pulse.

ZnO as a QD material has been used by Jin *et al.*[197] to fabricate photoconductive detectors in the UV range of the spectrum, operating at wavelengths down to 370 nm. The low free carrier densities in their films resulted in very low dark currents and below 400 nm responsivity reached over 60 A W^{-1} at mW cm^{-2} illumination levels, with rise and fall times of <0.1 and 1 s respectively.

The potential efficiency benefits of multi-exciton generation (MEG) in QD and QD hybrid films have often been cited in the introduction to papers on solar cells and photodetectors. In the context of extracting additional impact ionization generated charges the challenge has remained that of removing the carriers before Auger recombination with either another carrier pair (exciton) or a residual unpaired charge from a previous photoexcitation within the same QD reclaims the bonus carriers. Biexciton and trion recombination times are fast (few tens of ps or less) in spherical QDs making it hard to find a method to extract the charge in the form of primary photocurrent in either photodiodes or photovoltaic cells. However, the consequences of Auger recombination can lead to improvements in the signal detected in photoconductors, due to increased carrier trapping, leading to an increase in the photoconductive gain. This led many groups to search for one of the signatures of MEG in such circumstances – the observation of internal quantum efficiencies

 This journal is © The Royal Society of Chemistry 2017

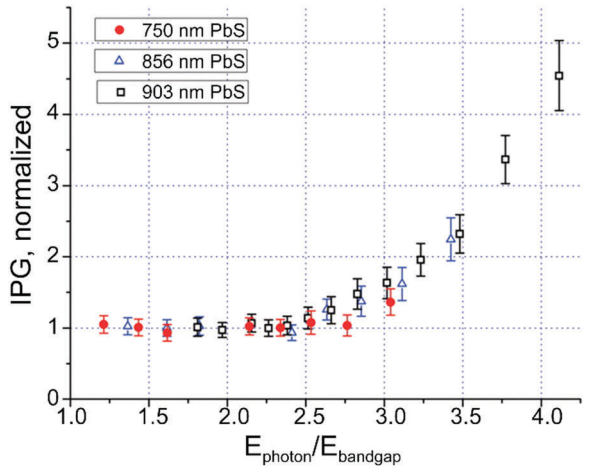

Fig. 13 Internal photoconductive gain spectra of three PbS QD-based devices having different quantum-confined bandgaps, plotted in (unitless) $E_{photon}/E_{bandgap}$. This quantity drives the internal photoconductive gain spectral behavior and is incompatible with direct ionization and compatible with MEG as a cause of the increase in trapped carriers. Reproduced with permission from ref. 200. Copyright 2009 American Association for the Advancement of Science.

exceeding 100%, *i.e.* the production of more than one electron per absorbed incident photon. Qi *et al.*[198] for example claimed external quantum efficiencies up to 150% at 510 nm for MEH-PPV/PbSe QD blends and the onset of higher than 100% efficiency for photon energies exceeding 2.7 times the QD bandgap, approximately the MEG threshold suggested for PbSe by Schaller and Klimov.[199] The observation of MEG derived photocurrent enhancements remained controversial for some time. Law *et al.*[136] made very careful analysis of the performance of their PbSe QD devices and concluded that after factoring out reflection and absorption factors the internal quantum efficiency (IQE) was not in fact exceeding 100% for their measurements. The same detailed analysis was later adopted by Sukhovatkin *et al.*[200] in the analysis of the wavelength dependence of the IQE of their PbS photoconductors (Fig. 13). Normalizing the internal photoconductive gain of several PbS devices with different sized QDs they observed a common trend with an onset in terms of the photon energy scaled by the QD bandgap energy of between 2.5 and 2.7 E_g and attributed the increased short wavelength gain to additional MEG/Auger recombination driven carrier trapping, but not from a direct increase in the primary photocurrent.

Much of the body of work on QD based photoconductive detectors overlaps with the spectral range of epitaxial semiconductors such as Si in the visible and in the near IR with Ge and InGaAs. It is difficult to see how or when QD photodetectors could supplant these mainstream detector technologies except perhaps in one or two niche aspects such as low cost/large area/solution processing applications. However, QD photodetectors are becoming much closer to a commercializable prospect for longer wavelength (*e.g.* beyond 2000 nm) detection and imaging applications where they could begin to compete with present day technologies that require either expensive or complex manufacturing processes and, in many cases, also require detectors to be cooled. Chen *et al.*[8] recently demonstrated wide frequency response (>1 MHz, 3 dB) and photoconductive gains of around 10 in simple spray coated HgTe detectors with QDs deposited from water based solutions and retaining the 1-TG ligands used during synthesis, *i.e.* without the need for ligand exchange to increase carrier mobilities. Detectivities of over 10^{10} Jones were obtained at room temperature. The fast response of these devices was attributed to the short electron trap lifetimes with this QD/ligand combination, which seem to be far shorter than those seen in comparable bandgap PbS devices.

Guyot-Sionnest's group have also extensively studied long wavelength HgTe QD and other Hg chalcogenide photodetectors and materials, favouring their growth by higher temperature hot-injection type synthesis using long chain alkylamine ligands. Critically, although they see the growth of distinct separate particles, the ligands and other synthesis conditions (precursor concentrations, *etc.*) lead to the growth of aggregated clusters of QDs where the QD spacing within each group is relatively small and helps to improve interdot electronic coupling.[7] Here again the type of ligand treatment or exchange used in PbS or PbSe QD devices was avoided, though this was investigated by the same group subsequently in studies comparing film carrier mobilities with organic linker treatments and with As_2S_3 ligands.[201] In their earlier work,[7] devices with a wavelength response to 5 μm showed a temperature dependent detectivity peaking at 10^9 Jones at close to 120 K, but falling to close to 5×10^7 Jones at room temperature (1 kHz, 5 V). More recent work[202] substantially extended the wavelength response for HgTe QD photoconductors to just beyond 12 μm with HgTe QD diameters reaching 20 nm. In this work stabilization of the larger particles during purification stages after synthesis was more of an issue, requiring the use of a long chain alkylammonium bromide ligand to keep the colloid dispersed and stable. During the device fabrication process therefore a ligand exchange with EDT was found to be necessary to cross-link the QD film and improve inter-dot coupling. For the 12 μm material the detectivity at 80 K had dropped to around 6.5×10^6 Jones and two time constants were seen in the response: one faster than 5 μs, and one on the ms timescale.

3.2. Photodiodes

As photodetectors, photodiodes can potentially operate at much higher speeds than a photoconductor in an equivalent material and similar dimensions for the active layer. As with solar cells there are several types of diode structure – Schottky junction and heterojunction designs and for signal detection purposes they may also be operated under reverse bias in a photoconductive rather than photovoltaic mode. In the photovoltaic arrangement the built-in field across the depletion region at the junction improves the rate of separation of the photogenerated carriers. In solar cells, the speed of response is immaterial but optimization of charge collection is paramount, so the active layer thickness should be taken as the sum of the depletion length and the charge diffusion distance. The latter is

the average distance a charge can travel in the absence of a field in a non-depleted region before recombination. For fast operation however, the diffusion process may be too slow, so collection of photogenerated charges in the diffusion zone may be dispensed with at the expense of some loss of sensitivity. Only much more rapidly collected charge aided by the built-in field may be collected for fastest operation, thus leading to the choice of the depletion depth as the limit for the active layer thickness.

The development of QD photodetectors shares its roots with the exploration of QDs as solar cell materials. Early work on the latter involved the use of materials such as CdSe QDs in hybrid blends with semiconducting polymers such as MEH-PPV. Greenham *et al.*[203] took this approach and studied the effect of the TOPO ligand used during synthesis on charge separation and the ratio of the blend components on carrier transport. The more effective performance was obtained from blends showing segregated hole and electron pathways through the polymer and CdSe NC aggregates respectively and essentially these were bulk heterojunction devices. Similar structures were also later studied by Jiang *et al.*,[98] who used PbSe QDs rather than CdSe NCs with a view to producing solar cells with extended IR collection and potentially also UV photon multiplication and collection *via* impact ionization. The former was certainly shown but no evidence of MEG contribution to the photocurrent was obtained. Type II alignment between PbSe QDs below 8 nm diameter and P3HT polymer was found and the larger sized dots allowed a photodiode response to over 2 μm with bias dependent responsivity.

Oertel *et al.*[204] fabricated a simple planar sandwich structure with a layer of PEDOT:PSS on ITO glass which was then coated with a 200 nm film of CdSe QDs. The latter was treated with butylamine after spin coating, and after rinsing and baking, a silver electrode was deposited. In this structure the work function of the silver top electrode and the CdSe conduction bands were almost matched in energy. The 3 dB frequency response extended to 50 kHz under 0 V bias and the detection limit was calculated to be 10 μW cm^{-2}, but the equivalent detectivity of these devices was only around 10^7 Jones, the fast recombination in the CdSe layer conferring speed of response at the expense of sensitivity. Clifford *et al.*[135] turned their attention to PbS QD based devices and used a higher QD conduction band to electrode (Al) workfunction difference to form a Schottky barrier of 0.4 eV at the top contact of their devices. Thorough characterization revealed a depletion width of 90–150 nm whilst 250 nm thick butylamine treated QD films were used, though solar as well as detector applications were considered. In the following work on the same type of Schottky devices (with combined butylamine, and oxidation treatments on the PbS QD layer) the speed of response as well as sensitivity was explored.[205] The 3 dB frequency response under 1 V reverse bias reached 60 kHz (3 dB) and the detectivity reached 10^{12} Jones, indicating that the use of the diode structure could avoid the heavy speed/sensitivity trade-off associated with QD photoconductors.

Rauch *et al.*[206] claimed the first demonstration of the use of PbS QDs in an imaging application, incorporating them as an IR sensitizer in a hybrid P3HT:PCBM:QD layer deposited over a pixelated amorphous silicon thin film transistor array. Band alignments of the three components were chosen such that the PbS QDs were positioned with type II alignment relative to both polymers. For the QD to PCBM interface, electron transfer to the polymer was favoured, whilst for the P3HT to QD interface, hole transfer into the former was effected. IR imaging of a static subject at 1310 nm with the array was shown, and low frame rate (5 Hz) moving images were also shown. In addition, discrete photodiodes with wavelength responses out to 1900 nm (5.2 nm diameter PbS QDs) and 2.5 kHz 3 dB bandwidth at 1310 nm wavelength and 1.6 mW cm^2 illumination levels were also reported.

Interband long wavelength photodetectors will necessarily involve the use of narrow bandgap QDs. Thermally activated excitation of carriers from mid-gap states may also contribute to the collected current as additional dark current. For very low bandgap materials this could also occur from the valence band itself making cooling unavoidable at very long wavelengths. However, even at bandgap energies that are not so small, the dark current degrades photodiode performance, limiting signal to noise ratio and best signal sensitivity. One approach to limit dark current has already been mentioned: QD surface treatments can significantly reduce mid gap states. A second approach (mostly in planar devices) is to reduce charge injection at the electrode to QD interface by inserting carrier blocking layers. This can be done at either or both sides of the QD layer so that under reverse bias, additional hole, electron or both types of carrier injection can be prevented.

Sarasqueta *et al.*[207] used such blocking layers: polymers such as TFB (poly[(9,9′-dioctylfluorenyl-2,7-diyl)-*co*-(4,4′-(*N*-(4-*sec*-butyl))diphenylamine)]) or TPD (poly(*N*,*N*′-bis(4-butylphenyl)-*N*,*N*′-bis(phenyl)benzidine)) to block electron injection; and C_{60} or ZnO nanoparticles to block hole injection, in conjunction with PbSe QDs of various sizes (Fig. 14). The use of ZnO nanoparticle blocking layers also beneficially improved device operating stability. For Shot noise dominated materials such as PbSe IR QDs the detectivity is simply related to the dark current density J_d as

$$D^* = \frac{R}{(2qJ_d)^{\frac{1}{2}}} \quad (1)$$

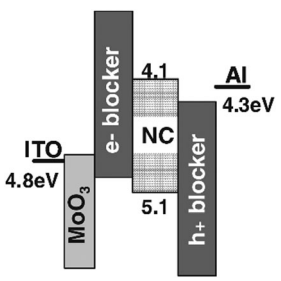

Fig. 14 A schematic representation of the energy band diagram necessary to block injection of charges under reversed bias for the nanocrystal (NC) based photodetector. Reproduced with permission from ref. 207. Copyright 2011 Wiley-VCH Verlag GmbH & Co. KGaA, Weinheim.

 This journal is © The Royal Society of Chemistry 2017

where R is the responsivity in A W^{-1}, J_d is in A cm^{-2} and q is the electronic charge.

Photodiodes with the optimum choice – TFB/PbSe/ZnO – had the best $R/(J_d)^{1/2}$ ratio with D^* reaching 10^{12} Jones (at 600 nm, around 10^{11} Jones at 1200 nm), comparable with values for commercial InGaAs photodetectors. Similarly, Pal *et al.*[208] formed p–n junction photodiodes from p-type PbS QDs in contact with a layer of n type ZnO or TiO_2. A layer of PEDOT:PSS between the PbS QDs and the ITO electrode acted as an electron blocking layer. The depletion zone formed by the pn junction leads to the collection of hole and electron currents driven by carrier drift under the influence of the electric field in that region. Under different bias levels the carrier drift times change (and are in general different for holes and electrons), leading to a bias dependent external quantum efficiency (EQE) spectrum. This resulted in flatter detectivity spectra over a wide range at high bias, with D^* values of $>10^{12}$ Jones over the visible to 750 nm range and $>10^{11}$ Jones in the near IR to 1100 nm.

HgTe QDs (synthesized in water) have also been incorporated into heterojunction structures to form IR photodiodes. Chen *et al.*[33] spray coated a 160 nm thick layer of HgTe QDs with 1-TG ligands onto ZnO coated ITO glass substrates and also onto ZnO coated substrates with an additional single layer of ZnO over-coated Au nanorods (40–50 nm wide × 90–110 nm long). A top electrode consisting of MoO_3/Au was added by evaporation under vacuum. The ZnO overcoating thickness was optimized to improve the performance. With no ZnO coating the gold nanorods partly quenched the HgTe photoresponse. For an optimal ZnO overcoating thickness of 4.5 nm however, the short circuit current density was enhanced by 340%, this being attributed to a combination of enhanced optical absorption due to the nanorod plasmon resonance coupled to the QDs and more efficient exciton dissociation and charge extraction driven by the nanorod near field. Peak detectivities reached 1.4×10^{10} Jones in the IR at 1200 nm, but in the absence of photoconductive gain, the frequency response was quite broad – 80 kHz at 1 mW cm^{-2} and 1 MHz at >100 mW cm^{-2} illumination levels.

4. Light-emitting devices (LEDs)

Whilst colloidal QD and light emitting polymer[209] materials research both had their origins in the 1980s, the use of QDs in LEDs was slower to take off than for the latter. Light emission from molecular organic materials such as Alq_3[210] (also used as an electron transport layer in QD LEDs) had been seen earlier and indeed light emission from small organic molecular compounds such as anthracene[211] could be traced back earlier still, so it is not surprising that organic LEDs (OLEDs) and polymer LEDs hit the commercial displays market long before QD LEDs. It is only recently that QD LEDs have started to be produced by companies such as QD Vision, and marketed in TV displays by companies such as LG Innotek, Samsung, *etc.* QD LED research has benefited from lessons learned in the development of OLEDs, to the extent that some of the OLED device physics and fabrication methods can be directly translated for QD LEDs. Yet the physics of the QDs themselves in terms of the excitation and emission processes is quite different, and the elaboration of which carrier processes are most critical and where and how to focus development effort has taken some time to fall into place. QD LEDs can be divided into two main categories: optically excited emitters where a conventional epitaxial blue or UV LED drives a layer of QD doped material applied over the emitter chip or in close proximity to the output of the device; and electroluminescent LEDs where the QDs themselves are directly excited by the passing of current through a QD containing film. The former, which we will refer to as QD phosphors, are down-conversion devices that make use of the high PL QY that can be obtained from more recently developed QD fluorophores. For white light emission the QDs may be mixed with other types of fluorescent materials, *e.g.* rare earth ions, to obtain a balanced emission color according to lighting or display standards. Such devices are targeted at applications such as computer display backlighting, room or outdoor lighting applications, each of which may have slightly different spectral requirements. The review by Erdem and Demir[212] gives an excellent account of the color science of QD LEDs, including an introduction to the related basics of human vision and photometry that shape LED design considerations for lighting applications. The review also summarizes progress in QD phosphor performance to that point in time.

The development of electroluminescent QD devices (which for convenience we will refer to as EL QDs, *etc.*, when distinguishing from QD phosphors) can be traced back to the early work of the Alivisatos group in 1994 on CdSe QD/PPV film devices.[213] In these relatively simple devices the EQE for emission was very low (0.001–0.01%) and upward progress in the efficiency and stability of EL devices was relatively slow. By the time of Rogach *et al.*'s[214] review in 2008, the best EL QD EQEs were only just approaching the 1% mark, and it was far from clear that QDs presented a clear commercial prospect for displays. Real progress in the emission efficiency did not come until 2011–2012 when several groups started to use inorganic oxide films, especially ZnO, as the electron transport/injection layer.[10,215,216] The combination of oxide layers with QD films had already benefited the development of QD-based heterojunction solar cells, and the fabrication and device physics was readily applicable to QD LEDs. By the time of Shirasaki *et al.*'s review in 2013,[11] the best QD EL EQE had jumped to 18%, just short of the 20% theoretical limit, and the commercial prospects were very clear. The work of the Bulovic and Bawendi groups[11,30,217,218] in developing a clear understanding of the critical role of the electric field in changing the electron and hole overlap for recombination and the need to balance the injection rates for both carriers was pivotal. Whilst there are many other potential mechanisms that might be anticipated to reduce emission efficiency of QD LEDs (*e.g.* Auger recombination involving charged QDs), field effects were found to be the most crucial by far.

In the following sections, we review the development and some of the work in each category of QD LED devices: first

QD phosphors, then EL QDs, with the rather more limited work on IR EL QDs discussed separately.

4.1. QD phosphors

Colloidal QDs, particularly core/shell heterostructures, can be synthesized to have very high solution PL QYs in some cases. Du *et al.*[219] reported efficiencies of 90% for $Zn_xCd_{1-x}Te$ QD alloys and recently Page *et al.*[220] (see also ref. 221) described a simple method to apply a chloride shell to organically grown CdTe QDs that increased their PL QY to 97%, though with limited temporal stability. However slightly lower PL QY (typically 80% or more) for QDs grown in either aqueous or organic solvents with good long term stability is well known.[222–224] For device applications the challenge has been to retain the high and stable solution PL QY in the solid state and to fabricate useful devices using such luminescent solids. Good long term stability, resistance to temperature and other environmental degradation mechanisms and retention of emission under strong excitation are all desirable properties for commercial devices. Methods to incorporate QDs into solids with high PL QY include co-dissolving in polymer solutions (both organic solvent and water soluble) to produce layers by casting or spin coating; intercalation into porous hosts such as layered double hydroxide flakes; inclusion in crystalline matrices such as sodium chloride or other salts.

Early work on white light emitting QD phosphors for display applications included work on organic solvent compatible QDs with a view to simply incorporating them in an organic solvent soluble polymer binder for film formation or casting as monoliths that could then be included in the packaging along with a blue or UV conventional epitaxial LED chip. Two main avenues to white light were popular – either the use of surface related emission from ''trap-rich'' QDs such as CdS or dual color emission from multishell heterostructures such as CdSe/ZnS/CdSe/ZnS as described by Sapra *et al.*[225] Whilst both the examples described were synthesized in organic solvents, it is also possible to form broad emission spectrum trap-rich QDs in water. Although the CdS was trap-rich, the PL QY was as high as 17% though the total integrated PL QY of the dual color emitter was higher at 30%. The latter emitted at around 500 nm and 612 nm since the inner ZnS shell was thick enough to decouple the core CdSe from the outer CdSe well. Heat treatment post-synthesis could be used to change the relative strengths of the two components, allowing the warmth of the resulting emission to be fine-tuned around the white region of the CIE color diagram. Jang *et al.*[226] chose to mix red emitting CdSe QDs with the Ce phosphor, $Sr_3SiO_5:Ce^{3+}$, with Li^+ doping to obtain green/yellow phosphors. The resulting combined QD/Ce^{3+} emitter was encapsulated over the output face of a blue emitting InGaN chip and white light emission with a color rendering index (CRI) of 90.1 and a luminous efficiency of 14 lm W^{-1} was obtained.

Panda *et al.*[227] adopted a different approach to white light emission by introducing two dopants, Cu^+ and Mn^{2+}, into ZnSe QDs. The Mn^{2+} emission was at 585 nm in the orange whilst the dominant Cu d-state emission was observed at 495 nm under blue illumination. A solid dried powder of the co-doped ZnSe material exhibited an integrated PL QY of 17%. Wang *et al.*[228] also made use of d-state/surface related Cu transitions[42] in ZnS coated CdS core/shell QDs to obtain broad red emission, which they teamed with YAG:Ce emission in the yellow. Using a blue emitting LED driver, topped with a mixture of the Ce phosphor and the doped QDs in an epoxy binder, they obtained a white light CRI of 86. The combination of the Ce emitter and the Cu doped core/shell QDs avoided the common reabsorption problem between fluorophores that often limits the efficiency of mixed phosphor combinations.

Notwithstanding the reabsorption issue, Chen *et al.*[229] demonstrated a relatively complex fabrication process using three QD emitter layers, CdSe for the red (R), $Cd_{1-x}Zn_xSe_{1-y}S_y$ for the green (G) and CdS for the blue (B). They produced both large (2 inch wafer scale) and pixelated substrates with RGB (red-green-blue) layers each separated with 80 μm thick poly-dimethylsiloxane (PDMS) films. On top of the stack a HfO_2/SiO_2 distributed Bragg grating structure was added to improve UV reflectivity, allowing better coupling of the UV LED array emission from the substrate wafer. This improved the luminous efficiency (to 100 lm W^{-1}) by ensuring more of the driver UV emission was absorbed in the QD layers. Each of the QD films was deposited by a pulsed spray deposition process from organic solutions in order to improve the film uniformity and give controlled thickness films.

Several groups have attempted to replace Cd containing QDs with other types of QD or nano-fluorophores though the regulatory pressure to do so has been relaxed to some degree with the realization that the net environmental burden may be increased by not rapidly adopting new energy saving lighting technologies and that the amount of heavy metals involved in QD LEDs is lower than in old style lighting, and encapsulated in a far less labile form. Materials based upon copper indium sulfide (CIS) are a popular choice. Song and Yang[230] grew CIS QD cores with a range of Cu/In ratios which on addition of a ZnS shell yielded PL QYs of 68–78% in the yellow to orange range of the spectrum. Color mixing the yellow emission with blue light from an epitaxial LED resulted in white emission with a CRI of 72 and a luminous efficiency of 63.4 lm W^{-1}. Sun *et al.*[231] mixed red and green types of zinc copper indium sulfide QDs with blue emitting carbon dots to form a white phosphor that was excited by UV emission from an epitaxial LED. The carbon dot PL QY was 49%. Stable and high blue emission efficiencies are often a problem for II–VI and other colloidal QD emitters, and a reason why blue epitaxial LEDs are often chosen as the excitation source. With the three color phosphor approach a CRI of 93 was achieved, with a slightly power dependent shift in color coordinates from (0.321, 0.312) at 10 mA to (0.351, 0.322) at 30 mA drive currents. By combining the mixture of green and red emitting $CuInS_2$-based QD with blue emitting chips, white light LEDs were fabricated showing a color rendering index of 95 and a luminous efficiency of ~70 lm W^{-1}.[232] By a similar strategy, green and red emitting Cu-doped ZnInS/ZnS QDs were also employed to fabricate white light LEDs with a color rendering index up to 96 and a luminous efficiency of 70–78 lm W^{-1}.[233]

 This journal is © The Royal Society of Chemistry 2017

III–V QD based white light phosphors have also been investigated by Kim *et al.*[234] Type I heterostructures of InP/GaP/ZnS core/shell/shell QDs were synthesized by organic solvent-based hot injection with the GaP thin shell added in order to mitigate the lattice strain between the InP core and the ZnS shell. This was suggested as a means to improve not only the PL QY (85%) but also the photochemical stability of the QDs. Red emitting QDs were mixed with a yellow emitting YAG:Ce phosphor in a silicone encapsulant and applied to a blue epitaxial LED. The white light emission (coordinates (0.3034, 0.2881)) had a CRI of 80.6 and a luminous efficiency of 54.7 lm W^{-1}.

In contrast to the foregoing works using organic solvent synthesized QDs, most of the white light phosphor development with water based materials has centred on CdTe QDs which can be synthesized with high PL QY and in large reaction volumes that are readily scalable to manufacturing levels. The challenge with aqueously grown QD materials is in finding a water compatible host into which they can be incorporated in order to preserve their good solution PL QY, without any degradation due to the formation of surface traps or any tendency to aggregate allowing FRET to transfer excitons to neighbouring QDs in the ensemble with low PL QY. Kalytchuk *et al.*[235] adopted a method used by Adam *et al.*[236,237] to include aqueously synthesized CdTe QDs in common salt matrices by mixing the QD solution with a saturated brine solution and allowing it to crystallize slowly. A range of CdTe QD sizes from 2.3 to 3.1 nm were used furnishing materials with emission peaks from 553 nm to 652 nm, very little red-shifted (12–18 nm) from the corresponding solution PL spectra. The PL decay curves of solutions and solids were also quite similar with average decay times in the 20–30 ns range. After inclusion in the salt crystals the composite was finely ground and the resulting luminescent fine powder could then be encapsulated in a PMMA binder and applied to the top of a UV LED to produce a series of down conversion monochrome LEDs.

Due to the excellent long term photostability and resistance to moisture ingress, silicone resins are a preferred material for regular LED packaging. In order to produce CdTe-based QD materials that are directly compatible with silicones, Mao *et al.*[238] first grew CdTe/CdS core/shell QDs using a two stage water-based microwave hydrothermal process. A third stage added a thin layer of ZnS and a silica shell by the addition of $Zn(CH_3COO)_2$, *N*-acetyl-L-cysteine, tetraethylorthosilicate, and ammonia in a modified Stöber reaction. The resulting silica coated red emitting core/shell QDs were isolated as dry powders and could be directly mixed with the silicone resin. A yellow emitting YAG:Ce phosphor was included and the mixture loaded onto blue emitting LED chips. A pair of white light LEDs were produced, one using a low power blue LED and one with a high power emitter package. The former generated white light with a CRI of 83.5 and a luminous efficiency of 53 lm W^{-1} at 20 mA drive current whilst the high power device had a CRI of 91.9 and an efficiency of 24.5 lm W^{-1} at 350 mA current. These performance figures were broadly comparable to those for the organically grown materials above.

Zhou *et al.*[239] used a self-assembly approach to convert aqueously grown QDs into solid phosphors. A number of different QDs – CdS; CdSe; CdTe; $CdSe_xTe_{1-x}$ and $Cd_xHg_{1-x}Te$ – were synthesized in water with an MPA surface ligand. CdSe QDs were also prepared by an organic solvent route and ligand exchanged with MPA in the same study. All of these carboxylic acid terminated QDs were cross-linked by the addition of hydrazine which formed amide bonds with the acid groups, thus establishing a QD solid network. The cross-linking process occurred over a period of typically 16 h to produce needle-like crystallites in the bottom of the reaction flask. With careful control over the amount of hydrazine used, rigid, water and solvent resistant 1D structured crystals could be prepared which retained the emission properties of the solutions, and for CdTe PL QYs ranged from 52 to 72% over most of the emission range. A six color phosphor was produced to demonstrate white light emission on a blue (450 nm) InGaN chip, using PDMS as an encapsulant. Undesirable FRET was avoided in the crystallization process by virtue of the controlled spacing of the QDs with the combined ligand and hydrazine linkage without aggregation of QDs at close particle range. The white light LED/phosphor had a CRI of 86 and a luminous efficiency of 37 lm W^{-1}.

An alternative method to building up QD composite films by making use of stacking between alternately charged layers of QDs and polyelectrolytes such as PDDA or poly(ethyleneimine) (PEI), *etc.*, has been shown by Liang *et al.*[240,241] In this method the polyelectrolyte was substituted by nano sheets of exfoliated layered double hydroxides (LDH) bearing plentiful divalent and trivalent cation sites on which to coordinate QDs. In the earlier work[240] white light phosphors were obtained by varying the ratio and deposition cycle pattern of two different types of CdTe QDs emitting at 535 nm and 635 nm. With the two dots in close proximity FRET was observed to strengthen the long wavelength emission at the expense of the short wavelength peak. White light LEDs were fabricated by applying the LDH/QD films to a blue emitting LED. In later work,[241] using CdTe and CdSe/ZnS core/shell QDs, PVA was added to the QD layers to further immobilize them within the structure as small clusters and ensure minimal opportunity for FRET. The core/shell QDs were incorporated into a white LED (WLED) structure to give a CRI of 91 but luminous efficiency was not stated.

In addition to incorporation into sodium chloride crystals, other crystalline salts can also be used as hosts. Chang *et al.*[242] produced WLEDs by applying mixed CdTe QD and YAG:Ce phosphors onto blue LEDs. The former was incorporated into a $BaSO_4$ crystalline host and the incorporation was much faster than that required for the common salt host, the co-precipitation process typically taking around 10 min in all. White light coordinates of (0.34, 0.33), a CRI of 88 and a luminous efficiency of 59 lm W^{-1} at 20 mA drive current were obtained using red emitting CdTe QDs.

4.2. Electroluminescent QD LEDs

Both aqueous and organic solvent grown QDs have featured in the development of electroluminescent QD LEDs. Early devices

such as those reported by Colvin *et al.*[213] borrowed heavily from the light emitting polymer field with CdSe QDs combined with PPV films, the latter functioning as a hole transport layer. With the PPV nearest the ITO anode and the QDs nearest the Mg cathode, emission could be obtained from both layers (green from PPV and yellow from the QDs) depending on the drive voltage, with charge accumulation of each type on opposite sides of the PPV/CdSe heterojunction. The external quantum efficiency (EQE) of these early devices was very low (0.001–0.01%) and air stability was very limited. Using water soluble CdSe QDs grown with thiolactic acid ligands and a water soluble precursor to PPV functioning as a polyelectrolyte Gao *et al.*[243] fabricated EL QD LEDs on ITO substrates with an Al top electrode. The polymer precursor was converted to PPV polymer after deposition using a layer by layer method by heating under vacuum, resulting in a multilayer QD/PPV thin film structure with broad emission peaking at 650 nm and EQE estimated as 0.0015%. In this case, no emission was observed from the PPV, which functioned purely as a hole transport layer. Once more, air stability was relatively limited (few hours). Mattoussi *et al.*[244] again used similar PPV-based materials as hole transport layers, but compared both bare CdSe and core/shell CdSe/ZnS QD devices. An early indication of the critical importance of the charge injection process was given by the fact that whilst the PL QY of the films increased with the addition of the ZnS shell, the EL efficiency did not. However, the EQEs of both core only and core/shell QDs had improved to 0.1% and the core/shell based devices were stable over 100 h of continuous operation. Several different sized QD samples were produced with emission peaks ranging from around 570 nm to 625 nm. Gao *et al.*[245] also improved the EQE performance of their water grown CdTe EL LEDs to around 0.1%, changing the active layer to a layer by layer deposited alternating stack of TGA capped CdTe QDs with PDDA in each bilayer. Up to 50 bilayers were deposited on ITO substrates and a top Al electrode added to complete the devices. A range of different QD sizes were used to produce LEDs with emission peaks from 540 nm to 650 nm. The relative EQE of the devices increased up to 5.7 times on going from the smallest emitters to the largest, which again was a pointer to the importance of the charge injection process as the difference between the Al work function and the QD conduction band rapidly falls as the particle size increases.

A more elaborate device structure using both electron and hole transport layers and for some test devices also an exciton blocking layer was investigated by Coe-Sullivan *et al.*[246] In the latter case the layer sequence was ITO/TPD/CdSe–ZnS core–shell QDs/TAZ/Alq_3/Mg:Ag/Ag, where TPD is *N*,*N*′-diphenyl-*N*,*N*′-bis(3-methylphenyl)-(1,1′-biphenyl)-4,4′-diamine (hole transport layer (HTL)), TAZ is 3-(4-biphenylyl)-4-phenyl-5-*tert*-butylphenyl-1,2,4-triazole (exciton blocking layer), and Alq_3 is tris-(8-hydroxyquinoline) aluminum (electron transport layer (ETL)). Apart from trying to improve the carrier transport towards the QD layer, the authors also aimed to take advantage of exciton generation in the organic layers under high current excitation which could efficiently be transferred to the QDs *via* a FRET mechanism. This was expected to be beneficial when using core/shell QDs as a means of bypassing the problem of charge tunnelling through the ZnS shell. The best EQE with this more engineered device structure reached 1.1%, an improvement on foregoing devices but still not that attractive.

Progress in improving the EL EQE over the ensuing years up until around 2012 was somewhat slow with a few small increments in performance but no great breakthroughs as a number of different strategies were explored. Bertoni *et al.*[247] continued to perfect the aqueous CdTe/PDDA layer by layer EL device fabrication process, raising the EQE to 0.51% with 50 bilayer devices, improved film quality and layer homogeneity. Simultaneous light and current measurements during voltage sweeps showed that the EL was a field dependent process, again pointing to the need for a focus on the carrier injection mechanisms. Chin *et al.*[248] used an alternative hot organic solvent route to grow CdTe nanoparticles which had rod or branched rod shapes. These were further capped with CdS shells and PL QYs as high as 52% were obtained. The EL test devices again included HTL and ETL layers but the best EQEs were only slightly smaller than those reported by Bertoni *et al.*[247]

The importance of carefully selecting the carrier transport layers was stressed by Anikeeva *et al.*[9] They replaced Alq_3 with 2,2′,2″-(1,3,5-benzenetriyl)-tris(1-phenyl-1-*H*-benzimidazole) (TPBi) since the latter had good spectral overlap between its PL and the QD absorption profiles used in their devices, this favouring FRET from the ETL to the QD emitters. This allowed them to dispense with any hole blocking layer and to use thin QD layers without the need to spatially separate the ETL from the QDs with little risk of back transfer to the TPBi film. The TPD HTL was also replaced with the more stable compound spiro-*N*,*N*′-diphenyl-*N*,*N*′-bis(3-methylphenyl)-(1,1′-biphenyl)-4,4′-diamine (spiroTPD). The authors also used solventless deposition processes (vacuum deposition for the ETL and HTL and contact transfer for the thin QD layer) to improve film morphology. With these improvements, EQEs of 1% in the red (CdZnSe alloy QDs), 2.6% in the green (ZnSe/CdSe/ZnS), 2.7% in the orange (CdSe/ZnS), and 0.4% in the blue (ZnCdS alloy QDs) were obtained.

In addition to their use in optically excited down conversion LEDs, layered double hydroxide sheets (LDHs) have also been used to form a solid host layer for aqueous CdTe QDs in EL devices.[249] In this instance a more rapid sequence of spin then dip iterations was used to alternately deposit QDs and then LDH sheets. Red emitting EL LEDs with a luminous efficiency of 0.2 lm W^{-1} were fabricated.

Organic solvent grown III–V colloidal QDs have also been explored as white light sources. Yang *et al.*[250] used InP/ZnS core/shell QDs grown by a one-pot solvothermal synthetic method to produce a range of QD emitters with narrow fluorescence from the blue (430 nm) through to the red (680 nm) regions of the spectrum. A series of different core size core/shell QDs synthesized by varying the In : Zn feed ratio were used to fabricate EL test devices. The PL QY reached 60% in the mid-range of the series but tailed off into the blue and the red regions. White light EL emission was demonstrated by combining the red emission from the core/shell QDs with blue green emission from a layer of poly-TPD organic emitter that also functioned as

 This journal is © The Royal Society of Chemistry 2017

a hole transporter. The CRI of the white light emitter was 91, with color coordinates (0.332, 0.338) and a high luminance of 270 cd m^{-2}.

An EPD QD deposition process to produce thin CdSe/ZnS core/shell QD layers on a ZnO ETL layer (on an ITO glass substrate) was demonstrated by Song *et al.*[251] The organically soluble QDs were dissolved in chloroform and 10% acetonitrile was added to encourage partial removal of the QD ligand. This also allowed some charging of the QDs which then enabled the EPD process to occur. After EPD, a 4,4′-*N*,*N*′-dicarbazolebiphenyl hole-transporting layer, a molybdenum oxide hole-injection layer, and an aluminum anode were added to complete the LED structure. The EQE of a red emitting LED reached 1.5%.

A perceived problem with QDs is the far higher Auger recombination rate than in the corresponding bulk materials. If multiple excitons are present in QDs at the same time, or if a QD is charged when a single exciton is also created within a QD (*i.e.* three charges are present simultaneously) fast Auger recombination processes will rapidly remove excitons non-radiatively until only a single exciton or a single charge remains. The latter, having acquired energy from the annihilated exciton(s), may have sufficient energy to eject a charge from the dot or may subsequently cool and lose the additional energy in the first instance as LO phonons. In case that a single cooled charge remains within the dot, it then lies in wait for the next exciton to be created and the process may be repeated. Concerned that such Auger processes might be responsible for the great gap between PL QYs and EL QYs in QD LEDs Pal *et al.*[252] fabricated LEDs using CdSe/CdS giant core/shell QDs. The possible limitations of this approach were that such QDs have volumes up to 100 times greater than those of the corresponding thin shell QDs and that the thick CdS shell might present a barrier for charge injection. The possible benefit would be a highly suppressed Auger recombination rate. In the event, an optimal shell thickness of 16 CdS monolayers furnished an EQE of 0.17% and a luminance of 2000 cd m^{-2}.

Although several groups had already fabricated QD LEDs using oxide electron transport layers (TiO_2 and SiO_2), Qian *et al.*[215] used a solution deposited nanocrystalline ZnO film as the ETL in their QD LED devices, citing the higher carrier mobilities as a reason for choosing a crystalline oxide over the amorphous oxides used by others. High brightness and power efficiencies of 31 000 cd m^{-2} and 3.8 lm W^{-1}; 68 000 cd m^{-2} and 8.2 lm W^{-1}; and 4200 cd m^{-2} and 0.17 lm W^{-1} were seen in orange/red, green and blue CdSe/ZnS core/shell QD LEDs, respectively. Un-encapsulated devices were run continuously under vacuum for up to 250 h at constant current with around a 50% droop in brightness. The three separate devices had colour coordinates that spanned a similar area to the NTSC TV display standard but the triangle they formed was slightly offset from the latter on the CIE color diagram, lacking in blue and red coverage.

A major stride forward in efficiency and brightness came with the use of an inverted device structure where the ZnO ETL layer was applied to the ITO substrate and various QD layers deposited upon that followed by one of several organic HTLs with HOMO levels selected with respect to the QDs used.[216] The HTL layer was coated with MoO_3 as a hole injection layer followed by an Al top electrode that functioned as the anode. The red, green and blue QD emitters were CdSe/CdS/ZnS, CdSe/ZnS and $Cd_{1-x}Zn_xS$/ZnS with PL QYs ranging from 70 to 80%. With this LED geometry, the red, green and blue efficiencies reached 7.3%, 5.8% and 1.7% and the brightness for each respective color was 23 040, 218 800 and 2250 cd m^{-2}. The three individual LEDs had good saturation and together covered a triangular region of the CIE diagram that encompassed most of the NTSC 1953 and 1987 color gamuts. The improved performance was credited to better electron injection, better charge balance with the device structure and careful engineering of the structure to ensure that most of the exciton recombination occurred in the QD emitter layer.

Following on from earlier work on field effect emission in ac driven QD LEDs by Bozyigit *et al.*[218] where direct current injection was prevented by adding insulating alumina layers to the two electrodes, Bozyigit *et al.*[217] examined the potential factors for PL quenching in LEDs: Auger recombination processes; charging effects; field driven exciton dissociation; or a field driven reduction of the electron–hole overlap. Backed by field-dependent PL measurements (monitoring of charge developed in test structures under ps optical excitation alongside time resolved PL measurements), the authors examined the changes in the hole and electron wavefunctions for a number of band structures corresponding to CdSe, CdSe/CdS and CdSe/ZnS QDs at field strengths comparable to those in LEDs (*e.g.* 4 MV cm^{-1}). Field induced charging was discounted as too weak an effect, but field induced reduction in the electron–hole wavefunction overlap was seen as the most significant mechanism for reducing the radiative recombination rate. Minimization of the overlap by both material and device design was identified as the major route to improving efficiency.

A significant improvement in the blue EL efficiency was reported by Lee *et al.*,[253] who increased the EQE value to 7.1% and the luminance to 2624 cd m^{-2}. The QDs were CdZnS/ZnS alloy core/shells with a shell thickness of 2.6 nm, whilst the ETL layer was again solution processed ZnO, though not in an inverted device geometry. PVK and PEDOT:PSS were used as the HTL and hole injection layer respectively, with PVK also acting as an effective electron blocking layer. The improved efficiency (around 4-fold better than that of previous blue EL LEDs) was credited to reduced Auger recombination due to the rather thick shell and reduction of the Auger rate by using a graded alloy composition rather than an abrupt composition interface between core and shell.

An extremely significant increase in red emission efficiency was reported in 2013 by Mashford *et al.*[10] with an EQE value of 18%. Taking into account a coupling efficiency of perhaps 20%, this corresponded to an internal efficiency of about 90%. They used CdSe/CdS core/shell QDs with an overall diameter of nominally 6 nm and therefore a much thinner shell than Lee *et al.*[253] and a shorter time core/shell synthesis, less likely to lead to a strongly graded core/shell interface. The key to the efficiency enhancement was the use of an inverted structure

with the ZnO ETL between the ITO electrode and the QD layer. Samples with nominally 2.5, 5, 7.5 and 10 QD monolayers were fabricated and tested, with the 7.5 QD layer device showing the maximum efficiency, whilst the thinner layer devices showed better operating stability. The critical factor was the degree of electrical coupling between the ZnO and QD layers which was critical in controlling charge transfer and maintaining charge balance for the QD emitters. The LEDs also exhibited below bandgap emission with turn on voltages below 2 V. This was explained in terms of electron accumulation at the QD/organic HTL layer where Auger assisted hole injection could then occur. The resulting reduction in the required drive voltage contributed to the improvement in the luminous power efficiency (>25 lm W^{-1}).

The highest EQE values are seen at lower drive currents, but at high current the brightness is limited by a drop off in the luminous efficiency termed efficiency roll-off. Shirasaki *et al.*[30] made detailed measurements of the simultaneous EL, PL and time resolved PL lifetimes of QDs in biased EL LED devices to determine the mechanism for the roll-off (Fig. 15). The potential mechanisms included radiative rate reduction *via* reduced electron–hole overlap under an applied field; increase of non-radiative rate due to exciton dissociation; hot carrier trapping in QD surface traps. The low PL QY of their devices (8%) coupled with the voltage dependent PL lifetime, but little change in the non-radiative rate led the authors to tentatively conclude that the roll-off is connected with a field dependent drop in the radiative rate such as might occur with a reduction in the carrier wavefunction overlap as suggested by Bozyigit *et al.*[217]

The EL QD LED development story and the key factors that have driven the improvements to reach 18% EQE devices along the way have been very comprehensively summarized by Shirasaki *et al.*[11] in the Bawendi and Bulovic groups' Mini Review of the field. They also offer some insight into the continuing research to combat emission quenching: the avenues under investigation to produce high brightness output with reduced efficiency roll-off; methods to improve the poor, 20% or so, output coupling; evaluation of the relative merits of direct *vs.* FRET methods to excite QDs; and finally efforts to reduce

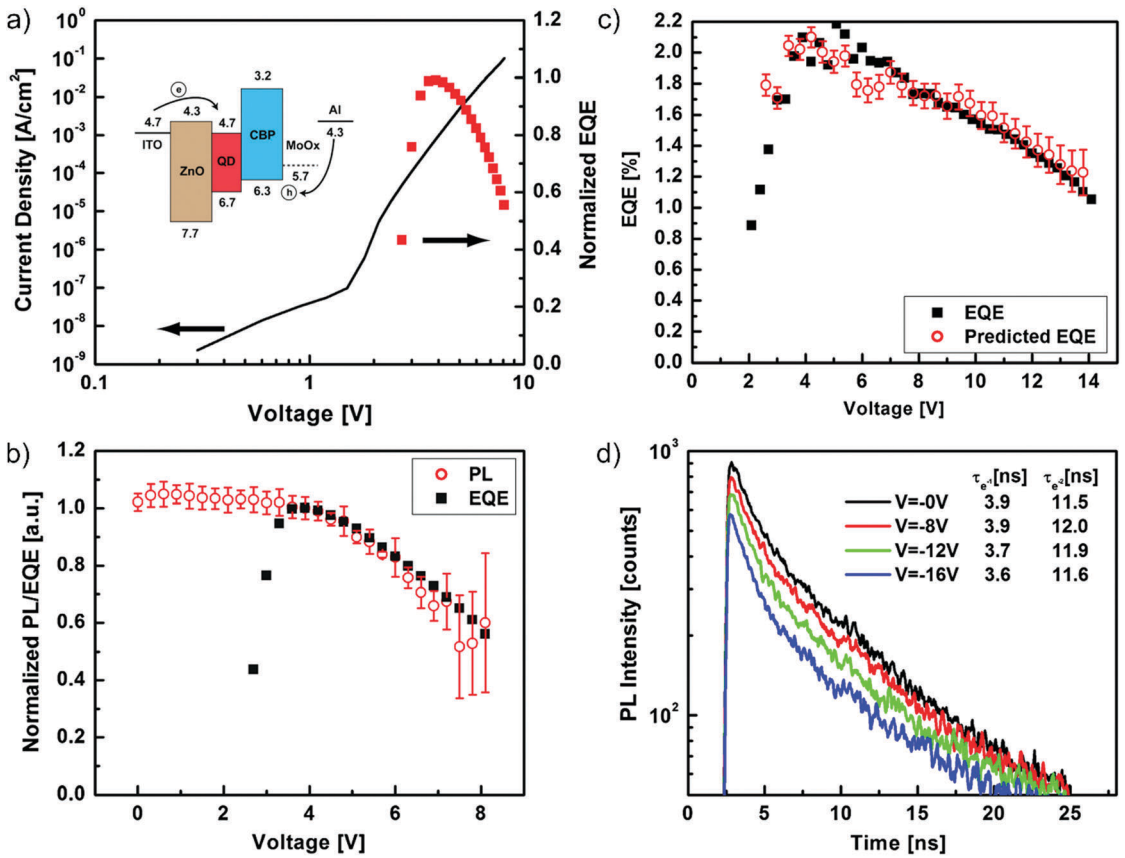

Fig. 15 (a) Current density–voltage and EQE–voltage characteristics of a QD-LED (with CdSe–ZnCdS core–shell QDs with a peak PL wavelength of 610 nm, provided by QD Vision, Inc.). Inset: Energy band diagram of the device, with indicated energy values referenced to the vacuum level. (b) EQE and QD PL intensity of the QD-LED (normalized at 4 V, when the peak EQE = 2%) as a function of voltage. Roll-off of the EQE above 4 V reflects reduced QD PL efficiency at high bias levels. (c) Measured EQE and predicted EQE as a function of voltage. EQE is predicted through the comparison of PL and EL data as described in the text. The agreement between the data and the prediction shows that the quantum confined Stark effect can self-consistently account for the QD-LED efficiency roll-off. (d) Transient PL of QDs in the QD-LED reverse biased at 0, 8, 12, and 16 V. Time constants of the decays (inset) are independent of the applied voltage, suggesting that the nonradiative exciton recombination rate is independent of the electric field. Reproduced with permission from ref. 30. Copyright 2013 American Physical Society.

This journal is © The Royal Society of Chemistry 2017

the QD production costs by at least a factor of 10 to compete with their OLED counterparts.

4.3. IR emitting EL LEDs

IR emitting electroluminescent QD LEDs are discussed here separately because some of the factors that strongly influence visible light emission and some factors that have been discounted as less significant in the visible have a different weighting when considering IR emission. Lower bandgaps may be expected to favour more efficient charge injection, whilst radiative rates will tend to be reduced as the bandgap becomes smaller according to Fermi's Golden Rule. Operation in the IR also leads to exciton energies comparable with the vibrational modes of surrounding near-surface molecules such as ligands, *etc.*, and the risk of the exciton's energy being transferred from the QD by an electronic/vibrational version of FRET,[254,255] or by non-adiabatic coupling mechanisms.[256]

One of the earliest examples of IR EL emission from a simple QD/polymer device was reported by Tessler *et al.*,[257] who adopted the approach used for previous visible light emitting LEDs by combining InAs/ZnSe low bandgap core/shell QDs with conjugated polymers based on PPV and poly[(9,9-dihexyl-fluorenyl-2,7-diyl)-*co*-(1,4-(benzo-[2,19,3]thiadiazole))]. These devices had relatively low EQEs, estimated to be around 0.5% for emission centred at 1300 nm, but for IR devices that was already a quite good efficiency. Bakueva *et al.*[258] similarly combined PbS QDs with PPV and poly *para*-phenylene polymers to demonstrate that size tunable EL emission was possible over the 1000–1600 nm wavelength range and estimated the internal quantum efficiency to be 1.2%.

IR QD LEDs based on more complex device structures were described by Steckel *et al.*[259] A range of PbSe QDs with emission peaks from 1.3 μm to 1.55 μm were sandwiched as monolayers between an Alq_3 ETL and a HTL of either TPD or NPD. EQE was estimated to be as low as 0.001% with these devices and the PL QY was also known to drop dramatically on forming dried thin films from as much as 20% to only 1.5%, limiting EL from the outset.

Early efforts with water-based IR QD materials were similarly limited in the EQE they could achieve though tunability across the 1000–1600 nm emission range was also readily demonstrated. Koktysh *et al.*[260] combined water-grown HgTe QDs with a methyl substituted poly(*para*-phenylene) polymer in a simple sandwich device construction and demonstrated 1300 nm EL with an EQE of 0.001%. In order to form the QD polymer composite the water soluble HgTe QDs were transferred into toluene and the thioglycerol ligands exchanged for dodecanethiol. Similar EQE performance had been obtained with HgTe QDs grown by the same method but without the ligand transfer step and deposited using a layer by layer method with PDDA and PEI as the counter charged polyelectrolytes.[261]

Recent improvements to IR QD LED performance have, like visible emitting QD LEDs, been partly due to improvements in device geometry. Sun *et al.*[262] fabricated PbS QD-based LEDs with a ZnO nanoparticle film ETL and PEDOT:PSS as a hole injector over an ITO/glass substrate. However, the most significant factor in the improvement of the EQE to 2% was the choice of organic spacer molecules that maintain the separation between QDs in the emitting layer. Comparison of EQEs with mercaptopropionic acid, mercaptohexanoic acid, mercaptooctanoic acid and mercaptoundecanoic acid as spacers showed the 8-carbon chain homologue to give the best performance. The adjustment of the interdot spacing was viewed as giving the best trade-off between exciton dissociation (leading ultimately to non-radiative recombination) and radiative recombination driven by efficient charge injection. Again the selection of well-balanced ETL and HTL layers was also stressed: the use of ZnO (which could be fine-tuned if necessary by photodoping, *etc.*) and PEDOT:PSS which could similarly be adjusted by varying the PSS to PEDOT ratio was seen as a major benefit for engineering the respective carrier supply rates. LED operating wavelengths could be tuned *via* the PbS QD sizes to range from 950 to 1700 nm. Although the luminous efficiencies are still low compared with those of visible range EL QD LEDs, the results given by Sun *et al.*[262] are quite good for IR materials and of a similar order to those for conventional epitaxial IR LEDs at comparable emission wavelengths.

5. Photocatalysis

Here we review some of the photocatalytic applications involving QDs, both those synthesized directly in aqueous solution and QDs and other nanostructures synthesized in hydrophobic solvents and then transferred into water *via* ligand exchange schemes. The purpose is to examine the range of QD materials in use, and to show how they are used in terms of their solution and ligand chemistry, *i.e.* how they are teamed with other co-catalysts and charge transport/donating molecules and substrates, rather than an in-depth study of photocatalysis mechanisms themselves. For that the reader should of course consult the references cited themselves or several more specialized review articles such as those by Wilker *et al.*,[15] Han and Eisenberg[263] or Wu *et al.*,[264] all of which include discussions of photosynthetic processes involving colloidal QDs, and compare these materials alongside other photoactive materials and in relation to photochemical processes other than hydrogen generation which we focus on specifically here. Combinations of semiconductor QDs with metal plasmonic nanoparticles have not been included; for a comprehensive review of these photocatalysts the review by Jiang *et al.*[64] is recommended. A review by Vaneski *et al.*[12] also describes the work in general on QD heterostructures and hierarchical 3D nanostructures in relation to photochemical water-splitting and hydrogen generation, surveying a wide variety of semiconductor materials and including complex nano-geometries. Their work also encompasses the combinations of QDs, nanorods, nanoribbons, *etc.*, with other co-catalysts including Pt-, Pd- and Co-based compounds and Fe–Fe hydrogenases.

The sustained photocatalytic splitting of water into both hydrogen and oxygen is an ultimate goal of the majority of work in this area. This is something that has already been realized

with other classes of photocatalysts, *e.g.* La doped $NaTaO_3$ microcrystals coated with NiO fine powders, but the expectation is that QD-based water splitting may have the capacity to do the same with much higher quantum efficiencies in due course. A great deal of effort continues to be devoted to optimizing the size, shape, heterostructure and material quality of the semiconductor nanoparticles, along with finding the best match for the co-catalysts and the most efficient methods to couple the two together. The majority of the research has involved the formulation and testing of materials addressing just one half of the water splitting problem, that of hydrogen generation which is realizable in dispersed aqueous mixtures of QDs, ligands, co-catalysts and hole scavengers. Operation is limited in more recent work by the ultimate stability of the latter and better photocatalysts may nowadays function for several weeks. To realize both halves of the water splitting goal simultaneous oxygen and hydrogen generation can be carried out in photoelectrochemical cells (PECs) where both photogenerated holes and electrons are used to generate the respective gases. Some examples of these employing QDs incorporated into and on solid substrates are also given.

Even in the early 1980s, before the development of colloidal semiconductor QDs had really started to get underway, it was recognized that finely dispersed semiconductor particles were promising as solar powered drivers for the electrochemical splitting of water, and to drive other useful photoelectrochemical reactions.[265–268] In this early work particle sizes were relatively large and the benefits of quantum confinement had yet to be fully realized, whilst growth methods relied on methods other than the steric or charge stabilized ligand methods now in common use. Meyer *et al.*[269] for example produced 12–15 nm diameter CdS colloidal particles using a micelle size control method, with the surfactant AOT forming a boundary between an octane phase and water at the inner boundary with the particles. The CdS particles were decorated with regions of Pt metal, with the CdS semiconductor supplying electrons to the metal catalyst under irradiation and these then going to form hydrogen gas by the reduction of an aqueous solution of thiophenol.

Nowadays semiconductor QDs as both spherical and anisotropic rods and other nanostructures and hetero-nanostructures have emerged, with a wide range of different growth methods that can cater to both hydrophilic and hydrophobic solvents. The improvements in synthetic sophistication allow for better separation and transfer of photogenerated charges, increased durability of the semiconductor nanostructure through the use of core/shell QDs, highly tailored surface functionalization (*e.g.* for binding hybrid complexes together) and size controlled bandgap and energy level engineering. Quantum confined NCs both as dispersed components in hybrid solutions (QDs with other catalysts, charge scavengers, *etc.*) and as parts of solid photoelectrodes in PECs began to emerge. Yu *et al.*[270] considered the design of type II InP/CdS and InP/ZnTe nanorod PECs where the core and shell dimensions and also the strain induced by lattice mismatch could be used to engineer not only the bandgap and thereby absorption characteristics, but also the separation of the photogenerated charges could be controlled. In the InP/CdS core/shell nanorod case electrons would tend to be located in the CdS shell whilst holes would be localized in the InP core. In the case of nanorods grown on an epitaxial substrate the core would be electrically connected with the external PEC circuit. In the InP/ZnTe case, the converse situation where holes are located in the shell and electrons are localized in the core could be arranged *via* an appropriate choice of core and shell sizes.

Whilst epitaxial nanostructure growth naturally lends itself to the formation of such nanorod assemblies on semiconductor substrates, colloidal and other related synthetic methods (hydro and solvothermal growth) can lead to the formation of a much richer range of particle shapes and heterostructures. Frame *et al.*,[271,272] for example, produced CdSe nanoribbons with a bandgap (2.7 eV) much wider than the CdSe bulk bandgap (1.7 eV). MoS_2 nanoplatelets formed by sonication of MoS_2 powder in the presence of butyllithium were added and absorbed onto the nanosheet surfaces. The nanoplatelets functioned as a co-catalyst in the photoreduction of water to hydrogen, enhancing the catalytic activity fourfold.

The use of spherical QDs and nanorods with dimensions in the size confinement regime has perhaps attracted the most interest in the area of water splitting over the last 8 years. Larger QDs in a given material have lower bandgaps (limited by the bandgap of the material in its bulk form) and have broader absorption spectra in the visible region. Quantum confinement effects push the valence and conduction bands apart; in most cases the lower effective mass of the electrons compared with the holes at the band edge results in a more rapid shift to higher energy for the conduction band than for the valence band as the particle diameter is reduced. The shifts in both levels contribute to a widening of the bandgap on making the diameter smaller. Holmes *et al.*[273] examined the impact of this on the photocatalytic activity of CdSe QDs in a simple system (just CdSe QDs stabilized with mercaptoethanol ligands in aqueous Na_2SO_3 solution) in order to establish the effect of the thermodynamic driving force ΔG for electron transfer from the QDs to the protons in their system. According to Gerischer theory[273–275] the hydrogen reduction rate is given as

$$k_{\mathrm{red}} \propto \exp\left[-\frac{(\Delta G - \lambda)^2}{4kT\lambda}\right] \qquad (2)$$

where ΔG is the difference between the conduction band edge potential and the proton reduction potential, $\Delta G = e(E_{\mathrm{CB}} - E^0_{\mathrm{red}})$, and λ is a reorganization term. At constant pH, E^0_{red} is a constant and $E_{\mathrm{CB}} \propto E_{\mathrm{gap}}$, so $k_{\mathrm{red}} \propto \exp(-E_{\mathrm{gap}})$. Thus, for a given amount of CdSe QDs, strong absorption is favoured by large dots whilst more rapid reaction is favoured by smaller dots. The optimum gas production rate is therefore a trade-off between the two; in Holmes *et al.*'s case the optimum QD size was for 2.2 nm diameter QDs with a generation rate of 53.7 mmol mol^{-1} CdSe. This was a relatively simple system to optimize from the QD dimensions point of view. Some of the following examples are rather more sophisticated, in some cases rather more complex heterostructures were used and

 This journal is © The Royal Society of Chemistry 2017

the overall reduction schemes involve interactions between more components (co-catalysts, *etc.*).

5.1. QD/metal co-catalysts

Catalytic metal decorated semiconductor nanoparticles generate hydrogen *via* the transfer of electrons from the conduction band of the QDs to the metal catalyst surface sites. However, the electrons may recombine with either the original or other holes before the reduction reaction can occur. Keeping the original geminate holes away from the electrons in the metal regions is therefore highly desirable. Amirav and Alivisatos produced a range of type I CdSe seed in CdS rod nanostructures with Pt decoration on the tips of the rods (Fig. 16).[276] In the ideal geometry the CdSe seeds are located near one end of the rod whilst the Pt site is at the opposite end. This then allows for good separation of photogenerated holes in the CdSe seed and electron transfer to the Pt tip. The highest quantum efficiencies for H_2 production were obtained with 60 nm long rods and 2.3 nm CdSe seeds with a value of 20%. The Pt tipped CdSe seeded CdS rods were seen to be substantially more stable than the same structures without the CdSe seeds as well as far more efficient. The non-seeded nanorods tended to lose the metal tips after even relatively short times, implicating the holes in the degradation process.

Zhu *et al.*[277] also made a comparative study of similar structures though without the Pt metallization. Quasi type II CdSe seed in CdS rods; CdS rods; and CdSe/CdS core/shell QDs with equal volume (same core size as the seed) and with equal lowest exciton energies to the seed in rod structures were studied. The particles were stabilized with water soluble MPA with excess ligand added in the additional role as a sacrificial hole scavenger. In measurements of the photoreduction of methylviologen (MV), and in hydrogen production (the latter assisted by the addition of colloidal Pt particles) the seed in rod structure out-performed the other heterostructures and the simple CdS rods (Fig. 17). The external quantum efficiency for H_2 generation reached 7.5% for the seed in rod structure.

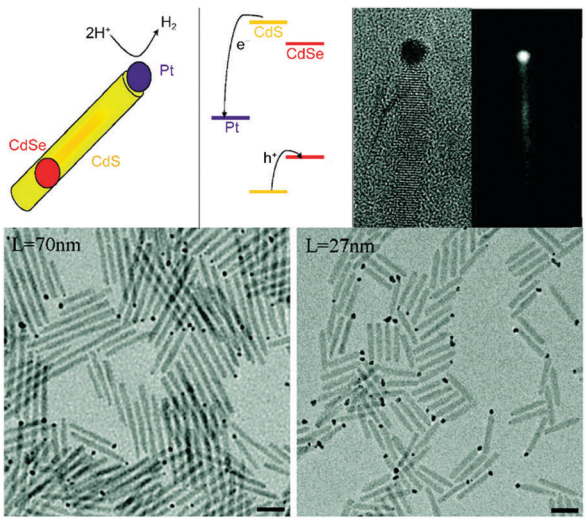

Fig. 16 (left top corner) An illustration of the multicomponent nano-heterostructure, composed of a Pt-tipped CdS rod with an embedded CdSe seed. (top middle) An illustration of the energy band diagram indicating that holes are confined to the CdSe while electrons are transferred to the Pt and are thus separated from the holes over three different components and by a tunable physical length. (bottom) TEM images of Pt tipped seeded rods with two different lengths, 27 and 70 nm on average (bar is 20 nm). (top right corner) The Pt tip is clearly seen in the HRTEM (with a 3 nm tip) and HAADF STEM (of a 40 nm long rod) micrographs. Reproduced with permission from ref. 276. Copyright 2010 American Chemical Society.

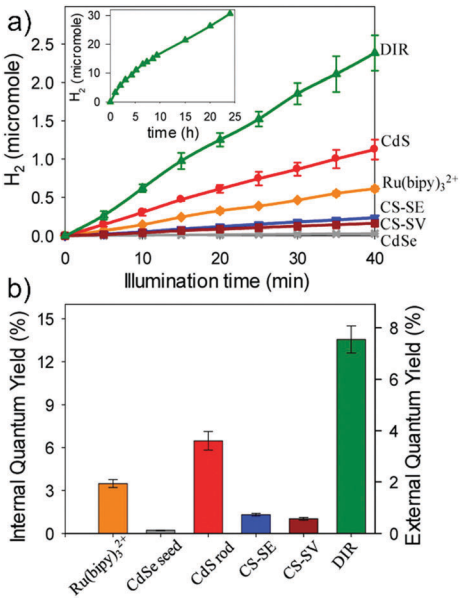

Fig. 17 (a) Kinetics of H_2 formation from water reduction using the sensitizers shown on the right: $Ru(bipy)_3^{2+}$ – tris(bipyridine)ruthenium(II) dye, CdSe seed, CdS rod, CS-SE – CdSe/CdS core/shell QDs of equivalent lowest exciton energy to dots in rods (DIRs), CS-SV CdSe/CdS core/shell QDs of equivalent volume to DIRs, DIR – CdSe/CdS dot in rod in the first 40 min. (Inset) The H_2 formation kinetics using CdSe/CdS dots in rods up to 24 h. Conditions: MV^{2+}, MPA, and NC concentration 50 mM, pH = 6.2 phosphate buffer; H_2 evolution catalyst (0.8 mM Pt nanoparticles); and illumination light (8 mW, 455 nm). (b) Internal (left axis) and external (right axis) quantum yields of H_2 evolution using different sensitizers. Reproduced with permission from ref. 277. Copyright 2012 American Chemical Society.

Whilst the photogenerated holes need to be kept away from their electron counterparts until the latter have been successfully consumed in the reduction of water to hydrogen, something further must be done with them – indefinite localization in the seed part of heterostructures, *etc.*, is not an option. As already mentioned, they may be involved in undermining the metal to semiconductor bonding in metal decorated hybrids, or they may be involved in the decomposition of the semiconductor structure itself. These issues were investigated by Acharya *et al.*[278] with ZnSe/CdS and ZnTe/CdSe/CdS seed in rod and core/shell seed in rod structures, each with and without Pt decoration on the end of the rods furthest from the seed. The eventual extraction of holes from the seed to the hole scavenger – in their case they used either MPA or mercaptoundecanoic acid – was determined by the alignment of the ligand/scavenger HOMO level relative to the valence band of either ZnSe or ZnTe. Hole transfer is energetically possible for ZnSe to MPA, but not for ZnTe to MPA for example. Thus, MPA may remove holes from ZnSe effectively

whereas for ZnTe they remain trapped within the seed region of the structures and may potentially degrade the operating stability and efficiency. In H_2 production tests the ZnSe/CdS/Pt materials generated gas whereas the ZnTe/CdS/Pt structures did not. Moreover, when the former stopped producing further H_2 on exhaustion of the sacrificial MPA ligand, further photocatalytic activity was resumed upon replenishing the solution with fresh ligand, *i.e.* the cessation was reversible and not a symptom of the complete breakdown of the heterostructure, highlighting the need to develop a rechargeable electron donating (hole accepting) ligand.

Further insight into the role of holes in metal decorated CdS rods can be found in the work of Berr *et al.*[279] in their transient absorption studies of electron transfer from CdS rods to Pt clusters on the sides of the rods they found that transfer was slower in the presence of $NaSO_3$ hole scavenger than without it. This was explained in terms of hole trapping on the surface of the CdS rods, close to the boundary between the semiconductor and the metal (which may have some relevance to earlier Pt degradation in metal tipped nanorod systems). With trapped holes closely located by a Pt cluster, Coulombic interaction with the geminate electron will also draw the latter towards both the trapped hole and the Pt cluster site, facilitating faster transfer into the latter *via* distortion of the electron wavefunction towards the surface and the metal. Of course, the electron is now located very close to a hole and the likelihood of recombination is strong and the chances of surviving long enough to take part in a multielectron reduction reaction are very low. The point is made though that with the scavenger the electron transfer rate is not a maximum, the trade-off in such a simple structure is based on both CdS to Pt transfer and the recombination rate and these are controlled by both the structure and the scavenger kinetics. The latter was addressed further in a follow-up study[280] of the effectiveness of a number of different hole scavengers, sulfite, triethanolamine (TEA), ethylenediaminetetraacetic acid (EDTA) and methanol (MeOH), with Pt decorated CdS nanorods stabilized with either MPA or cysteine (Fig. 18). The ligands themselves may also play a role in the scavenging mechanism, MPA being a common choice in this capacity as well. The hydrogen generating capacity was found to correlate with the scavenger HOMO levels, with the higher thermodynamic driving force for hole transfer arising for the sulfite. The faster rate of hole transfer ensured that the electrons could then get on with their task with less hindrance. The sulfite/MPA combination gave the greatest H_2 generation efficiency. Comparison of the nanorods before and after use also indicated that methanol and EDTA led to rod shortening and aggregation, leading to colloid destabilization.

Whilst many nanorod and seed in rod syntheses rely on high temperature/hot injection methods to favour anisotropic growth of hexagonal material, use for water splitting requires that the photocatalyst be water soluble and this then entails a ligand and solvent exchange at some point for materials grown in hydrophobic conditions. However, Vaneski *et al.*[27] made use of a method to synthesize both CdS and CdSe/CdS tetrapods directly in water/ethylenediamine mixtures at room temperature, dispensing with the need for a ligand exchange step. Ligands such as MPA, cysteine, and TGA could all be added and improved the stabilization but did not disturb the growth process. After the formation of the tetrapods additional Pt decoration was carried out using ascorbic acid as a mild reducing agent to convert the metal chloride to surface deposited clusters. In the case of the CdSe/CdS tetrapods, hole localization in the CdSe tetrahedral core occurred with electrons being initially confined to the CdS arms. Triethanolamine/ascorbic acid formed the hole scavenging species and hydrogen production of 24 mmol per g tetrapods per h was obtained under AM 1.5G illumination. A range of synthetic methods to synthesize such metal decorated nanorods, tetrapods and other hybrid photocatalytic structures were reviewed by the same group.[281]

Alternatives to the use of precious metals as Pt in such hybrid nanoparticles have been investigated for several reasons: cost

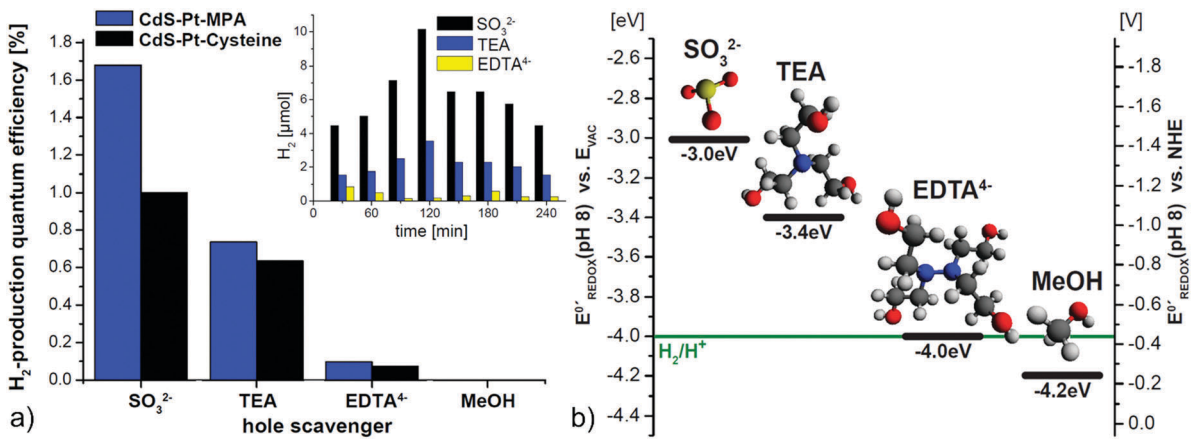

Fig. 18 (a) Comparison of H_2 production quantum efficiencies for Pt-decorated CdS nanorods using SO_3^{2-}, TEA, $EDTA^{4-}$, and MeOH as hole scavengers. Data for different ligands (*i.e.*, MPA and cysteine) are shown. In all cases SO_3^{2-} shows the largest hydrogen generation followed by TEA, $EDTA^{4-}$, and MeOH. The inset shows hydrogen evolution as a function of time for MPA-stabilized nanorods and SO_3^{2-}, TEA, and $EDTA^{4-}$ as hole scavengers. (b) Schematic plot of the energy levels of the electrons of SO_3^{2-}, TEA, $EDTA^{4-}$, and MeOH that are involved in the reduction of the photohole *vs.* vacuum and on normal hydrogen electrode (NHE) scale. Reproduced with permission from ref. 280. Copyright 2012 American Institute of Physics.

This journal is © The Royal Society of Chemistry 2017

in some instances; operating efficiency; and also from the point of improved stability. Shemesh *et al.*[282] coated the tips of CdS nanorods with the conductor Pd_4S *via* a high temperature organic synthesis, and alternatively decorated the same type of nanorods with PdO *via* an aqueous route. Both types of decorated CdS showed H_2 photocatalytic activity with production rates depending strongly on the nature of the coverage with the palladium sulfide/oxide, with smaller clusters giving higher generation rates. Molybdenum sulfides, which feature both in industrial catalysis and also in nature incorporated into biological enzymes, have also been explored by Tang *et al.*,[283] who produced CdSe seeded CdS nanorods coated with a thin layer of the sulfide. The interest in these sulfides derives from the fact that sulfur atoms on under-coordinated surface sites can bind hydrogen atoms with virtually zero free energy making them an ideal place to assemble H_2 molecules. The MoS_3 precursor was $(NH_4)_2MoS_4$ which was applied in organic solution, the coated rods being transferred into neutral aqueous solution after purification. Peak H_2 generating activities of almost 90 mmol g^{-1} h^{-1} were obtained for 2.8 nm diameter CdSe seeds in 65 nm long MoS_3 coated CdS rods.

Simon *et al.*[284] decorated CdS nanorods with Ni as a cheaper alternative to Pt or Pd catalysts. The slower rate of transfer of electrons from the semiconductor to the metal clusters (compared with the precious metals) can present a problem because competing recombination with nearby holes on the surface will then remove electrons before they can deprotonate water molecules. Improvement to the hole scavenging rate to redress this problem was obtained by using hydroxyl ions/hydroxyl radicals as a hole relay to carry holes away rapidly from the nanorod surface to the sacrificial hole scavenger (ethanol in this case). This hole shuttling mechanism (rather than direct hole scavenging by ethanol) becomes active at high pH (around pH 14) due to a favourable cross-over in the hydroxyl anion oxidation electrochemical potential and the CdS valence band energy in this pH range. The much smaller size of the hydroxyl ion/radical compared with the ethanol/acetaldehyde scavenger/oxidized product allows more rapid removal of holes from the surface. H_2 production reached almost 20 mmol g^{-1} h^{-1} at pH 14.7 with such decorated nanorods.

In addition to decorated nanorods and hetero-nanorods, many groups have also investigated the factors that influence the photocatalytic activity of spherical QDs and core/shell QDs. Water-grown citrate capped CdSe QDs were known not to have significant photocatalytic activity on their own in water, but Thibert *et al.*[285] demonstrated that the addition of a thiolate hole scavenger could allow limited activity. Ten-fold improvement could be obtained however by the addition of a CdS shell to form a type I structure. Although a type I band alignment would restrict both electrons and holes to the core it is still possible for the carriers to tunnel to the surface on the timescale necessary for the photoreduction step. The reason for the improvement on addition of the CdS shell was attributed to the passivation of deeper electron traps at the CdSe surface (which hinder the activity of the bare core QDs). Although this then introduces an energy barrier for electron escape, tunnelling is sufficiently fast enough to allow electrons with sufficient reduction potential to make it to the CdS outer surface.

Li *et al.*[286] incorporated Ni^{2+} ions into the surface of their CdSe QDs and CdSe/CdS core/shell QDs *via* the addition of nickel salts ($NiCl_2$) to MPA stabilized aqueous QD solutions. Given the smaller ionic radius of Ni^{2+} (83 pm) compared with Cd^{2+} (109 pm) it is entirely feasible that surface ion exchange at least may readily occur. Surface bound Ni^{2+} ions were proposed as sites for the photoreduction of water on receiving excited electrons *via* tunnelling through the CdS shell. Two hole scavenging mechanisms were suggested, where the latter also tunnelled to the surface and oxidized either a propan-2-ol scavenger or a hydroxyl anion. However the fact that the peak H_2 generation was observed at a low pH (5.1) may mitigate against the latter mechanism (see earlier discussion regarding Simon *et al.*[284] work on Ni decorated CdS nanorods and pH dependence). Nevertheless, H_2 generation with a rate of 1.5 mmol g^{-1} h^{-1} was observed.

The influence of the band alignment in CdSe/CdS core/shell QDs decorated with Ni clusters was explored by Ehrat *et al.*[14] The decoration was carried out in an aqueous alkaline environment by photoreduction of added nickel salt. They synthesized a range of different sized CdSe cores and coated some with two monolayers of CdS and one CdSe core diameter with a range of different shell thicknesses. This range of core diameters and shell thicknesses tuned the band alignment across the threshold for type I to quasi type II alignment, thus allowing the impact of the ease of access of photogenerated electrons to the surface Ni regions on H_2 generation to be studied (Fig. 19). PL lifetimes and QYs were correlated with H_2 production rates for each of the structures (PL measurements on non-decorated core shells). Quasi type II structures show longer lifetimes and increased segregation of the electrons and holes. They differ from structures with full type II band alignment in that the amplitude of the electron wavefunction is spread across both core and shell, whilst the hole wavefunction remains more strongly localized in the core with little penetration into the shell. For smaller cores, evidence of quasi type II alignment was seen; for larger diameter cores the PL lifetimes increased with increasing thickness which may reflect the fact that the electron could still occupy the shell due to tunnelling even though the structure became type I. The authors also suggested that with Ni clusters present a Schottky barrier may be formed at the metal/CdS interface on transfer of an electron, further enhancing carrier separation (and H_2 production). Interestingly there were two nearly equivalent best cases for H_2 production: either small quasi type II or large thicker shell type I core–shells showed almost the same performance.

5.2. QD/enzyme co-catalysts

The search for lower cost alternative catalysts for use in conjunction with colloidal QDs has led several groups to follow the examples of nature and turn to either naturally occurring photosynthetic enzymes or to produce synthetic mimics of such materials. Found in phototropic organisms these hydrogenases contain metal–metal sites that act as a centre for the

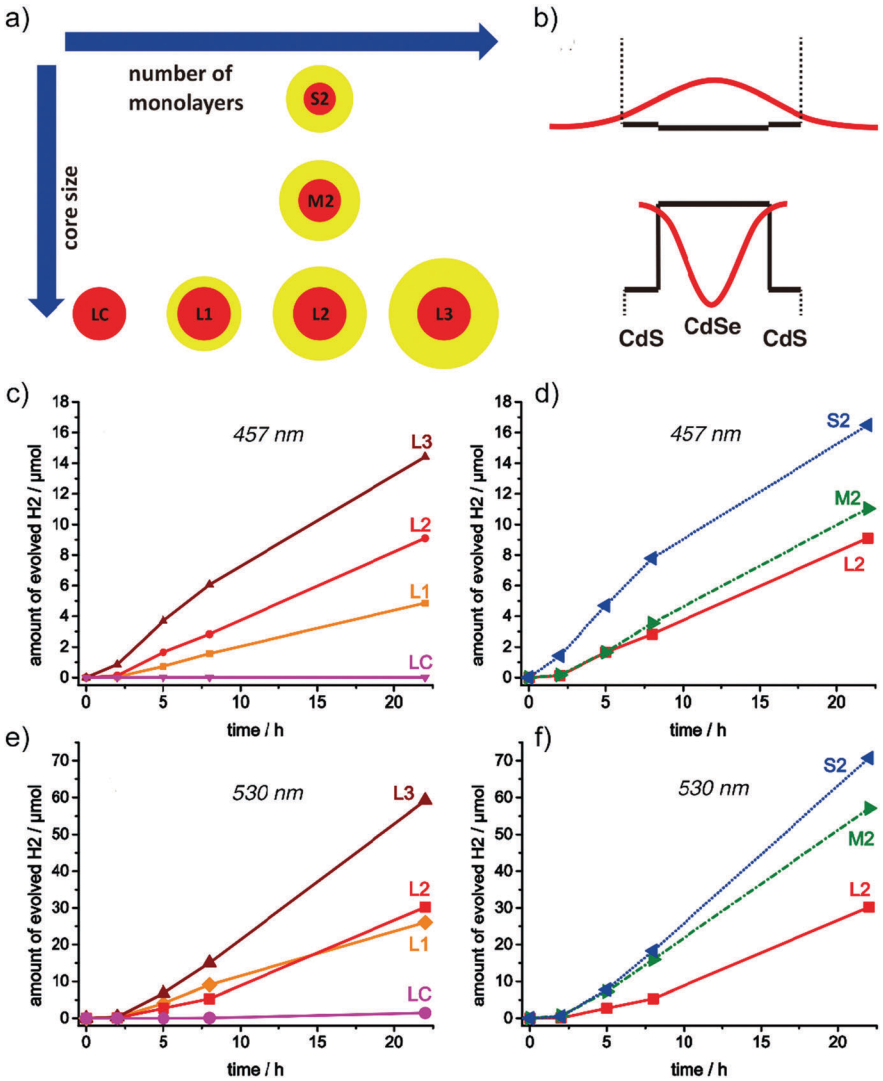

Fig. 19 Schematic illustration of the CdSe/CdS core/shell QDs. (a) Number of monolayers was varied for the larger (3.1 nm) particles. Three different sizes (S, M and L) of particles with 2 monolayers on CdS were also studied. (b) The energy diagram of the QD showing the hole wavefunction localized in the core and delocalized electron wavefunction. Photocatalytic H_2 generation under (c) and (d) 457 nm and (e) and (f) 530 nm laser illumination, varying (c) and (e) the number of monolayers and (d) and (f) core size. Reproduced with permission from ref. 14. Copyright 2015 Walter De Gruyter GmbH.

assembly of hydrogen molecules with the hydrogen atoms supplied by other photochemical agents. Here the latter role is taken by colloidal QDs. Brown *et al.*[36,37] have used naturally occurring *Clostridium acetobutylicum* [Fe–Fe] hydrogenase (CaI) with both CdTe QDs and CdS nanorods, both covered by MPA ligands. The CaI forms a complex with the carboxylate group on the MPA ligands thereby locating the metal centres close to the QD surface, facilitating rapid electron transfer from the QD to the CaI iron–sulfur clusters. Ascorbic acid was used as the sacrificial hole scavenger in both cases. Optimization of the CdTe QD-based system resulted in 1.8% quantum efficiency of H_2 production under AM 1.5G illumination and 9% under monochromatic (532 nm) light. In conjunction with the CdS nanorods the monochromatic QY was 20% measured under 405 nm illumination. Long term stability in these systems was limited by CdTe photodegradation in the first case and loss of MPA from the CdS nanorods in the second case that eventually compromised the hole scavenging pathway as well as colloidal stability. Greene *et al.*[287] also teamed CdTe QDs with a hydrogenase, choosing instead a Ni–Fe hydrogenase derived from *Thiocapsa roseopersicina* (Tr). Again, close coupling to the CdTe QDs was mediated by the use of MPA as the ligand and ascorbic acid was present as the hole scavenger. The justification for this particular hydrogenase was its good chemical stability in a range of buffers, wide pH range and O_2 tolerance, though, as in the work of Brown *et al.*, eventual photo-oxidation of the ligand limited the overall operating times. Hydrogen production in this case had a quantum efficiency of 4%. FTIR difference (excitation on–excitation off) spectra revealed the presence of a number of photoreduction intermediate states when the dye $Ru(bpy)_3^{2+}$ was used in place of the CdTe QDs, but no intermediates when using the QDs. This highlighted the fact that the latter could supply multiple electrons per enzyme reduction cycle whereas the molecular sensitizer could only transfer

 This journal is © The Royal Society of Chemistry 2017

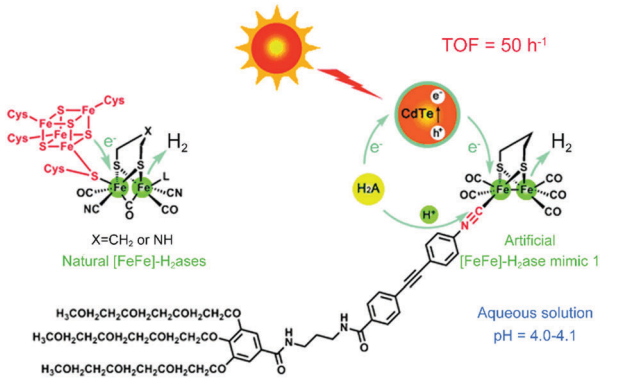

Fig. 20 The structure of natural [FeFe]-H_2ases and artificial [FeFe]-H_2ase mimic 1. Reproduced with permission from ref. 288. Copyright 2011 Wiley-VCH Verlag GmbH & Co. KGaA, Weinheim.

electrons sequentially and so some cycles did not complete and were ineffective with the latter. QDs on the contrary could accumulate multiple electrons ready for fast transfer and complete photoreduction without being blocked until each hole was sequentially removed, *i.e.* the latter process could catch up with independent timing whilst the electrons were acquired and transferred within the enzyme cycle.

The development of far cheaper synthetic mimics of the natural hydrogenase (which require costly isolation and purification steps) was initially limited to organic solvent soluble compounds with poor photochemical stability. However Wang *et al.*[288] succeeded in producing a water soluble (pH 4–4.1) [Fe–Fe] hydrogenase mimic (Fig. 20) which could extend the operating times from 1 h to 8 h with a steady generation rate over the first 6 h.

Further improvements to the stability and H_2 production with similar diiron hydrogenase mimics were obtained by Jian *et al.*[35] and Wang *et al.*[289] In the former case the CdTe QD/MPA/hydrogenase complexes were microencapsulated within chitosan shells. The plentiful hydroxyl groups on the latter are beneficial to maintain CdTe QD colloidal stability at the low operating pH values (4.5) restricting their aggregation especially when faced with MPA photodecomposition. With restriction to the interior of the chitosan domains, the hydrogenase mimic did not require a solubilizing hydrophilic chain unit such as used by Wang *et al.*[288] In the later publication by Wang *et al.*[289] polyacrylic acid with an aromatic side chain linked to the mimic was used and CdSe QDs and ascorbic acid (as the hole scavenger) were absorbed within the resulting water soluble polymer network. In this intimately mixed restricted environment, the H_2 quantum yield reached 5.07%, with operating times of up to 8 h under 450 nm illumination.

5.3. Other co-catalysts

In addition to the precious metals and hydrogenases and hydrogenase mimics already described, other co-catalysts have been used with QDs. Although we have already described work with nickel salt added to MPA capped QDs by Li *et al.*,[286] far higher activity and durability (up to 2 weeks of hydrogen production) were obtained by Han *et al.*[290] using dihydrolipoic acid (DHLA) capped CdSe QDs and DHLA–Ni^{2+} chelates as the co-catalysts, with ascorbic acid as the hole scavenger. DHLA was used to render the initially hydrophobic CdSe QDs water soluble, but also binds strongly to the nickel ions. The CdSe QD diameters investigated restricted light absorption to only 25% of the visible range, but monochromatic illumination (520 nm) indicated that H_2 quantum efficiencies of up to 36% could be obtained in water, and up to 59% in 1 : 1 ethanol/water mixtures. Operating times were found to be limited by the ascorbic acid depletion. Replenishment of the latter allowed hydrogen production to be resumed.

Several groups have investigated the use of molecular complexes of cobalt, coupled directly to the surface of QDs as the photoreduction sites. Huang *et al.*[291] coupled the cobaloxime catalyst with CdSe/ZnS core/shell QDs and studied the carrier generation, transfer and recombination dynamics. Electron transfer times were much faster than recombination times (105 ps compared with >3 ns) measured in toluene solution by transient absorption spectroscopy. H_2 generation also in toluene, with triethanolamine as both the hole scavenger and proton source, saw generation of up to 10^4 mol H_2 per mol catalyst over a period of 10 h but was ultimately limited by photocorrosion of the QDs. Das *et al.*[292] used several water soluble $[Co(bdt)_2]^-$ anions (bdt = bis dithiolene, with various combinations of hydrogen, methyl and chlorine functionalization on the phenyl ring) in conjunction with CdSe QDs, and also compared performance with Ni^{2+}–DHLA co-catalysts. In other studies (*e.g.* Han *et al.*[290]), the latter was found to benefit from the desorption of the DHLA ligand from the QD surface whereas the Co(III) and other co-catalyst based systems did not. Das *et al.*[292] therefore used more tightly binding tridentate thiols to solubilize their QDs, reasoning that this would prevent the ligands from being easily desorbed and interfering with the Co complex operation. Linear H_2 generation from aqueous solutions over periods exceeding 48 h was observed with the trithiol capped CdSe QDs with the best Co co-catalyst being $[Co(tdt)_2]^-$ (tdt = toluene-3,4-dithiolate).

A cationic version of the Co(III) co-catalyst was used by Gimbert-Surinach *et al.*[293] with MPA capped CdTe QDs. Kinetics studies established the scheme for hydrogen evolution shown in Fig. 21 with the two step priming of the Co(III) → Co(II) → Co(I)

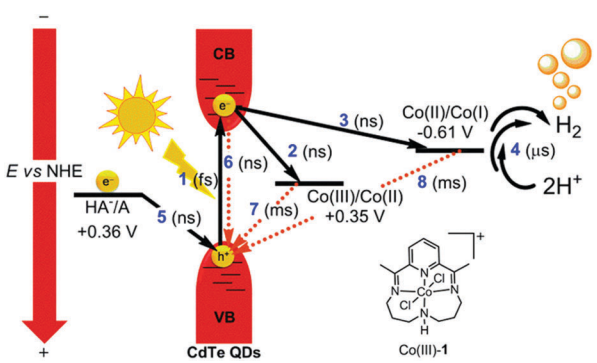

Fig. 21 Energetics and kinetics scheme for the photocatalytic hydrogen-evolving system based on CdTe QDs, cobalt molecular catalyst Co(III)-1, and ascorbic acid/sodium ascorbate. Reproduced with permission from ref. 293. Copyright 2014 American Chemical Society.

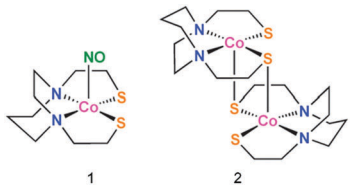

Fig. 22 Structures of molecular cobalt complexes used as co-catalysts with CdTe QDs. Reproduced with permission from ref. 294. Copyright 2015 The Royal Society of Chemistry.

photoreduction site by the transfer of multiple electrons from the QDs being seen as a strongly viable pathway compared with the various back electron transfer and recombination channels. H_2 generation quantum yield was found to be around 10% at best with these materials, but with operating times limited to a few hours.

The relative merits of QD coordinated *vs.* non-coordinated Co(III) complexes were investigated by Han *et al.*,[294] who compared the PL quenching and H_2 generation behavior of TGA stabilized CdTe QDs operating with two metallodithiolate complexes (Fig. 22). Complex **1** in Fig. 22 was found to coordinate *via* the sulfur atoms and bind to the CdTe QD surface whereas the dimeric complex **2** did not attach to the QD surface. PL quenching for the latter was less efficient and was attributed to collisional interactions rather than surface adsorption. The difference in the strength of the interaction of the two complexes with the QDs and how this affected electron transfer were strongly reflected in the H_2 generation rates: with complex **1** the quantum efficiency was 5.32% and operation extended to over 70 h whereas the more weakly interacting complex **2** showed a quantum efficiency of 1.49% and a more limited operation time of 30 h.

5.4. Applications of QDs in photoelectrochemical cells

The foregoing sections of this review described research on one half of the water splitting challenge, the generation of hydrogen gas, with the removal of photogenerated holes being dealt with by using a hole scavenger/electron donor to return the QDs to their neutral state in a timely manner and thus avoid the risk of recombination. Ultimately however the operating time of such photocatalytic conversion materials may be limited by the depletion or degeneration of the hole scavenger if other constituents do not fail first. If the production of oxygen gas is required alongside the hydrogen, or if an alternative use for the separated photogenerated holes is required, then one solution is to use a pair of electrically connected photoelectrodes where the photoreduction and photo-oxidation occur at a charge extracting/injecting substrate. This then dispenses with the need for a hole scavenger in the PEC, though hole/electron shuttles may still be useful to efficiently move charge from the sensitizer to the substrate. Here again, the coupling of QDs to one or other of the electrode substrates is a subject of much research. We will give just a few examples showing how QDs may be coupled to either the anode or the cathode to generate oxygen or hydrogen and supply the counter charge for generation of the corresponding gas at the oppositely charged interface.

The incorporation of QDs into or onto oxide nanotube or nanowire arrays grown on conducting substrates has been investigated by many groups. As such this is very similar to some of the work cited on QDSSCs where the n-type oxide can collect photogenerated electrons from the QDs leaving the geminate holes to oxidize water to form oxygen. The use of p-type QDs such as CdTe is advantageous with n-type oxides for efficient charge separation across the heterointerface between the two materials. Chen *et al.*[295] deposited MPA stabilized CdTe QDs on ZnO nanowires formed on an FTO substrate and characterized their photochemical response in a PEC with a simple Pt plate as the cell counter electrode and a Na_2SO_4 electrolyte. Though not characterized for hydrogen/oxygen generation, the photoconversion efficiency was determined to be 1.83%. Sheng *et al.*[296] used a more elaborate cell design building on the many lessons from QDSSCs. TiO_2 nanotube arrays grown on Ti foil were coated with MPA capped CdTe QDs grown by hydrothermal synthesis. In order to improve the QD durability in the electrolyte used (Na_2SO_3/Na_2S at pH 11.5), the CdTe QDs were coated *in situ* with CdS using several SILAR deposition cycles. In addition to improving resistance to photocorrosion, this also creates a type II heterointerface between the CdTe and the CdS shell, favouring hole localization in the CdTe and electron localization in the CdS. From there the electrons were transferred to the TiO_2 and collected on the Ti foil which was electrically connected to a Pt counter electrode. The photoconversion efficiency of this cell was 6.12% measured under AM 1.5G 1 Sun illumination and photocurrents up to 9.17 mA cm^{-2} were obtained. Oxygen evolution at the nanotube photoanode and hydrogen generation at the Pt cathode were both observed and analysis of the hydrogen content indicated a generation rate of 1.56 mmol W^{-1} h^{-1}. Under illumination, the photocurrent of the CdTe/CdS PEC declined by 5% in the first hour of operation.

The principle for using substrate immobilized QDs at the photocathode was demonstrated by Nann *et al.*[297] InP QDs grown with long chain ligands (hexadecylamine, and zinc salts of stearic and undecanoic acid) were deposited from toluene solution on gold electrodes treated with benzenedithiol. A multilayer deposition process of deposition, drying, and treatment with the dithiol replaced the long chain ligands and cross-linked each successive layer. The [Fe–Fe] hydrogenase mimic, $[Fe_2S_2(CO)_6]$, was introduced into the voids in the dried QD film by deposition from toluene followed by drying to complete the photocathode. The anode was a Pt mesh and the electrolyte an aqueous solution of $NaBF_4$. The current yield was around 60% and after 1 h of illumination at 395 nm 16.2 nmoles of H_2 were generated.

6. Other applications: thermal sensing with QDs

For certain materials and sizes, the fluorescence of QDs is strongly dependent on the local temperature, making them potentially suitable as fluorescent nanothermometers for

 This journal is © The Royal Society of Chemistry 2017

intracellular thermal sensing. In general, an increase in temperature produces a decrease in the fluorescence intensity (quenching), which is accompanied by a spectral shift. The magnitude of both effects (luminescence quenching and spectral shift) depends strongly on the material constituting the QDs and on their size.[298]

Jaque and coworkers[299] systematically investigated the temperature dependence of the two-photon emission of CdTe QDs of different sizes (from ≈1–8 nm), and thermal sensitivities as high as 0.2 °C have been achieved based on multiphoton excited CdTe QDs with extremely small sizes close to 1 nm. Yang and coworkers[300] used streptavidin coated QDs as nanothermometers to get the local temperature response inside single living cells upon external chemical and physical stimuli. The PL spectral shifts from endocytosed QDs were used to map intracellular heat generation in NIH/3T3 cells following Ca^{2+} stress and cold shock.

Using a different mechanism to the previous examples, Zhang and coworkers reported a ligand decoration strategy to enlarge the lattice dilation of QDs, which greatly enhances the characteristic sensitivity of a QD-based thermometer. Macrocyclic compounds (such as thiolated cyclodextrin) when covalently coupled to QDs transmit thermally induced forces to the lattice of CdTe QDs after temperature changes due to their conformation-related torsional rearrangement. Such forces can be detected *via* the deformation potential related shifts in the conduction and valence bands and thereby the bandgap of the QDs[301] (such strain effects are described in the recent review by Jing *et al.*[42]). As an example, β-cyclodextrin-decorated CdTe QDs exhibited a 0.28 nm shift of their spectra per degree centigrade, 2.4-fold higher than those of monothiol-ligand decorated QDs where changes are mainly due to intrinsic lattice dilation.[302]

The temperature dependence of both band edge and surface related trap state luminescence intensity and PL lifetimes can be used to sense temperature changes around QDs (see Fig. 23). Kalytchuk *et al.*[303] recently explored different temperature sensing modes in a range of different sized CdTe QDs (2.3, 2.5, 2.8, 3.0, 3.2 nm) embedded in common salt (NaCl) matrices. In each case the band edge luminescence grew in intensity and blue shifted as the temperature was decreased, but at the same time surface related emission also increased. The ratio of surface to band edge luminescence was greater for the smaller QDs. Decreasing the temperature also increased the PL lifetimes of each emission type but with differing temperature exponents.

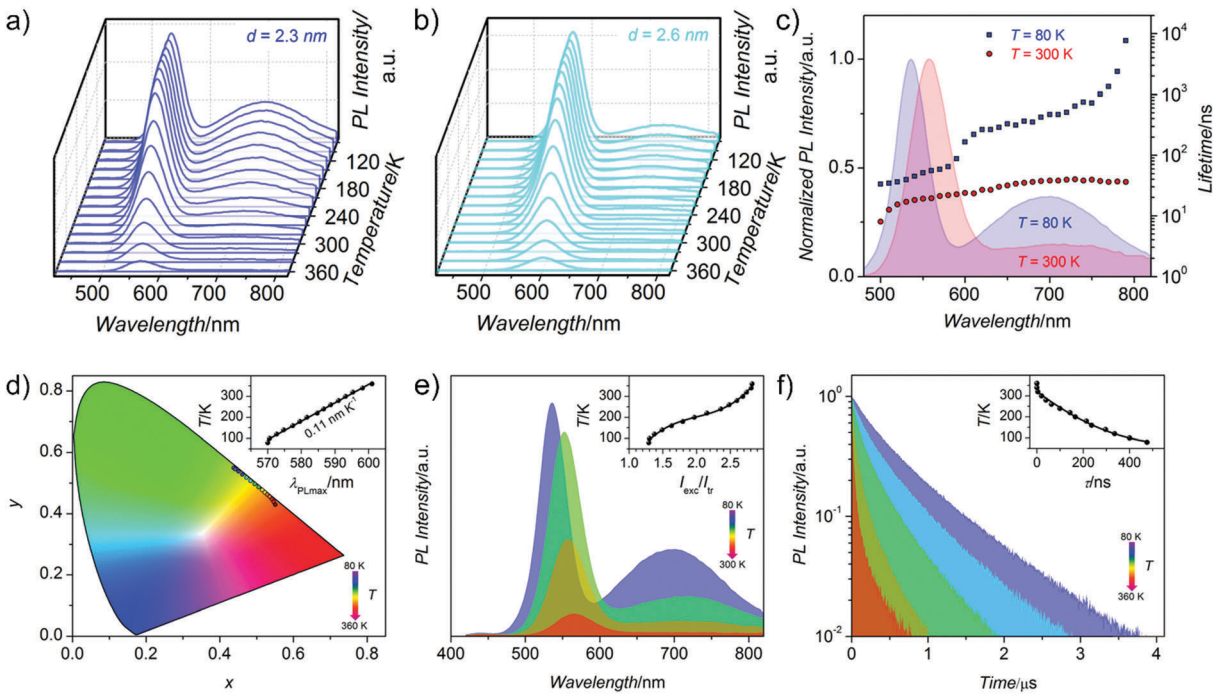

Fig. 23 Normalized 3D plots of the temperature-dependent emission taken in the temperature range from 80 to 360 K with a step of 20 K for CdTe QDs@NaCl powders with a QD size of (a) 2.3 and (b) 2.6. (c) Normalized PL emission profiles of the CdTe QDs@NaCl powder (2.3 nm diameter QDs) at 80 and 300 K (highlighted in blue and red, respectively) and the corresponding wavelength-dependent time-resolved PL lifetimes (symbols). Three detection schemes of luminescence temperature sensing realized with CdTe QDs@NaCl powders: (d) luminescence thermochromic imaging. CIE chromaticity diagram showing the trajectory of (*x*, *y*) coordinates of the CdTe QDs@NaCl powder (2.6 nm diameter QDs) as a function of temperature from 80 to 360 K. The inset shows the linear temperature-induced peak wavelength shift according to eqn (3); (e) ratiometric luminescence thermal sensing using dual emission from the CdTe QDs@NaCl powder (2.3 nm diameter QDs) over a wide temperature range (80–360 K). The inset shows the calculated ratiometric response (integrated area of the excitonic PL relative to trap-related PL) plotted *versus* temperature (where the line follows eqn (4)); (f) PL lifetime thermal sensing. PL decay curves for the CdTe QDs@NaCl powder (2.3 nm diameter QDs) for the trap-related emission at different temperatures. The inset plots the temperature variation of the PL lifetime extracted from the fitting of the decay curves (see the Experimental section for details) plotted *versus* temperature in the range of 80–360 K with the solid line following the calibration curve given by eqn (5). Reproduced with permission from ref. 303. Copyright 2016 Wiley-VCH Verlag GmbH & Co. KGaA, Weinheim.

These temperature dependencies allowed three different sensing modes: (i) luminescence thermochromic imaging where the peak PL emission wavelength can be used to determine temperature, *e.g.*, for 2.6 nm diameter QDs the relationship

$$T = -4921.7 + 8.8\lambda_{\mathrm{PLmax}} \quad (3)$$

could be used as a temperature scale; (ii) ratiometric sensing of the PL intensities of the surface to band edge emission peaks, I_r, according to the relationship

$$T = -1138.4 + 1841.5I_r - 877.5I_r^2 + 146.0I_r^3 \quad (4)$$

for 2.3 nm diameter QDs; and (iii) PL lifetime sensing where the $1/e$ PL lifetime, τ, can be used in the relationship

$$T = 321.8 - 0.85\tau + 7.2 \times 10^{-4}\tau^2 \quad (5)$$

also for 2.3 nm QDs. Method (i) is a useful means of mapping temperature distributions over a surface coated with a film of the QD temperature sensing probe material. The ratiometric method (ii) is insensitive to variations in the probe areal concentration, fluctuations in excitation intensity, variations in detection efficiency, optical occlusions, *etc.* Method (iii) has the merits of not being affected by light scattering, reflections, intensity fluctuations or probe volume/geometry.

7. Conclusions and outlook

The synthetic advances in QD fabrication methods over the past thirty years and perhaps most of all in the last decade have given rise to nanomaterials that are finally starting to fulfil long held promises for technological applications. Foremost of these are the applications in optoelectronics discussed above – QDs may prove to be highly effective and beneficial in display, lighting, sensing and energy generation applications. In reaching the level of maturity to be considered as commercially viable, QDs have had to show and will need to continue to demonstrate that they can make the transition from the lab bench to manufacturing and then operate robustly throughout a realistic product lifetime. This has required the development of sophisticated heterostructures underpinned by a firm understanding of both the synthetic methodology and the nanoscale semiconductor and other physics behind both materials and devices. For many types of optoelectronic devices it has also been necessary to develop further chemical strategies to process the QD materials into solid films with good electrical and optical properties. Here surface chemistry, nanoscale characterization and detailed spectroscopic measurement methods have played a vital role in allowing the QDs to perform to their full potential. In some cases, for example in solar cells and photocatalysts, QDs have been specifically functionalized in order to form hybrid or composite assemblies – a great example of chemistry and physics working hand in hand to develop highly engineered materials for a specific target application. Synthetic methods such as the emerging heat-up approach have started to address the scale – scale up and associated material production cost issues that may also be critical in getting QDs into widespread commercial use.

The strides made in visible light emitting QD LEDs have already made QD displays a reality – in this field the challenges going forward are to improve brightness further and to combat the drop in efficiency at high drive current so that similar QDs may then also be able to make an impact in energy efficient lighting (both indoor and outdoor) applications. Lighting accounts for the consumption of 15–20% of global electricity output, so the economic and environmental benefits of a reduced demand are quite clear. We will come back to the prospects for high brightness QD lighting a little later, but improvements in the EQE for displays is a topic highly relevant for portable displays in that this can support longer battery operation times/permit use of lower capacity, lighter batteries. Even QD emitters that have near 100% internal quantum efficiency can only couple about 20% of that light to the outside world due to the difference in the dielectric permittivity of the semiconductor and the surrounding material. Present best EQEs are already reaching close to 20%,[10] so further improvements are likely to come from pairing QD emitters with plasmonic[304] and photonic micro- and nanostructures,[302] where the dielectric mismatch can be partially offset.

On the energy generation side QDs may ultimately offer benefits in terms of cleaner electricity production, but here, for any major mainstream adoption, the battle to reduce the power cost is currently a rather difficult one for QDs to fight without major improvements in EQE and demonstrated manufacturing cost. One ultimate goal is to bring the generation cost down below that incurred by burning fossil fuels. The 2015 US figure for the Levelized Cost of Energy (LCOE) for coal is around 9.5 cents kW^{-1} h^{-1} and for natural gas 7.5 cents kW^{-1} h^{-1}, whilst for (mainly silicon) solar cell generation it is around 12.5 cents kW^{-1} h^{-1}. A present day typical commercial silicon PV panel has an efficiency of a little over 20%, whilst the Shockley Queisser limit imposes an upper limit of around 30%.[40] Thus, even silicon PVs have to find both a manufacturing cost and EQE breakthrough in order to stand a chance of decisively beating fossil fuel pricing. Related to manufacture, single crystal silicon PVs are expensive to produce in terms of material and energy costs and this in turn is a dominant contributor to the LCOE for solar panels using such PVs. This has driven the development of thin film polysilicon PVs, *etc.* but also mitigates in favour of all other thin film PV technologies including QD based solar cells. Any manufacturing process that uses less energy (lower temperatures/faster production times) will be more competitive. Typically, current commercial silicon PVs will spend the first few years (*e.g.* 3–5) repaying the overall installation costs and mitigating the CO_2 released during their manufacture (*e.g.* in generating the energy required for production). If QD PVs can start to match conventional PVs in terms of performance and service lifetimes, then the potentially lower manufacturing costs and energy inputs could be a key advantage.

In terms of performance, the current state of the art for QD based solar cells has PCEs around 12%,[67] compared with 22% for perovskite film based solar cells.[41] Both technologies have

 This journal is © The Royal Society of Chemistry 2017

to yet to demonstrate credible warranted operating lifetimes though this is now a major focus for the latter.[305] Whilst significant improvements in QD PCEs are of course likely to be very useful, the demonstration of a low manufacturing cost could be just as significant, if the QD PV itself is a major contributor to the overall installed panel cost.

The question for the humble materials scientists is whether we can find any substantial material improvements to radically shift the balance. A commonly held view is that carrier multiplication may be able to boost solar cell performance, which is far more favourable in many QDs than in bulk crystalline silicon.[42] However, the exact quantification of the benefits with realistic QD thresholds and slopes[306] shows that the improvement to the theoretical QD solar cell performance attributable to multiplication is rather modest or even highly marginal.[307] More recent theoretical work has suggested that the use of core/shell structures and attractive rather than repulsive biexciton binding energies are a prerequisite to realizing any significant improvement in solar cell performance.[308] Whilst any MEG effect would help, clearly the main effort should be applied elsewhere in the solar cell, with improvements in carrier extraction and collection probably being far more important.

Visible range QD photodetectors will find it hard to compete with standard discrete bulk silicon photodiodes since the latter are virtually a few pennies per device technology. Any new QD technology in this market must offer either vastly improved performance or some integration or other functionality advantage. The former is difficult – cooled silicon CCDs can operate at extremely low, single photon counting levels, but less high spec QD photodetectors could be integrated with other QD microelectronic components, *e.g.* QD field effect transistors (FETs)[309] and potentially printable circuits constructed on flexible, non-epitaxial substrates.[310,311] In addition to FETs, other key electronic structures have already been demonstrated in QDs: Schottky junctions, (depleted) heterojunctions, p–i–n structures, so there is already a potential QD microelectronic toolbox. A key step to making this type of technology more commercially attractive is to improve carrier mobilities in QD films.[311] Recent work by Kagan and coworkers[312] has demonstrated high electron mobilities in CdSe QDs which are certainly useful and may be a signature of band-like carrier transport.[313] As an indirect semiconductor it is also difficult to make silicon emit light efficiently though it has been demonstrated in doped and quantum confined silicon structures. There may therefore be a niche area where visible range QD light emitters integrated with QD microelectronic functions could usefully compete with existing bulk silicon technology.

Low light level signals from photodetectors generally require amplification before being used and this is often essentially a charge multiplication process. In photomultiplier tubes several serial two- or three-fold multiplications can amass a net gain of at least 10^5 if not more, but with very good signal to noise ratios. The solid state equivalent is the avalanche photodiode (APD) where multiplication takes place in several sequential impact ionization (inverse of Auger recombination) steps with kinetic energy being supplied to the incident and multiplied charges *via* an applied electric field. Gain in photodiodes using this effect is distinct from the current gain in photoconductive (non-photodiode) QD devices already widely seen (as described in Section 3). Photodiode structures with avalanche mode gain would be able to operate at much higher frequencies than such photoconductors. It is already well known that carrier multiplication without an externally applied field can occur in many types of QDs[42] and indeed similar strategies to those used in bulk APD design can be copied in QD versions of the same materials to enhance multiplication.[314,315] A potentially fruitful approach might be to explore the possibility of multiple impact ionization chains in QD films under applied electric fields as a means of producing a QD APD.

In the IR, beyond the bandgaps for silicon and established materials such as InGaAs the photodetector playing field is a little more even. All IR semiconductor technologies face the same physics – the radiative recombination rates all fall at least linearly as the transition frequency drops, rapidly making the radiative transition of little concern for photodetectors. Non-radiative recombination processes are the major competition for photocurrent extraction and there are already signs that in terms of detectivities QD based IR photodetectors are beginning to compete with commercial devices, and may offer serious advantages in operation due to the reduced need for cooling.

To achieve good IR photodetector performance, it is vital that the several different types of non-radiative recombination processes that can occur in this region[256] are understood and appropriate efforts devoted to taking steps to minimize them. Synthetic strategies giving better surface quality can reduce the number of surface traps and thwart polaron formation which is instrumental in one mechanism for coupling the energy of excitons to near surface vibrational modes in ligands, *etc.* An alternative mechanism *via* resonant energy transfer as an adiabatic electronic donor to vibrational state acceptor process must be addressed by either removing the acceptor altogether (using non-IR absorbing ligands or host materials[316]) or at least putting the acceptor further away from the donor by interposing a shell layer.

Alongside such strategies to minimize the loss of photogenerated carriers by non-radiative relaxation, the photocurrent can be improved by better electron and hole extraction and transport to the respective electrodes. In the latter respect, again QDs with improved carrier mobilities are desirable. There is some evidence that near field effects in QD/plasmonic hybrids can also enhance the former.[33]

Whilst visible emitting QD LEDs are already a success story, the challenges for IR LEDs are somewhat harder. Such devices would again be useful for low cost and portable sensor applications (as light sources rather than detectors) but here the challenge is how to improve the rather low radiative rates in the face of much more rapid non-radiative recombination. As for IR photodetectors, reducing the non-radiative rate is a primary approach, but increasing the radiative rate can be viewed as more of a fundamental challenge. Most simple dielectric environments can only reduce rather than accelerate radiative recombination, but coupling QDs to photonic cavities could

offer a means to improve radiative rates. Combining QDs with photonic nanostructures also offers other potential advantages as well (*e.g.* improved LED EQEs as mentioned above). A recent article by Eggleston *et al.*[317] also offers another approach to using an external resonator coupled to QDs to enhance spontaneous radiative emission rates that might be further explored for IR LED devices.

Burning fossil fuels does a great deal of harm to the planet's biosphere – and aside from electricity generation, our dependence on fossil fuel based transport is a major contributor to the environmental toll. QDs may offer at least part of the solution by direct photocatalytic conversion of sunlight to hydrogen gas and indeed a further objective would be complete water splitting to produce both hydrogen and oxygen simultaneously. Whilst we have seen that QD photocatalysed hydrogen generation is already well known, challenges remain with regard to improvement of overall generation efficiency, durability of both the QD and co-catalyst combinations and also the hole scavengers.

In contemplating the progress so far and the challenges remaining for QDs in commercial applications there is one clear and simple observation that can be made: so far, the leading QD applications such as biomedical probes, television screen down conversion phosphors, *etc.*, have in common that the QDs operate *via* the absorption of light, whereas applications that require the injection or extraction of charges (photodetectors, QD microelectronics, LEDs, *etc.*) have proved a much greater challenge and are much more difficult to bring to market. Improvements and innovations in carrier injection, extraction and transport are therefore going to have a great deal of value when it comes to future commercialization.

So, what is coming over the materials horizon that might help with all of these QD applications? Undoubtedly in many instances there is plenty of scope for improvements simply by continuing to develop functional structures of QDs coupled to other nanoparticles and molecules. The development of thicker shelled (>10 shell monolayers) QDs[318,319] and core/shell QDs with graded, less sharp transitions between the core and shell[320,321] has proved to be useful in partly combating Auger relaxation and has started to open up a pathway to devices that can exploit multiexciton optoelectronic effects. Whilst Klimov's and other groups were instrumental in showing that with the bandgap tunability benefits of 3D quantum confinement came the additional headache of enhanced Auger recombination[322,323] it seems now that it is possible to reduce the severity of the latter by toning down the confinement to 1D. By fabricating CdSe, CdS and CdTe nanoplatelets Ithurria *et al.*[324,325] showed evidence of enhanced exciton radiative recombination rates and long biexciton lifetimes. Rowland *et al.*[326] similarly showed long biexciton lifetimes (up to 500 ps) and also demonstrated FRET and multiexciton transfer between platelets. Good overlap between adjacent platelets may also prove to favour improved carrier mobilities. This could be useful not only in generally improving the performance of QD electronic structures, but in depleted heterojunction solar cells, for example, it may conceivably extend the carrier diffusion region, helping to improve the useful absorption depth and short circuit photocurrents and device fill factors.

Recently Izquierdo *et al.*[327] have extended the nanoplatelet template to HgTe and HgSe by first synthesizing Cd chalcogenides and then ion exchanging the Cd^{2+} for Hg^{2+} ions to produce materials emitting close to 900 nm in the near IR. If the reduced confinement can still allow bandgap tuning into the mid-IR whilst also exhibiting slow biexciton recombination this may well prove to be a candidate material for QD IR APD detectors.

Sustained multiexciton populations in semiconductor nanoplatelets may possibly be of interest in the development of steady state, electrically driven lasers. Geiregat *et al.*[328] have already demonstrated extension of the gain-lifetime to around 100 ns using doped HgTe QDs and suggest that this is close to the level necessary to support steady state operation under electrical excitation. It will be of interest to explore whether HgTe nanoplatelets can also maintain sufficient excited state population to permit electrically driven operation.

Wider bandgap nanoplatelets may also prove to be ideal for high brightness QD lighting applications – provided biexciton lifetimes can be made to approach the single exciton radiative recombination times, whilst the areal emitted photon fluence will have to exceed that which could be obtained from an identical mass of QDs to be beneficial.

Longer biexciton lifetimes would also be highly beneficial in solar cell applications, provided the additional carriers can be extracted rapidly enough, before radiative recombination occurs. Enhanced biexciton sustainability is not just beneficial where carrier multiplication occurs – even without MEG there are potential benefits. In concentrated solar systems the PV elements must be able to efficiently convert high incident fluences (*e.g.* $\times 100$ Suns) to photocurrent without losing excitons in multiply occupied QDs to Auger recombination. Of course, these are quite extreme conditions and there are plenty of other practical issues to solve before nanoplatelets might be used in such situations, but it is worth pondering their benefits in such applications.

Acknowledgements

The authors acknowledge funding from the National Natural Science Foundation of China (81530057, 81671755, 21203210), from the Research Grants Council of the Hong Kong S.A.R., China (CityU 11302114, T23-713/11), and from the Germany/Hong Kong Joint Research Scheme sponsored by the Research Grants Council of Hong Kong and the German Academic Exchange Service (G-CityU110/14).

Notes and references

1 G. H. Carey, A. L. Abdelhady, Z. Ning, S. M. Thon, O. M. Bakr and E. H. Sargent, *Chem. Rev.*, 2015, **15**, 12732–12763.
2 E. H. Sargent, *Nat. Photonics*, 2012, **6**, 133–135.
3 C. R. Kagan, E. Lifshitz, E. H. Sargent and D. V. Talapin, *Science*, 2016, **353**(6302), aac5523.
4 M. X. Liu, O. Voznyy, R. Sabatini, F. P. Garcia de Arquer, R. Munir, A. H. Balawi, X. Z. Lan, F. J. Fan, G. Walters,

 This journal is © The Royal Society of Chemistry 2017

A. R. Kirmani, S. Hoogland, F. Laquai, A. Amassian and E. H. Sargent, *Nat. Mater.*, 2016, DOI: 10.1038/NMAT4800.
5 E. H. Sargent, *Adv. Mater.*, 2008, **20**, 3958–3964.
6 S. A. McDonald, G. Konstantatos, S. G. Zhang, P. W. Cyr, E. J. D. Klem, L. Levina and E. H. Sargent, *Nat. Mater.*, 2005, **4**, 138–142.
7 S. Keuleyan, E. Lhuillier, V. Brajuskovic and P. Guyot-Sionnest, *Nat. Photonics*, 2011, **5**, 489–493.
8 M. Y. Chen, H. Yu, S. V. Kershaw, H. H. Xu, S. Gupta, F. Hetsch, A. L. Rogach and N. Zhao, *Adv. Funct. Mater.*, 2014, **24**, 53–59.
9 P. O. Anikeeva, J. E. Halpert, M. G. Bawendi and V. Bulovic, *Nano Lett.*, 2009, **9**, 2532–2536.
10 B. S. Mashford, M. Stevenson, Z. Popovic, C. Hamilton, Z. Zhou, C. Breen, J. Steckel, V. Bulovic, M. Bawendi, S. Coe-Sullivan and P. T. Kazlas, *Nat. Photonics*, 2013, **7**, 407–412.
11 Y. Shirasaki, G. J. Supran, M. G. Bawendi and V. Bulovic, *Nat. Photonics*, 2013, **7**, 13–23.
12 A. Vaneski, J. Schneider, A. S. Susha and A. L. Rogach, *J. Photochem. Photobiol., C*, 2014, **19**, 52–61.
13 M. J. Berr, P. Wagner, S. Fischbach, A. Vaneski, J. Schneider, A. S. Susha, A. L. Rogach, F. Jackel and J. Feldmann, *Appl. Phys. Lett.*, 2012, **100**, 223903.
14 F. Ehrat, T. Simon, J. K. Stolarczyk and J. Feldmann, *Z. Phys. Chem.*, 2015, **229**, 205–219.
15 M. B. Wilker, K. J. Schnitzenbaumer and G. Dukovic, *Isr. J. Chem.*, 2012, **52**, 1002–1015.
16 L. Carbone and P. D. Cozzoli, *Nano Today*, 2010, **5**, 449–493.
17 P. D. Cozzoli and L. Manna, in *Bio-Applications of Nanoparticles*, ed. W. C. W. Chan, 2007, vol. 620, pp. 1–17.
18 H. McDaniel, P. E. Heil, C. L. Tsai, K. Kim and M. Shim, *ACS Nano*, 2011, **5**, 7677–7683.
19 J. M. Luther, H. M. Zheng, B. Sadtler and A. P. Alivisatos, *J. Am. Chem. Soc.*, 2009, **131**, 16851–16857.
20 D. J. Milliron, S. M. Hughes, Y. Cui, L. Manna, J. B. Li, L. W. Wang and A. P. Alivisatos, *Nature*, 2004, **430**, 190–195.
21 D. V. Talapin, J. H. Nelson, E. V. Shevchenko, S. Aloni, B. Sadtler and A. P. Alivisatos, *Nano Lett.*, 2007, **7**, 2951–2959.
22 A. Fiore, R. Mastria, M. G. Lupo, G. Lanzani, C. Giannini, E. Carlino, G. Morello, M. De Giorgi, Y. Li, R. Cingolani and L. Manna, *J. Am. Chem. Soc.*, 2009, **131**, 2274–2282.
23 J. E. Govan, E. Jan, A. Querejeta, N. A. Kotov and Y. K. Gun'ko, *Chem. Commun.*, 2010, **46**, 6072–6074.
24 L. Manna, E. C. Scher and A. P. Alivisatos, *J. Am. Chem. Soc.*, 2000, **122**, 12700–12706.
25 C. Nobile, S. Kudera, A. Fiore, L. Carbone, G. Chilla, T. Kipp, D. Heitmann, R. Cingolani, L. Manna and R. Krahne, *Phys. Status Solidi A*, 2007, **204**, 483–486.
26 S. L. Teich-McGoldrick, M. Bellanger, M. Caussanel, L. Tsetseris, S. T. Pantelides, S. C. Glotzer and R. D. Schrimpf, *Nano Lett.*, 2009, **9**, 3683–3688.
27 A. Vaneski, J. Schneider, A. S. Susha and A. L. Rogach, *APL Mater.*, 2014, **2**, 012104.
28 http://www.nanosysinc.com/#lcd-revolution.
29 J. McKittrick and L. E. Shea-Rohwer, *J. Am. Ceram. Soc.*, 2014, **97**, 1327–1352.
30 Y. Shirasaki, G. J. Supran, W. A. Tisdale and V. Bulovic, *Phys. Rev. Lett.*, 2013, **110**, 217403.
31 L. Su, X. Zhang, Y. Zhang and A. L. Rogach, *Top. Curr. Chem.*, 2016, **374**, 42.
32 E. Lhuillier, S. Keuleyan and P. Guyot-Sionnest, *Nanotechnology*, 2012, **23**, 175705.
33 M. Chen, L. Shao, S. V. Kershaw, H. Yu, J. Wang, A. L. Rogach and N. Zhao, *ACS Nano*, 2014, **8**, 8208–8216.
34 M. Chen, H. Yu, S. V. Kershaw, H. Xu, S. Gupta, F. Hetsch, A. L. Rogach and N. Zhao, *Adv. Funct. Mater.*, 2014, **24**, 53–59.
35 J.-X. Jian, Q. Liu, Z.-J. Li, F. Wang, X.-B. Li, C.-B. Li, B. Liu, Q.-Y. Meng, B. Chen, K. Feng, C.-H. Tung and L.-Z. Wu, *Nat. Commun.*, 2013, **4**, 2695.
36 K. A. Brown, M. B. Wilker, M. Boehm, G. Dukovic and P. W. King, *J. Am. Chem. Soc.*, 2012, **134**, 5627–5636.
37 K. A. Brown, S. Dayal, X. Ai, G. Rumbles and P. W. King, *J. Am. Chem. Soc.*, 2010, **132**, 9672–9680.
38 K. A. Brown, Q. Song, D. W. Mulder and P. W. King, *ACS Nano*, 2014, **8**, 10790–10798.
39 T. Nann, S. K. Ibrahim, P. M. Woi, S. Xu, J. Ziegler and C. J. Pickett, *Angew. Chem., Int. Ed.*, 2010, **49**, 1574–1577.
40 W. Shockley and H. J. Queisser, *J. Appl. Phys.*, 1961, **32**, 510–519.
41 L. Dou, A. B. Wong, Y. Yu, M. Lai, N. Kornienko, S. W. Eaton, A. Fu, C. G. Bischak, J. Ma, T. Ding, N. S. Ginsberg, L.-W. Wang, A. P. Alivisatos and P. Yang, *Science*, 2015, **349**, 1518–1521.
42 L. H. Jing, S. V. Kershaw, Y. L. Li, X. D. Huang, Y. Y. Li, A. L. Rogach and M. Y. Gao, *Chem. Rev.*, 2016, **116**, 10623–10730.
43 K. Hola, Y. Zhang, Y. Wang, E. P. Giannelis, R. Zboril and A. L. Rogach, *Nano Today*, 2014, **9**, 590–603.
44 X. M. Li, M. C. Rui, J. Z. Song, Z. H. Shen and H. B. Zeng, *Adv. Funct. Mater.*, 2015, **25**, 4929–4947.
45 M. L. Mastronardi, E. J. Henderson, D. P. Puzzo and G. A. Ozin, *Adv. Mater.*, 2012, **24**, 5890–5898.
46 F. Priolo, T. Gregorkiewicz, M. Galli and T. F. Krauss, *Nat. Nanotechnol.*, 2014, **9**, 19–32.
47 M. Dasog, J. Kehrle, B. Rieger and J. G. C. Veinot, *Angew. Chem., Int. Ed.*, 2016, **55**, 2322–2339.
48 D. D. Vaughn and R. E. Schaak, *Chem. Soc. Rev.*, 2013, **42**, 2861–2879.
49 A. J. Nozik, M. C. Beard, J. M. Luther, M. Law, R. J. Ellingson and J. C. Johnson, *Chem. Rev.*, 2010, **110**, 6873–6890.
50 S. Emin, S. P. Singh, L. Y. Han, N. Satoh and A. Islam, *Sol. Energy*, 2011, **85**, 1264–1282.
51 M. R. Kim, Z. Xu, G. Chen and D. Ma, *Chem. – Eur. J.*, 2014, **20**, 11256–11275.
52 X. Lan, S. Masala and E. H. Sargent, *Nat. Mater.*, 2014, **13**, 233–240.
53 M. R. Kim and D. Ma, *J. Phys. Chem. Lett.*, 2015, **6**, 85–99.
54 S. G. Kwon and T. Hyeon, *Acc. Chem. Res.*, 2008, **41**, 1696–1709.

55 F. Hetsch, X. Xu, H. Wang, S. V. Kershaw and A. L. Rogach, *J. Phys. Chem. Lett.*, 2011, **2**, 1879–1887.
56 S. Ruhle, M. Shalom and A. Zaban, *ChemPhysChem*, 2010, **11**, 2290–2304.
57 D. A. Hines and P. V. Kamat, *ACS Appl. Mater. Interfaces*, 2014, **6**, 3041–3057.
58 H. Liu, J. Tang, I. J. Kramer, R. Debnath, G. I. Koleilat, X. Wang, A. Fisher, R. Li, L. Brzozowski, L. Levina and E. H. Sargent, *Adv. Mater.*, 2011, **23**, 3832–3837.
59 A. H. Ip, A. J. Labelle and E. H. Sargent, *Appl. Phys. Lett.*, 2013, **103**, 263905.
60 K. Ramasamy, M. A. Malik, N. Revaprasadu and P. O'Brien, *Chem. Mater.*, 2013, **25**, 3551–3569.
61 S. P. Mondal and S. K. Ray, *Proc. Natl. Acad. Sci., India, Sect. A*, 2012, **82**, 21–29.
62 H. Fu and S.-W. Tsang, *Nanoscale*, 2012, **4**, 2187–2201.
63 F. Purcell-Milton and Y. K. Gun'ko, *J. Mater. Chem.*, 2012, **22**, 16687–16697.
64 R. B. Jiang, B. X. Li, C. H. Fang and J. F. Wang, *Adv. Mater.*, 2014, **26**, 5274–5309.
65 T. Franzl, T. A. Klar, S. Schietinger, A. L. Rogach and J. Feldmann, *Nano Lett.*, 2004, **4**, 1599–1603.
66 J. van Embden, A. S. R. Chesman and J. J. Jasieniak, *Chem. Mater.*, 2015, **27**, 2246–2285.
67 J. Du, Z. Du, J.-S. Hu, Z. Pan, Q. Shen, J. Sun, D. Long, H. Dong, L. Sun, X. Zhong and L.-J. Wan, *J. Am. Chem. Soc.*, 2016, **138**, 4201–4209.
68 I. Robel, V. Subramanian, M. Kuno and P. V. Kamat, *J. Am. Chem. Soc.*, 2006, **128**, 2385–2393.
69 I. Mora-Sero, J. Bisquert, T. Dittrich, A. Belaidi, A. S. Susha and A. L. Rogach, *J. Phys. Chem. C*, 2007, **111**, 14889–14892.
70 K. S. Leschkies, R. Divakar, J. Basu, E. Enache-Pommer, J. E. Boercker, C. B. Carter, U. R. Kortshagen, D. J. Norris and E. S. Aydil, *Nano Lett.*, 2007, **7**, 1793–1798.
71 A. Kongkanand, K. Tvrdy, K. Takechi, M. Kuno and P. V. Kamat, *J. Am. Chem. Soc.*, 2008, **130**, 4007–4015.
72 Q. Shen, J. Kobayashi, L. J. Diguna and T. Toyoda, *J. Appl. Phys.*, 2008, **103**, 084304.
73 H. J. Lee, J.-H. Yum, H. C. Leventis, S. M. Zakeeruddin, S. A. Haque, P. Chen, S. I. Seok, M. Grätzel and M. K. Nazeeruddin, *J. Phys. Chem. C*, 2008, **112**, 11600–11608.
74 J. H. Bang and P. V. Kamat, *ACS Nano*, 2009, **3**, 1467–1476.
75 H. Lee, M. Wang, P. Chen, D. R. Gamelin, S. M. Zakeeruddin, M. Grätzel and M. K. Nazeeruddin, *Nano Lett.*, 2009, **9**, 4221–4227.
76 I. Mora-Sero, S. Gimenez, F. Fabregat-Santiago, R. Gomez, Q. Shen, T. Toyoda and J. Bisquert, *Acc. Chem. Res.*, 2009, **42**, 1848–1857.
77 G. Sixto, M.-S. Iván, M. Lorena, G. Nestor, L.-V. Teresa, G. Roberto, J. D. Lina, S. Qing, T. Taro and B. Juan, *Nanotechnology*, 2009, **20**, 295204.
78 S. H. Im, Y. H. Lee, S. I. Seok, S. W. Kim and S.-W. Kim, *Langmuir*, 2010, **26**, 18576–18580.
79 A. Salant, M. Shalom, I. Hod, A. Faust, A. Zaban and U. Banin, *ACS Nano*, 2010, **4**, 5962–5968.
80 X. Hu, Q. X. Zhang, X. M. Huang, D. M. Li, Y. H. Luo and Q. B. Meng, *J. Mater. Chem.*, 2011, **21**, 15903–15905.
81 Z. J. Ning, C. Z. Yuan, H. N. Tian, Y. Fu, L. Li, L. C. Sun and H. Agren, *J. Mater. Chem.*, 2012, **22**, 6032–6037.
82 H. McDaniel, N. Fuke, J. M. Pietryga and V. I. Klimov, *J. Phys. Chem. Lett.*, 2013, **4**, 355–361.
83 J. Wang, I. Mora-Sero, Z. X. Pan, K. Zhao, H. Zhang, Y. Y. Feng, G. Yang, X. H. Zhong and J. Bisquert, *J. Am. Chem. Soc.*, 2013, **135**, 15913–15922.
84 Z. X. Pan, K. Zhao, J. Wang, H. Zhang, Y. Y. Feng and X. H. Zhong, *ACS Nano*, 2013, **7**, 5215–5222.
85 D. A. Hines and P. V. Kamat, *J. Phys. Chem. C*, 2013, **117**, 14418–14426.
86 K. M. Coughlin, J. S. Nevins and D. F. Watson, *ACS Appl. Mater. Interfaces*, 2013, **5**, 8649–8654.
87 D. Pan, D. Weng, X. Wang, Q. Xiao, W. Chen, C. Xu, Z. Yang and Y. Lu, *Chem. Commun.*, 2009, 4221–4223, DOI: 10.1039/B905151A.
88 J. H. Luo, H. Y. Wei, F. Li, Q. L. Huang, D. M. Li, Y. H. Luo and Q. B. Meng, *Chem. Commun.*, 2014, **50**, 3464–3466.
89 L. Tao, Y. Xiong, H. Liu and W. Z. Shen, *Nanoscale*, 2014, **6**, 931–938.
90 A. N. Jumabekov, F. Deschler, D. Böhm, L. M. Peter, J. Feldmann and T. Bein, *J. Phys. Chem. C*, 2014, **118**, 5142–5149.
91 S. Kim, J. H. Heo, J. H. Noh, S.-W. Kim, S. H. Im and S. I. Seok, *ChemPhysChem*, 2014, **15**, 1024–1027.
92 Z. L. Chen, F. Y. Liu, Q. S. Zeng, Z. K. Cheng, X. H. Du, G. Jin, H. Zhang and B. Yang, *J. Mater. Chem. A*, 2015, **3**, 10969–10975.
93 J. Huang, B. Xu, C. Yuan, H. Chen, J. Sun, L. Sun and H. Ågren, *ACS Appl. Mater. Interfaces*, 2014, **6**, 18808–18815.
94 S. Jiao, Q. Shen, I. Mora-Sero, J. Wang, Z. X. Pan, K. Zhao, Y. Kuga, X. H. Zhong and J. Bisquert, *ACS Nano*, 2015, **9**, 908–915.
95 D. S. Ginger and N. C. Greenham, *Phys. Rev. B: Condens. Matter Mater. Phys.*, 1999, **59**, 10622–10629.
96 W. U. Huynh, J. J. Dittmer and A. P. Alivisatos, *Science*, 2002, **295**, 2425–2427.
97 I. Gur, N. A. Fromer, C.-P. Chen, A. G. Kanaras and A. P. Alivisatos, *Nano Lett.*, 2007, **7**, 409–414.
98 X. Jiang, R. D. Schaller, S. B. Lee, J. M. Pietryga, V. I. Klimov and A. A. Zakhidov, *J. Mater. Res.*, 2007, **22**, 2204–2210.
99 L. Wang, Y. Liu, X. Jiang, D. Qin and Y. Cao, *J. Phys. Chem. C*, 2007, **111**, 9538–9542.
100 J. Bang, J. Park, J. H. Lee, N. Won, J. Nam, J. Lim, B. Y. Chang, H. J. Lee, B. Chon, J. Shin, J. B. Park, J. H. Choi, K. Cho, S. M. Park, T. Joo and S. Kim, *Chem. Mater.*, 2010, **22**, 233–240.
101 H. Z. Zhong and G. D. Scholes, *J. Am. Chem. Soc.*, 2009, **131**, 9170–9171.
102 H. Z. Zhong, Y. Zhou, Y. Yang, C. H. Yang and Y. F. Li, *J. Phys. Chem. C*, 2007, **111**, 6538–6543.
103 S. Dayal, H. Z. Zhong, N. Kopidakis, G. D. Scholes and G. Rumbles, *J. Photonics Energy*, 2015, **5**, 057409.
104 Y. C. Li, H. Z. Zhong, R. Li, Y. Zhou, C. H. Yang and Y. F. Li, *Adv. Funct. Mater.*, 2006, **16**, 1705–1716.

 This journal is © The Royal Society of Chemistry 2017

105 Z. Yi, L. Yunchao, Z. Haizheng, H. Jianhui, D. Yuqin, Y. Chunhe and L. Yongfang, *Nanotechnology*, 2006, **17**, 4041.
106 H. T. Wei, H. Z. Sun, H. Zhang, W. L. Yu, F. Zhai, Z. X. Fan, W. J. Tian and B. Yang, *J. Mater. Chem.*, 2012, **22**, 9161–9165.
107 J. Briscoe, D. E. Gallardo, S. Hatch, V. Lesnyak, N. Gaponik and S. Dunn, *J. Mater. Chem.*, 2011, **21**, 2517–2523.
108 I. Gur, N. A. Fromer, M. L. Geier and A. P. Alivisatos, *Science*, 2005, **310**, 462–465.
109 S. Kitada, E. Kikuchi, A. Ohno, S. Aramaki and S. Maenosono, *Solid State Commun.*, 2009, **149**, 1853–1855.
110 Y. Li, R. Mastria, A. Fiore, C. Nobile, L. Yin, M. Biasiucci, G. Cheng, A. M. Cucolo, R. Cingolani, L. Manna and G. Gigli, *Adv. Mater.*, 2009, **21**, 4461–4466.
111 D. Gross, I. Mora-Sero, T. Dittrich, A. Belaidi, C. Mauser, A. J. Houtepen, E. Da Como, A. L. Rogach and J. Feldmann, *J. Am. Chem. Soc.*, 2010, **132**, 5981–5983.
112 A. G. Pattantyus-Abraham, I. J. Kramer, A. R. Barkhouse, X. Wang, G. Konstantatos, R. Debnath, L. Levina, I. Raabe, M. K. Nazeeruddin, M. Grätzel and E. H. Sargent, *ACS Nano*, 2010, **4**, 3374–3380.
113 N. Zhao, T. P. Osedach, L.-Y. Chang, S. M. Geyer, D. Wanger, M. T. Binda, A. C. Arango, M. G. Bawendi and V. Bulovic, *ACS Nano*, 2010, **4**, 3743–3752.
114 Z. X. Cai, G. X. Chen, X. Huang and M. H. Ma, *Sens. Actuators, B*, 2011, **157**, 368–373.
115 X. H. Wang, G. I. Koleilat, J. Tang, H. Liu, I. J. Kramer, R. Debnath, L. Brzozowski, D. A. R. Barkhouse, L. Levina, S. Hoogland and E. H. Sargent, *Nat. Photonics*, 2011, **5**, 480–484.
116 M. J. Greaney, S. Das, D. H. Webber, S. E. Bradforth and R. L. Brutchey, *ACS Nano*, 2012, **6**, 4222–4230.
117 N. Yaacobi-Gross, N. Garphunkin, O. Solomeshch, A. Vaneski, A. S. Susha, A. L. Rogach and N. Tessler, *ACS Nano*, 2012, **6**, 3128–3133.
118 I. J. Kramer, D. Zhitomirsky, J. D. Bass, P. M. Rice, T. Topuria, L. Krupp, S. M. Thon, A. H. Ip, R. Debnath, H.-C. Kim and E. H. Sargent, *Adv. Mater.*, 2012, **24**, 2315–2319.
119 H. Liu, D. Zhitomirsky, S. Hoogland, J. Tang, I. J. Kramer, Z. Ning and E. H. Sargent, *Appl. Phys. Lett.*, 2012, **101**, 151112.
120 S. M. Willis, C. Cheng, H. E. Assender and A. A. R. Watt, *Nano Lett.*, 2012, **12**, 1522–1526.
121 P. Maraghechi, A. J. Labelle, A. R. Kirmani, X. Lan, M. M. Adachi, S. M. Thon, S. Hoogland, A. Lee, Z. Ning, A. Fischer, A. Amassian and E. H. Sargent, *ACS Nano*, 2013, **7**, 6111–6116.
122 I. J. Kramer, G. Moreno-Bautista, J. C. Minor, D. Kopilovic and E. H. Sargent, *Appl. Phys. Lett.*, 2014, **105**, 163902.
123 Z. Chen, H. Zhang, Q. Zeng, Y. Wang, D. Xu, L. Wang, H. Wang and B. Yang, *Adv. Energy Mater.*, 2014, **4**, 1400235.
124 G.-H. Kim, B. Walker, H.-B. Kim, J. Y. Kim, E. H. Sargent, J. Park and J. Y. Kim, *Adv. Mater.*, 2014, **26**, 3321–3327.
125 H. Wang, T. Kubo, J. Nakazaki and H. Segawa, *Phys. Status Solidi RRL*, 2014, **8**, 961–965.
126 D. C. J. Neo, C. Cheng, S. D. Stranks, S. M. Fairclough, J. S. Kim, A. I. Kirkland, J. M. Smith, H. J. Snaith, H. E. Assender and A. A. R. Watt, *Chem. Mater.*, 2014, **26**, 4004–4013.
127 A. K. Rath, F. Pelayo Garcia de Arquer, A. Stavrinadis, T. Lasanta, M. Bernechea, S. L. Diedenhofen and G. Konstantatos, *Adv. Mater.*, 2014, **26**, 4741–4747.
128 S. C. Boehme, T. A. Walvis, I. Infante, F. C. Grozema, D. Vanmaekelbergh, L. D. A. Siebbeles and A. J. Houtepen, *ACS Nano*, 2014, **8**, 7067–7077.
129 D. K. Ko, P. R. Brown, M. G. Bawendi and V. Bulovic, *Adv. Mater.*, 2014, **26**, 4845–4850.
130 P. K. Santra, A. F. Palmstrom, J. T. Tanskanen, N. Yang and S. F. Bent, *J. Phys. Chem. C*, 2015, **119**, 2996–3005.
131 C. Hefeng, L. Zeke, Z. Xiangxiang, P. Jun, H. Long, X. Songman, L. Miao, M. Wanli, T. Jiang and L. Huan, *Nanotechnology*, 2015, **26**, 035401.
132 M. Nam, J. Park, K. Lee, S.-W. Kim, H. Ko, I. K. Han and D.-H. Ko, *J. Mater. Chem. A*, 2015, **3**, 10585–10591.
133 J. M. Luther, M. Law, M. C. Beard, Q. Song, M. O. Reese, R. J. Ellingson and A. J. Nozik, *Nano Lett.*, 2008, **8**, 3488–3492.
134 K. W. Johnston, A. G. Pattantyus-Abraham, J. P. Clifford, S. H. Myrskog, S. Hoogland, H. Shukla, E. J. D. Klem, L. Levina and E. H. Sargent, *Appl. Phys. Lett.*, 2008, **92**, 122111.
135 J. P. Clifford, K. W. Johnston, L. Levina and E. H. Sargent, *Appl. Phys. Lett.*, 2007, **91**, 253117.
136 M. Law, M. C. Beard, S. Choi, J. M. Luther, M. C. Hanna and A. J. Nozik, *Nano Lett.*, 2008, **8**, 3904–3910.
137 G. I. Koleilat, L. Levina, H. Shukla, S. H. Myrskog, S. Hinds, A. G. Pattantyus-Abraham and E. H. Sargent, *ACS Nano*, 2008, **2**, 833–840.
138 D. A. R. Barkhouse, A. G. Pattantyus-Abraham, L. Levina and E. H. Sargent, *ACS Nano*, 2008, **2**, 2356–2362.
139 M.-J. Choi, J. Oh, J.-K. Yoo, J. Choi, D. M. Sim and Y. S. Jung, *Energy Environ. Sci.*, 2014, **7**, 3052–3060.
140 K. W. Johnston, A. G. Pattantyus-Abraham, J. P. Clifford, S. H. Myrskog, D. D. MacNeil, L. Levina and E. H. Sargent, *Appl. Phys. Lett.*, 2008, **92**, 151115.
141 R. Debnath, J. Tang, D. A. Barkhouse, X. Wang, A. G. Pattantyus-Abraham, L. Brzozowski, L. Levina and E. H. Sargent, *J. Am. Chem. Soc.*, 2010, **132**, 5952–5953.
142 C. Piliego, L. Protesescu, S. Z. Bisri, M. V. Kovalenko and M. A. Loi, *Energy Environ. Sci.*, 2013, **6**, 3054–3059.
143 W. H. Weber and J. Lambe, *Appl. Opt.*, 1976, **15**, 2299–2300.
144 A. Goetzberger and W. Greube, *Appl. Phys.*, 1977, **14**, 123–139.
145 R. Reisfeld and S. Neuman, *Nature*, 1978, **274**, 144–145.
146 J. S. Batchelder, A. H. Zewai and T. Cole, *Appl. Opt.*, 1979, **18**, 3090–3110.
147 J. Bomm, A. Büchtemann, A. J. Chatten, R. Bose, D. J. Farrell, N. L. A. Chan, Y. Xiao, L. H. Slooff, T. Meyer, A. Meyer, W. G. J. H. M. van Sark and R. Koole, *Sol. Energy Mater. Sol. Cells*, 2011, **95**, 2087–2094.
148 K. Barnham, J. L. Marques, J. Hassard and P. O'Brien, *Appl. Phys. Lett.*, 2000, **76**, 1197–1199.
149 A. J. Chatten, K. W. J. Barnham, B. F. Buxton, N. J. Ekins-Daukes and M. A. Malik, *Semiconductors*, 2004, **38**, 909–917.
150 A. J. Chatten, K. W. J. Barnham, B. F. Buxton, N. J. Ekins-Daukes and M. A. Malik, *Sol. Energy Mater. Sol. Cells*, 2003, **75**, 363–371.

151 S. J. Gallagher, B. C. Rowan, J. Doran and B. Norton, *Sol. Energy*, 2007, **81**, 540–547.
152 A. Schüler, M. Python, M. V. del Olmo and E. de Chambrier, *Sol. Energy*, 2007, **81**, 1159–1165.
153 S. J. Gallagher, B. Norton and P. C. Eames, *Sol. Energy*, 2007, **81**, 813–821.
154 S. M. Reda, *Acta Mater.*, 2008, **56**, 259–264.
155 D. Şahin, B. Ilan and D. F. Kelley, *J. Appl. Phys.*, 2011, **110**, 033108.
156 V. Sholin, J. D. Olson and S. A. Carter, *J. Appl. Phys.*, 2007, **101**, 123114.
157 F. Meinardi, A. Colombo, K. A. Velizhanin, R. Simonutti, M. Lorenzon, L. Beverina, R. Viswanatha, V. I. Klimov and S. Brovelli, *Nat. Photonics*, 2014, **8**, 392–399.
158 S. Kalytchuk, S. Gupta, O. Zhovtiuk, A. Vaneski, S. V. Kershaw, H. Fu, Z. Fan, E. C. H. Kwok, C.-F. Wang, W. Y. Teoh and A. L. Rogach, *J. Phys. Chem. C*, 2014, **118**, 16393–16400.
159 F. Meinardi, H. McDaniel, F. Carulli, A. Colombo, K. A. Velizhanin, N. S. Makarov, R. Simonutti, V. I. Klimov and S. Brovellii, *Nat. Nanotechnol.*, 2015, **10**, 878–885.
160 X. M. Hu, R. D. Kang, Y. Y. Zhang, L. G. Deng, H. Z. Zhong, B. S. Zou and L. J. Shi, *Opt. Express*, 2015, **23**, A858–A867.
161 T. A. Klar, T. Franzl, A. L. Rogach and J. Feldmann, *Adv. Mater.*, 2005, **17**, 769–773.
162 A. Ruland, C. Schulz-Drost, V. Sgobba and D. M. Guldi, *Adv. Mater.*, 2011, **23**, 4573–4577.
163 S. Chanyawadee, R. T. Harley, D. Taylor, M. Henini, A. S. Susha, A. L. Rogach and P. G. Lagoudakis, *Appl. Phys. Lett.*, 2009, **94**, 233502.
164 M. T. Nimmo, L. M. Caillard, W. De Benedetti, H. M. Nguyen, O. Seitz, Y. N. Gartstein, Y. J. Chabal and A. V. Malko, *ACS Nano*, 2013, **7**, 3236–3245.
165 J. D. Olson, Y. W. Rodriguez, L. D. Yang, G. B. Alers and S. A. Carter, *Appl. Phys. Lett.*, 2010, **96**, 242103.
166 J. Jasieniak, B. I. MacDonald, S. E. Watkins and P. Mulvaney, *Nano Lett.*, 2011, **11**, 2856–2864.
167 B. I. MacDonald, A. Martucci, S. Rubanov, S. E. Watkins, P. Mulvaney and J. J. Jasieniak, *ACS Nano*, 2012, **6**, 5995–6004.
168 Y. Cao, M. S. Denny, J. V. Caspar, W. E. Farneth, Q. Guo, A. S. Ionkin, L. K. Johnson, M. Lu, I. Malajovich, D. Radu, H. D. Rosenfeld, K. R. Choudhury and W. Wu, *J. Am. Chem. Soc.*, 2012, **134**, 15644–15647.
169 C. K. Miskin, W.-C. Yang, C. J. Hages, N. J. Carter, C. S. Joglekar, E. A. Stach and R. Agrawal, *Prog. Photovoltaics*, 2015, **23**, 654–659.
170 H. Zhou, W.-C. Hsu, H.-S. Duan, B. Bob, W. Yang, T.-B. Song, C.-J. Hsu and Y. Yang, *Energy Environ. Sci.*, 2013, **6**, 2822–2838.
171 I. Kim, K. Kim, Y. Oh, K. Woo, G. Z. Cao, S. Jeong and J. Moon, *Chem. Mater.*, 2014, **26**, 3957–3965.
172 M. G. Panthani, J. M. Kurley, R. W. Crisp, T. C. Dietz, T. Ezzyat, J. M. Luther and D. V. Talapin, *Nano Lett.*, 2014, **14**, 670–675.
173 G. Konstantatos and E. H. Sargent, *Nat. Nanotechnol.*, 2010, **5**, 391–400.
174 G. Konstantatos and E. H. Sargent, *Infrared Phys. Technol.*, 2011, **54**, 278–282.
175 D. V. Talapin, J. S. Lee, M. V. Kovalenko and E. V. Shevchenko, *Chem. Rev.*, 2010, **110**, 389–458.
176 C. A. Leatherdale, C. R. Kagan, N. Y. Morgan, S. A. Empedocles, M. A. Kastner and M. G. Bawendi, *Phys. Rev. B: Condens. Matter Mater. Phys.*, 2000, **62**, 2669–2680.
177 M. V. Jarosz, V. J. Porter, B. R. Fisher, M. A. Kastner and M. G. Bawendi, *Phys. Rev. B: Condens. Matter Mater. Phys.*, 2004, **70**, 195327.
178 D. Yu, B. L. Wehrenberg, P. Jha, J. Ma and P. Guyot-Sionnest, *J. Appl. Phys.*, 2006, **99**, 104315.
179 V. J. Porter, S. Geyer, J. E. Halpert, M. A. Kastner and M. G. Bawendi, *J. Phys. Chem. C*, 2008, **112**, 2308–2316.
180 H. Kim, K. Cho, H. Song, B. Min, J.-S. Lee, G.-T. Kim, S. Kim, S. H. Kim and T. Noh, *Appl. Phys. Lett.*, 2003, **83**, 4619–4621.
181 H. Kim, K. Cho, B. Park, J.-H. Kim, J. W. Lee, S. Kim, T. Noh and E. Jang, *Solid State Commun.*, 2006, **137**, 315–319.
182 M. Böberl, M. V. Kovalenko, S. Gamerith, E. J. W. List and W. Heiss, *Adv. Mater.*, 2007, **19**, 3574–3578.
183 M. Böberl, M. V. Kovalenko, G. Pillwein, G. Brunthaler and W. Heiss, *Appl. Phys. Lett.*, 2008, **92**, 261113.
184 G. Konstantatos, I. Howard, A. Fischer, S. Hoogland, J. Clifford, E. Klem, L. Levina and E. H. Sargent, *Nature*, 2006, **442**, 180–183.
185 G. Konstantatos, J. Clifford, L. Levina and E. H. Sargent, *Nat. Photonics*, 2007, **1**, 531–534.
186 G. Konstantatos and E. H. Sargent, *Appl. Phys. Lett.*, 2007, **91**, 173505.
187 E. J. D. Klem, H. Shukla, S. Hinds, D. D. MacNeil, L. Levina and E. H. Sargent, *Appl. Phys. Lett.*, 2008, **92**, 212105.
188 S. Hinds, L. Levina, E. J. D. Klem, G. Konstantatos, V. Sukhovatkin and E. H. Sargent, *Adv. Mater.*, 2008, **20**, 4398–4402.
189 G. Konstantatos, L. Levina, A. Fischer and E. H. Sargent, *Nano Lett.*, 2008, **8**, 1446–1450.
190 G. Konstantatos, L. Levina, J. Tang and E. H. Sargent, *Nano Lett.*, 2008, **8**, 4002–4006.
191 S. A. McDonald, P. W. Cyr, L. Levina and E. H. Sargent, *Appl. Phys. Lett.*, 2004, **85**, 2089–2091.
192 A. Biebersdorf, R. Dietmüller, A. S. Susha, A. L. Rogach, S. K. Poznyak, D. V. Talapin, H. Weller, T. A. Klar and J. Feldmann, *Nano Lett.*, 2006, **6**, 1559–1563.
193 H.-Y. Chen, K. F. LoMichael, G. Yang, H. G. Monbouquette and Y. Yang, *Nat. Nanotechnol.*, 2008, **3**, 543–547.
194 T. P. Osedach, N. Zhao, S. M. Geyer, L.-Y. Chang, D. D. Wanger, A. C. Arango, M. C. Bawendi and V. Bulović, *Adv. Mater.*, 2010, **22**, 5250–5254.
195 K. Szendrei, F. Cordella, M. V. Kovalenko, M. Böberl, G. Hesser, M. Yarema, D. Jarzab, O. V. Mikhnenko, A. Gocalinska, M. Saba, F. Quochi, A. Mura, G. Bongiovanni, P. W. M. Blom, W. Heiss and M. A. Loi, *Adv. Mater.*, 2009, **21**, 683–687.
196 A. Pourret, P. Guyot-Sionnest and J. W. Elam, *Adv. Mater.*, 2009, **21**, 232–235.

 This journal is © The Royal Society of Chemistry 2017

197 Y. Jin, J. Wang, B. Sun, J. C. Blakesley and N. C. Greenham, *Nano Lett.*, 2008, **8**, 1649–1653.
198 D. Qi, M. Fischbein, M. Drndić and S. Šelmić, *Appl. Phys. Lett.*, 2005, **86**, 093103.
199 R. D. Schaller and V. I. Klimov, *Phys. Rev. Lett.*, 2004, **92**, 186601.
200 V. Sukhovatkin, S. Hinds, L. Brzozowski and E. H. Sargent, *Science*, 2009, **324**, 1542–1544.
201 E. Lhuillier, S. Keuleyan, H. Liu and P. Guyot-Sionnest, *Chem. Mater.*, 2013, **25**, 1272–1282.
202 S. E. Keuleyan, P. Guyot-Sionnest, C. Delerue and G. Allan, *ACS Nano*, 2014, **8**, 8676–8682.
203 N. C. Greenham, X. Peng and A. P. Alivisatos, *Phys. Rev. B: Condens. Matter Mater. Phys.*, 1996, **54**, 17628–17637.
204 D. C. Oertel, M. G. Bawendi, A. C. Arango and V. Bulović, *Appl. Phys. Lett.*, 2005, **87**, 213505.
205 J. P. Clifford, G. Konstantatos, K. W. Johnston, S. Hoogland, L. Levina and E. H. Sargent, *Nat. Nanotechnol.*, 2009, **4**, 40–44.
206 T. Rauch, M. Boberl, S. F. Tedde, J. Furst, M. V. Kovalenko, G. Hesser, U. Lemmer, W. Heiss and O. Hayden, *Nat. Photonics*, 2009, **3**, 332–336.
207 G. Sarasqueta, K. R. Choudhury, J. Subbiah and F. So, *Adv. Funct. Mater.*, 2011, **21**, 167–171.
208 B. N. Pal, I. Robel, A. Mohite, R. Laocharoensuk, D. J. Werder and V. I. Klimov, *Adv. Funct. Mater.*, 2012, **22**, 1741–1748.
209 J. H. Burroughes, D. D. C. Bradley, A. R. Brown, R. N. Marks, K. Mackay, R. H. Friend, P. L. Burns and A. B. Holmes, *Nature*, 1990, **347**, 539–541.
210 C. W. Tang and S. A. VanSlyke, *Appl. Phys. Lett.*, 1987, **51**, 913–915.
211 W. Helfrich and W. G. Schneider, *Phys. Rev. Lett.*, 1965, **14**, 229–231.
212 T. Erdem and H. V. Demir, *Nanophotonics*, 2013, **2**, 57–81.
213 V. L. Colvin, M. C. Schlamp and A. P. Alivisatos, *Nature*, 1994, **370**, 354–357.
214 A. L. Rogach, N. Gaponik, J. M. Lupton, C. Bertoni, D. E. Gallardo, S. Dunn, N. L. Pira, M. Paderi, P. Repetto, S. G. Romanov, C. O'Dwyer, C. M. S. Torres and A. Eychmüller, *Angew. Chem., Int. Ed.*, 2008, **47**, 6538–6549.
215 L. Qian, Y. Zheng, J. Xue and P. H. Holloway, *Nat. Photonics*, 2011, **5**, 543–548.
216 J. Kwak, W. K. Bae, D. Lee, I. Park, J. Lim, M. Park, H. Cho, H. Woo, D. Y. Yoon, K. Char, S. Lee and C. Lee, *Nano Lett.*, 2012, **12**, 2362–2366.
217 D. Bozyigit, O. Yarema and V. Wood, *Adv. Funct. Mater.*, 2013, **23**, 3024–3029.
218 D. Bozyigit, V. Wood, Y. Shirasaki and V. Bulovic, *J. Appl. Phys.*, 2012, **111**, 113701.
219 J. Du, X. L. Li, S. J. Wang, Y. Z. Wu, X. P. Hao, C. W. Xu and X. Zhao, *J. Mater. Chem.*, 2012, **22**, 11390–11395.
220 R. C. Page, D. Espinobarro-Velazquez, M. A. Leontiadou, C. Smith, E. A. Lewis, S. J. Haigh, C. Li, H. Radtke, A. Pengpad, F. Bondino, E. Magnano, I. Pis, W. R. Flavell, P. O'Brien and D. J. Binks, *Small*, 2015, **11**, 1548–1554.
221 C. T. Smith, M. A. Leontiadou, R. Page, P. O'Brien and D. J. Binks, *Adv. Sci.*, 2015, **2**, 1500088.
222 K. Gong, J. E. Martin, L. E. Shea-Rohwer, P. Lu and D. F. Kelley, *J. Phys. Chem. C*, 2015, **119**, 2231–2238.
223 E. Jang, S. Jun and L. Pu, *Chem. Commun.*, 2003, 2964–2965.
224 X. T. Gao, J. Wu, X. Wei, C. H. He, X. Y. Wang, G. S. Guo and Q. S. Pu, *J. Mater. Chem.*, 2012, **22**, 6367–6373.
225 S. Sapra, S. Mayilo, T. A. Klar, A. L. Rogach and J. Feldmann, *Adv. Mater.*, 2007, **19**, 569–572.
226 H. S. Jang, H. Yang, S. W. Kim, J. Y. Han, S. G. Lee and D. Y. Jeon, *Adv. Mater.*, 2008, **20**, 2696–2702.
227 S. K. Panda, S. G. Hickey, H. V. Demir and A. Eychmüller, *Angew. Chem., Int. Ed.*, 2011, **50**, 4432–4436.
228 X. Wang, X. Yan, W. Li and K. Sun, *Adv. Mater.*, 2012, **24**, 2742–2747.
229 K.-J. Chen, H.-C. Chen, K.-A. Tsai, C.-C. Lin, H.-H. Tsai, S.-H. Chien, B.-S. Cheng, Y.-J. Hsu, M.-H. Shih, C.-H. Tsai, H.-H. Shih and H.-C. Kuo, *Adv. Funct. Mater.*, 2012, **22**, 5138–5143.
230 W.-S. Song and H. Yang, *Chem. Mater.*, 2012, **24**, 1961–1967.
231 C. Sun, Y. Zhang, Y. Wang, W. Liu, S. Kalytchuk, S. V. Kershaw, T. Zhang, X. Zhang, J. Zhao, W. W. Yu and A. L. Rogach, *Appl. Phys. Lett.*, 2014, **104**, 261106.
232 B. K. Chen, H. Z. Zhong, M. X. Wang, R. B. Liu and B. S. Zou, *Nanoscale*, 2013, **5**, 3514–3519.
233 X. Yuan, J. Hua, R. S. Zeng, D. H. Zhu, W. Y. Ji, P. T. Jing, X. D. Meng, J. L. Zhao and H. B. Li, *Nanotechnology*, 2014, **25**, 435202.
234 S. Kim, T. Kim, M. Kang, S. K. Kwak, T. W. Yoo, L. S. Park, I. Yang, S. Hwang, J. E. Lee, S. K. Kim and S.-W. Kim, *J. Am. Chem. Soc.*, 2012, **134**, 3804–3809.
235 S. Kalytchuk, O. Zhovtiuk and A. L. Rogach, *Appl. Phys. Lett.*, 2013, **103**, 103105.
236 M. Adam, Z. Wang, A. Dubavik, G. M. Stachowski, C. Meerbach, Z. Soran-Erdem, C. Rengers, H. V. Demir, N. Gaponik and A. Eychmüller, *Adv. Funct. Mater.*, 2015, **25**, 2638–2645.
237 M. Adam, R. Tietze, N. Gaponik and A. Eychmüller, *Z. Phys. Chem.*, 2015, **229**, 109–118.
238 L.-H. Mao, Q.-H. Zhang, Y. Zhang, C.-F. Wang and S. Chen, *Ind. Eng. Chem. Res.*, 2014, **53**, 16763–16770.
239 D. Zhou, M. Liu, M. Lin, X. Y. Bu, X. T. Luo, H. Zhang and B. Yang, *ACS Nano*, 2014, **8**, 10569–10581.
240 R. Liang, S. Xu, D. Yan, W. Shi, R. Tian, H. Yan, M. Wei, D. G. Evans and X. Duan, *Adv. Funct. Mater.*, 2012, **22**, 4940–4948.
241 R. Liang, D. Yan, R. Tian, X. Yu, W. Shi, C. Li, M. Wei, D. G. Evans and X. Duan, *Chem. Mater.*, 2014, **26**, 2595–2600.
242 Y. Chang, X. Yao, Z. Zhang, D. Jiang, Y. Yu, L. Mi, H. Wang, G. Li, D. Yu and Y. Jiang, *J. Mater. Chem. C*, 2015, **3**, 2831–2836.
243 M. Y. Gao, B. Richter and S. Kirstein, *Adv. Mater.*, 1997, **9**, 802–805.
244 H. Mattoussi, L. H. Radzilowski, B. O. Dabbousi, E. L. Thomas, M. G. Bawendi and M. F. Rubner, *J. Appl. Phys.*, 1998, **83**, 7965–7974.

245 M. Y. Gao, C. Lesser, S. Kirstein, H. Möhwald, A. L. Rogach and H. Weller, *J. Appl. Phys.*, 2000, **87**, 2297–2302.
246 S. Coe-Sullivan, W.-K. Woo, J. S. Steckel, M. Bawendi and V. Bulović, *Org. Electron.*, 2003, **4**, 123–130.
247 C. Bertoni, D. Gallardo, S. Dunn, N. Gaponik and A. Eychmüller, *Appl. Phys. Lett.*, 2007, **90**, 034107.
248 T. K. C. Patrick, W. S. Jan, S. v. B. Svetlana and A. J. J. René, *Nanotechnology*, 2008, **19**, 205602.
249 J. S. Bendall, M. Paderi, F. Ghigliotti, N. L. Pira, V. Lambertini, V. Lesnyak, N. Gaponik, G. Visimberga, A. Eychmüller, C. M. S. Torres, M. E. Welland, C. Gieck and L. Marchese, *Adv. Funct. Mater.*, 2010, **20**, 3298–3302.
250 X. Yang, D. Zhao, K. S. Leck, S. T. Tan, Y. X. Tang, J. Zhao, H. V. Demir and X. W. Sun, *Adv. Mater.*, 2012, **24**, 4180–4185.
251 K. W. Song, R. Costi and V. Bulovic, *Adv. Mater.*, 2013, **25**, 1420–1423.
252 B. N. Pal, Y. Ghosh, S. Brovelli, R. Laocharoensuk, V. I. Klimov, J. A. Hollingsworth and H. Htoon, *Nano Lett.*, 2012, **12**, 331–336.
253 K.-H. Lee, J.-H. Lee, W.-S. Song, H. Ko, C. Lee, J.-H. Lee and H. Yang, *ACS Nano*, 2013, **7**, 7295–7302.
254 A. Aharoni, D. Oron, U. Banin, E. Rabani and J. Jortner, *Phys. Rev. Lett.*, 2008, **100**, 057404.
255 S. Keuleyan, J. Kohler and P. Guyot-Sionnest, *J. Phys. Chem. C*, 2014, **118**, 2749–2753.
256 Q. Wen, S. V. Kershaw, S. Kalytchuk, O. Zhovtiuk, C. Reckmeier, M. I. Vasilevskiy and A. L. Rogach, *ACS Nano*, 2016, **10**, 4301–4311.
257 N. Tessler, V. Medvedev, M. Kazes, S. Kan and U. Banin, *Science*, 2002, **295**, 1506–1508.
258 L. Bakueva, S. Musikhin, M. A. Hines, T.-W. F. Chang, M. Tzolov, G. D. Scholes and E. H. Sargent, *Appl. Phys. Lett.*, 2003, **82**, 2895–2897.
259 J. S. Steckel, S. Coe-Sullivan, V. Bulovic and M. G. Bawendi, *Adv. Mater.*, 2003, **15**, 1862–1866.
260 D. S. Koktysh, N. Gaponik, M. Reufer, J. Crewett, U. Scherf, A. Eychmüller, J. M. Lupton, A. L. Rogach and J. Feldmann, *ChemPhysChem*, 2004, **5**, 1435–1438.
261 S. V. Kershaw and A. L. Rogach, *Z. Phys. Chem.*, 2015, **229**, 23–64.
262 L. Sun, J. J. Choi, D. Stachnik, A. C. Bartnik, B.-R. Hyun, G. G. Malliaras, T. Hanrath and F. W. Wise, *Nat. Nanotechnol.*, 2012, **7**, 369–373.
263 Z. J. Han and R. Eisenberg, *Acc. Chem. Res.*, 2014, **47**, 2537–2544.
264 L. Z. Wu, B. Chen, Z. J. Li and C. H. Tung, *Acc. Chem. Res.*, 2014, **47**, 2177–2185.
265 M. Graetzel, *Acc. Chem. Res.*, 1981, **14**, 376–384.
266 J. R. Darwent and G. Porter, *J. Chem. Soc., Chem. Commun.*, 1981, 145–146, DOI: 10.1039/C39810000145.
267 J. R. Darwent, *J. Chem. Soc., Faraday Trans. 2*, 1981, **77**, 1703–1709.
268 K. Kalyanasundaram, E. Borgarello and M. Graetzel, *Helv. Chim. Acta*, 1981, **64**, 362–366.
269 M. Meyer, C. Wallberg, K. Kurihara and J. H. Fendler, *J. Chem. Soc., Chem. Commun.*, 1984, 90–91, DOI: 10.1039/C39840000090.
270 Z. G. Yu, C. E. Pryor, W. H. Lau, M. A. Berding and D. B. MacQueen, *J. Phys. Chem. B*, 2005, **109**, 22913–22919.
271 F. A. Frame, E. C. Carroll, D. S. Larsen, M. Sarahan, N. D. Browning and F. E. Osterloh, *Chem. Commun.*, 2008, 2206–2208, DOI: 10.1039/B718796C.
272 F. A. Frame and F. E. Osterloh, *J. Phys. Chem. C*, 2010, **114**, 10628–10633.
273 M. A. Holmes, T. K. Townsend and F. E. Osterloh, *Chem. Commun.*, 2012, **48**, 371–373.
274 H. Gerischer, *Electrochim. Acta*, 1990, **35**, 1677–1699.
275 R. Memming, in *Electron Transfer I*, ed. J. Mattay, Springer Berlin Heidelberg, 1994, ch. 3, vol. 169, pp. 105–181.
276 L. Amirav and A. P. Alivisatos, *J. Phys. Chem. Lett.*, 2010, **1**, 1051–1054.
277 H. Zhu, N. Song, H. Lv, C. L. Hill and T. Lian, *J. Am. Chem. Soc.*, 2012, **134**, 11701–11708.
278 K. P. Acharya, R. S. Khnayzer, T. O'Connor, G. Diederich, M. Kirsanova, A. Klinkova, D. Roth, E. Kinder, M. Imboden and M. Zamkov, *Nano Lett.*, 2011, **11**, 2919–2926.
279 M. J. Berr, A. Vaneski, C. Mauser, S. Fischbach, A. S. Susha, A. L. Rogach, F. Jäckel and J. Feldmann, *Small*, 2012, **8**, 291–297.
280 M. J. Berr, P. Wagner, S. Fischbach, A. Vaneski, J. Schneider, A. S. Susha, A. L. Rogach, F. Jäckel and J. Feldmann, *Appl. Phys. Lett.*, 2012, **100**, 223903.
281 A. Vaneski, A. S. Susha, J. Rodríguez-Fernández, M. Berr, F. Jäckel, J. Feldmann and A. L. Rogach, *Adv. Funct. Mater.*, 2011, **21**, 1547–1556.
282 Y. Shemesh, J. E. Macdonald, G. Menagen and U. Banin, *Angew. Chem., Int. Ed.*, 2011, **50**, 1185–1189.
283 M. L. Tang, D. C. Grauer, B. Lassalle-Kaiser, V. K. Yachandra, L. Amirav, J. R. Long, J. Yano and A. P. Alivisatos, *Angew. Chem., Int. Ed.*, 2011, **50**, 10203–10207.
284 T. Simon, N. Bouchonville, M. J. Berr, A. Vaneski, A. Adrovic, D. Volbers, R. Wyrwich, M. Doblinger, A. S. Susha, A. L. Rogach, F. Jackel, J. K. Stolarczyk and J. Feldmann, *Nat. Mater.*, 2014, **13**, 1013–1018.
285 A. Thibert, F. A. Frame, E. Busby, M. A. Holmes, F. E. Osterloh and D. S. Larsen, *J. Phys. Chem. Lett.*, 2011, **2**, 2688–2694.
286 Z.-J. Li, J.-J. Wang, X.-B. Li, X.-B. Fan, Q.-Y. Meng, K. Feng, B. Chen, C.-H. Tung and L.-Z. Wu, *Adv. Mater.*, 2013, **25**, 6613–6618.
287 B. L. Greene, C. A. Joseph, M. J. Maroney and R. B. Dyer, *J. Am. Chem. Soc.*, 2012, **134**, 11108–11111.
288 F. Wang, W.-G. Wang, X.-J. Wang, H.-Y. Wang, C.-H. Tung and L.-Z. Wu, *Angew. Chem., Int. Ed.*, 2011, **50**, 3193–3197.
289 F. Wang, W.-J. Liang, J.-X. Jian, C.-B. Li, B. Chen, C.-H. Tung and L.-Z. Wu, *Angew. Chem., Int. Ed.*, 2013, **52**, 8134–8138.
290 Z. Han, F. Qiu, R. Eisenberg, P. L. Holland and T. D. Krauss, *Science*, 2012, **338**, 1321–1324.
291 J. Huang, K. L. Mulfort, P. Du and L. X. Chen, *J. Am. Chem. Soc.*, 2012, **134**, 16472–16475.
292 A. Das, Z. Han, M. G. Haghighi and R. Eisenberg, *Proc. Natl. Acad. Sci. U. S. A.*, 2013, **110**, 16716–16723.

 This journal is © The Royal Society of Chemistry 2017

293 C. Gimbert-Surinach, J. Albero, T. Stoll, J. Fortage, M. N. Collomb, A. Deronzier, E. Palomares and A. Llobet, *J. Am. Chem. Soc.*, 2014, **136**, 7655–7661.

294 K. Han, M. Wang, S. Zhang, S. L. Wu, Y. Yang and L. C. Sun, *Chem. Commun.*, 2015, **51**, 7008–7011.

295 H. M. Chen, C. K. Chen, Y.-C. Chang, C.-W. Tsai, R.-S. Liu, S.-F. Hu, W.-S. Chang and K.-H. Chen, *Angew. Chem., Int. Ed.*, 2010, **49**, 5966–5969.

296 P. T. Sheng, W. L. Li, J. Cai, X. Wang, X. Tong, Q. Y. Cai and C. A. Grimes, *J. Mater. Chem. A*, 2013, **1**, 7806–7815.

297 T. Nann, S. K. Ibrahim, P.-M. Woi, S. Xu, J. Ziegler and C. J. Pickett, *Angew. Chem., Int. Ed.*, 2010, **49**, 1574–1577.

298 D. Jaque, B. d. Rosal, E. M. Rodríguez, L. M. Maestro, P. Haro-González and J. G. Solé, *Nanomedicine*, 2014, **9**, 1047–1062.

299 L. M. Maestro, C. Jacinto, U. R. Silva, F. Vetrone, J. A. Capobianco, D. Jaque and J. G. Solé, *Small*, 2011, **7**, 1774–1778.

300 J. M. Yang, H. Yang and L. W. Lin, *ACS Nano*, 2011, **5**, 5067–5071.

301 L. H. Jing, S. V. Kershaw, T. Kipp, S. Kalytchuk, K. Ding, J. F. Zeng, M. X. Jiao, X. Y. Sun, A. Mews, A. L. Rogach and M. Y. Gao, *J. Am. Chem. Soc.*, 2015, **137**, 2073–2084.

302 D. Zhou, M. Lin, X. Liu, J. Li, Z. L. Chen, D. Yao, H. Z. Sun, H. Zhang and B. Yang, *ACS Nano*, 2013, **7**, 2273–2283.

303 S. Kalytchuk, O. Zhovtiuk, S. V. Kershaw, R. Zbořil and A. L. Rogach, *Small*, 2016, **12**, 466–476.

304 G. Lozano, S. R. K. Rodriguez, M. A. Verschuuren and J. Gomez Rivas, *Light: Sci. Appl.*, 2016, **5**, e16080.

305 J. Liu, S. K. Pathak, N. Sakai, R. Sheng, S. Bai, Z. Wang and H. J. Snaith, *Adv. Mater. Interfaces*, 2016, **3**, 1600571.

306 G. Nair, L.-Y. Chang, S. M. Geyer and M. G. Bawendi, *Nano Lett.*, 2011, **11**, 2145–2151.

307 D. J. Binks, *Phys. Chem. Chem. Phys.*, 2011, **13**, 12693–12704.

308 S. Tomic, J. M. Miloszewski, E. J. Tyrrell and D. J. Binks, *IEEE J. Photovoltaics*, 2016, **6**, 179–184.

309 F. Hetsch, N. Zhao, S. V. Kershaw and A. L. Rogach, *Mater. Today*, 2013, **16**, 312–325.

310 W.-k. Koh, S. R. Saudari, A. T. Fafarman, C. R. Kagan and C. B. Murray, *Nano Lett.*, 2011, **11**, 4764–4767.

311 D. K. Kim, Y. Lai, B. T. Diroll, C. B. Murray and C. R. Kagan, *Nat. Commun.*, 2012, **3**, 1216.

312 J.-H. Choi, A. T. Fafarman, S. J. Oh, D.-K. Ko, D. K. Kim, B. T. Diroll, S. Muramoto, J. G. Gillen, C. B. Murray and C. R. Kagan, *Nano Lett.*, 2012, **12**, 2631–2638.

313 A. Shabaev, A. L. Efros and A. L. Efros, *Nano Lett.*, 2013, **13**, 5454–5461.

314 S. V. Kershaw, S. Kalytchuk, O. Zhovtiuk, Q. Shen, T. Oshima, W. Yindeesuk, T. Toyoda and A. L. Rogach, *Phys. Chem. Chem. Phys.*, 2014, **16**, 25710–25722.

315 A. Bejaoui, M. I. Alonso, M. Garriga, M. Campoy-Quiles, A. R. Goñi, F. Hetsch, S. V. Kershaw, A. L. Rogach, C. H. To, Y. Foo and J. A. Zapien, *Appl. Surf. Sci.*, DOI: 10.1016/j.apsusc.2016.09.070.

316 M. V. Kovalenko, R. D. Schaller, D. Jarzab, M. A. Loi and D. V. Talapin, *J. Am. Chem. Soc.*, 2012, **134**, 2457–2460.

317 M. S. Eggleston, K. Messer, L. Zhang, E. Yablonovitch and M. C. Wu, *Proc. Natl. Acad. Sci. U. S. A.*, 2015, **112**, 1704–1709.

318 Y. Chen, J. Vela, H. Htoon, J. L. Casson, D. J. Werder, D. A. Bussian, V. I. Klimov and J. A. Hollingsworth, *J. Am. Chem. Soc.*, 2008, **130**, 5026–5027.

319 B. Mahler, P. Spinicelli, S. Buil, X. Quelin, J. P. Hermier and B. Dubertret, *Nat. Mater.*, 2008, **7**, 659–664.

320 G. E. Cragg and A. L. Efros, *Nano Lett.*, 2010, **10**, 313–317.

321 W. K. Bae, L. A. Padilha, Y. S. Park, H. McDaniel, I. Robel, J. M. Pietryga and V. I. Klimov, *ACS Nano*, 2013, **7**, 3411–3419.

322 V. I. Klimov, *J. Phys. Chem. B*, 2006, **110**, 16827–16845.

323 I. Robel, R. Gresback, U. Kortshagen, R. D. Schaller and V. I. Klimov, *Phys. Rev. Lett.*, 2009, **102**, 177404.

324 S. Ithurria and B. Dubertret, *J. Am. Chem. Soc.*, 2008, **130**, 16504–16505.

325 S. Ithurria, M. D. Tessier, B. Mahler, R. P. S. M. Lobo, B. Dubertret and A. L. Efros, *Nat. Mater.*, 2011, **10**, 936–941.

326 C. E. Rowland, I. Fedin, H. Zhang, S. K. Gray, A. O. Govorov, D. V. Talapin and R. D. Schaller, *Nat. Mater.*, 2015, **14**, 484–489.

327 E. Izquierdo, A. Robin, S. Keuleyan, N. Lequeux, E. Lhuillier and S. Ithurria, *J. Am. Chem. Soc.*, 2016, **138**, 10496–10501.

328 P. Geiregat, A. Houtepen, L. Kishore Sagar, C. Delerue, D. Van Thourhout and Z. Hens, Thresholdless Optical Gain using Colloidal HgTe Nanocrystals, in *CLEO: 2014*, OSA Technical Digest (online), Optical Society of America, 2014, paper FTh4C.4.